THE FLOWER CONSTELLATIONS -

THEORY, DESIGN PROCESS, AND APPLICATIONS

A Dissertation

by

MATTHEW PAUL WILKINS

Submitted to the Office of Graduate Studies of
Texas A&M University
in partial fulfillment of the requirements for the degree of

DOCTOR OF PHILOSOPHY

December 2004

Major Subject: Aerospace Engineering

THE FLOWER CONSTELLATIONS - THEORY, DESIGN PROCESS, AND APPLICATIONS

A Dissertation

by

MATTHEW PAUL WILKINS

Submitted to Texas A&M University
in partial fulfillment of the requirements
for the degree of

DOCTOR OF PHILOSOPHY

Approved as to style and content by:

Daniele Mortari (Co-Chair of Committee)	Kyle T. Alfriend (Co-Chair of Committee)
John L. Junkins (Member)	Srinivas R. Vadali (Member)
J. Maurice Rojas (Member)	Walter Haisler (Head of Department)

December 2004

Major Subject: Aerospace Engineering

ABSTRACT

The Flower Constellations -

Theory, Design Process, and Applications. (December 2004)

Matthew Paul Wilkins, B.S., M.S., Texas A&M University

Co–Chairs of Advisory Committee: Dr. Daniele Mortari
Dr. Kyle T. Alfriend

In this research, constellations of satellites all having orbits compatible with rotating reference frames are considered. That is to say, no matter how many satellites are considered for the constellation, when viewed from an arbitrarily defined rotating reference frame of interest, they all follow a single, identical relative trajectory. In this regard, one could think of the relative trajectories as “space trajectories on a rotating reference frame.”

In particular, this research concerns itself with reference frames constrained to rotate with the planet under consideration (e.g. the Earth Centered Earth Fixed (ECEF) frame, a frame rotating with the Earth). When the axis of symmetry of these constellations is aligned with the spin axis of the planet, then the ground track as projected onto the planet surface will be repeating.

Flower Constellations are identified by eight parameters. Five are integer parameters: the number of *petals* (N_p), the number of sidereal days to repeat the ground track (N_d), the number of satellites (N_s), and two integers to govern the phasing (F_n and F_d). Three are orbit parameters that are generally equal for all satellites: the argument of perigee (ω), the orbit inclination (i), and the perigee altitude (h_p). Each of these parameters has a unique effect on the overall design of a *Flower Constellation*.

Based upon specific choices of these parameters, some broad categories of constellation types are presented along with some unique cases. Often, a large number of satellites

are used to completely visualize these constellations. While *Flower Constellations* lend themselves to micro- and nano-satellite constellations very easily, they are also readily scalable to any mission requirement. Also investigated are inverse design techniques where the governing equations are solved for the *Flower Constellation* parameters to achieve a desired final constellation or formation shape.

Flower Constellations present beautiful and interesting dynamical features that allow us to explore a wide range of potential applications that include: telecommunications, Earth and deep space observation, global positioning systems, and new kinds of formation flying schemes among others. To demonstrate their potential, some specific *Flower Constellations* are described and discussed. Finally, the effect of perturbations such as the Earth's oblateness are investigated and options for mitigating perturbations are discussed.

Thanks, as always, to my parents Paul and Beverly Wilkins.

ACKNOWLEDGMENTS

This dissertation is the culmination of close to two years of work. I would like to thank Daniele Mortari, my co-chair and co-inventor of the *Flower Constellations* for all of his advice, his insight, and his contributions to this work. Daniele was the first to formally express the phasing relationship that has been adopted for use in this dissertation. Additionally, he wrote the reorientation method that is used in this work. As my research into the many mysteries of the *Flower Constellations* progressed, Dr. Mortari was always there to give guidance and bounce ideas off of. I am forever grateful for the wonderful working relationship that we had and hopefully will continue to have in the future.

I would also like to acknowledge my committee members who have given assistance in so many ways. From moral support to technical support, the *Flower Constellations* would not be what they are today without them. Dr. Alfriend and Dr. Junkins were two of the first to hear about the *Flower Constellations*, and I appreciate the time they took to listen to the many inane ramblings about flowers in space! They're thoughtful insights and constructive criticisms helped to point Dr. Mortari and myself in the right direction on how to approach this problem. Dr. Vadali provided invaluable insight into the problem of formation flying and how to apply *Flower Constellations* toward that end. Dr. J. Maurice Rojas, was of invaluable assistance in mathematically proving some of the more intriguing aspects of the *Flower Constellation* theory. Without his insight and mathematical expertise to point me in the write direction, I would not have been able to complete this work.

I would like to thank Christian Bruccoleri for his continued work on the *Flower Constellation* Visualization and Analysis Tool. Without his tireless efforts, many of the results presented herein would not be possible. I also appreciate his patience with our groups' demands for further improvements to the software. I would like to thank the *Spacecraft Technology Center* for the generous use of their facilities and personnel.

I would also like to mention all those who have expressed interest in the *Flower Constellation* concept. At the various technical conferences I have attended, many people have expressed amazement at the beauty of the constellations and formations. Their excitement regarding the *Flower Constellations* mirrors our own and makes the long hours of research worth while. I am very appreciative of the kind remarks by John Draim in his Breakwall Memorial Lecture at the 55^{th} International Astronautical Congress where he listed the fledgling *Flower Constellations* amongst other great constellation concepts. I look forward to many more exciting years of working with the *Flower Constellations*!

TABLE OF CONTENTS

CHAPTER Page

I THEORY OF THE *FLOWER CONSTELLATIONS* 1

A. Survey of Similar Satellite Constellations 2
1. HEO/MIO 5
2. JOCOS 6
3. LOOPUS 7
4. COBRA 9
B. Essential Theory of the *Flower Constellations* 10
1. Compatible Orbits 11
2. Finding the Nodal Period 12
3. Solving for a and e 14
4. Satellite Phasing 14
a. Symmetric Schemes 18
b. Restricted Schemes 20
c. Non-symmetric Schemes 20
d. Incomplete Schemes 21
5. Switched *Flower Constellations* 21
6. Re-Orientation of a *Flower Constellation* 22
7. *Flower Constellations* about Other Planets and Frames of Reference 24
C. Secondary Closed Paths - Existence and Uniqueness 25

II THE FORWARD DESIGN PROCESS 35

A. Choosing a *Flower Constellation* 37
1. Shape Considerations 38
a. Inclination 38
b. Argument of the Perigee 38
c. Height of Perigee 40
2. Selecting N_p and N_d 41
3. Phasing Considerations 44
4. Some Consequences of Parameter Selection 47
a. Similitude of *Flower Constellations* 48
b. Specifying the number of satellites per orbit 49
c. Specifying the number of orbits 49

CHAPTER Page

d. Planes of Satellites 50
B. Categories of *Flower Constellations* 51
1. Basic Flowers 52
2. Secondary Open Paths 52
3. Planar Patterns 54
4. Helixes 54
5. Figure 8's 54
6. Rings 56
7. Nearly Straight Lines of Satellites 57
8. Spirals 58
C. Spin Rate of Secondary Paths 58

III APPLYING THE FC THEORY: EXAMPLE PROBLEMS 62

A. Basic Design Procedure 62
B. Common Phasing Choices 64
C. Galileo Constellation Example 66
D. JOCOS Example 66
E. LOOPUS Examples 68
1. Example from Dondl Section 5.2 70
2. Example from Dondl Section 6 71
F. COBRA Example 72
G. Constructing Secondary Closed Paths 72
H. Potential Applications 75
1. Global Navigation Systems 75
2. Formation Flying Schemes 78
a. Follow the Leader 78
b. Asymmetric *Flower Constellations* 79
c. Extreme *Flower Constellations* 79

IV CONSTELLATION DESIGN VIA PROJECTION OF AN ARBITRARY SHAPE ONTO A FLOWER CONSTELLATION SURFACE 83

A. Projection from an Arbitrary View Plane 85
1. Some Definitions 85
2. Solving for the Unknowns 88
3. Finding the RAAN and MA 92
4. A Triangle Formation Example 95
B. Projection From the Mercator Map 98

CHAPTER Page

1. Geocentric Projection With a Circle Formation Example . 98
2. Parallel Projection 101
C. Other Examples 104
D. Reorientation of the Constellation/Formation 104

V PERTURBATION THEORY AND ITS EFFECT ON FC DESIGN . 109

A. Resonance Concerns 110
1. Station Keeping in the Presence of Resonance Effects for Nearly Circular Orbits 115
2. Station Keeping in the Presence of Resonance Effects for Eccentric Resonant Orbits 117
3. Resonance and the Critical Inclination 117
B. Variation of the Orbit Elements 120
1. Numerical Simulations 123
2. Incorporating Higher Order Zonal Harmonics 125
C. Effects of Third-Body Interactions 125
D. Effect of Solar Radiation Pressure 135
E. Frozen Orbits 138

VI CONCLUSIONS AND FUTURE WORK 140

REFERENCES 142

APPENDIX A 147

APPENDIX B 153

APPENDIX C 154

VITA 161

LIST OF TABLES

TABLE		Page
I	The *Sistema Quadrifoglio* (Four-Leaf Clover System) with $a = 20270.418\,km$ and $e = 0.655747$.	2
II	Parameters of HEO orbits.	6
III	Planetary constants.[20]	25
IV	Lower bound on τ as a function of minimum altitude.	42
V	Orbital parameters given for the 6+1 JOCOS system.[11]	68
VI	Satellite phasing for a 10 satellite triangle formation based upon a 10-1 *Flower Constellation*.	97
VII	Satellite phasing for a 8 satellite circle formation based upon a 10-1 *Flower Constellation*.	101
VIII	New orbital parameters for a 10 satellite triangle formation originally based upon a 10-1 *Flower Constellation* that has been reoriented 90° from the original axis of symmetry.	107
IX	Tesseral terms used by Delhaise and Henrard[32] to study the problem of resonance in mean motion for critically inclined orbits.	120
X	Integer symbols.	148
XI	Satellite Phasing for a 8-1-9-1-9 *Flower Constellation*.	154
XII	Satellite phasing for a 4-1-4-1-4 *Flower Constellation*.	154
XIII	Satellite phasing for a 769-257-4-1-4 *Flower Constellation*.	155
XIV	Satellite phasing for a 3-1-4-1-7 *Flower Constellation*.	155
XV	Satellite phasing for a 4-1-5-1-5 *Flower Constellation*.	155

TABLE Page

XVI Satellite phasing for a 3-1-4 and 3-2-4 *Flower Constellation*. 156

XVII Satellite phasing for a 12-1-13-1-13 *Flower Constellation*. 156

XVIII Satellite phasing for a 12-1-26-1-26 *Flower Constellation*. 157

XIX Satellite phasing for a 31-11-30-7-10 *Flower Constellation*. 158

XX Satellite phasing for a 37-18-57-6-19 *Flower Constellation*. 159

XXI Satellite phasing for a 15-7-49-23-49 *Flower Constellation*. 160

LIST OF FIGURES

FIGURE		Page
1	A snapshot of the *Sistema Quadrifoglio* (Four-Leaf Clover System) at initial time.	3
2	The *Flower Constellation* representation of a JOCOS 6+1 constellation. See Chapter III for details.	7
3	The *Flower Constellation* representation of a LOOPUS constellation. See Chapter III for details.	8
4	A *Flower Constellation* representation of a COBRA constellation. See Chapter III for details.	10
5	Admissible locations for satellites in a 3-1 *Flower Constellation.*	15
6	A 5-2 *Flower Constellation* can accept two satellites per orbit.	17
7	Comparison of the sequence of allowable values for the RAAN and mean anomaly angles.	26
8	When specific choices of parameters are made, then the pattern of pairs of RAAN and mean anomaly angles will repeat before the complete range is filled.	29
9	By graphing the RAAN versus mean anomaly over mod(2π), one can see that as the satellites are placed, distinct banding can appear depending upon the values of A and B.	33
10	Here the RAAN is plotted versus mean anomaly over mod(2π) in a polar plot.	34
11	A 8-1-9 *Flower Constellation* with various choices of inclination.	37
12	Two cases of a 4-1-4 *Flower Constellation* with the argument of perigee equal to 270° or 225°.	39

FIGURE Page

13 Two cases of a 3-1 *Flower Constellation* with different heights of perigee (h_p). 40

14 Varying τ has a direct impact on the anomalistic orbit period. 41

15 Case 1: A 3-1 *Flower Constellation*, Case 2: A 769-257 *Flower Constellation*. 43

16 Case 1: A 3-1 *Flower Constellation*with 50 satellites, Case 2: A 769-257 *Flower Constellation*with 50 satellites. 44

17 This figure illustrates a polar view of ECI orbits and the effect of various choices of F_n and F_d for a 3-1-4 and a 3-2-4 *Flower Constellation* with $i = 63.4^\circ$ and $\omega = 270^\circ$. 46

18 Increasing the value of F_d beyond N_s causes the spacing between ECI orbits to shrink. 47

19 The basic "Figure 8" configuration is represented here by a 12-1-13 *Flower Constellation*with $F_n = 1, F_d = 13$, $i = 116.6^\circ$,$h_p = 1666\ km$, and $\omega = 270^\circ$. 48

20 In this case, an equatorial view of a 3-1-6-1-6 *Flower Constellation* with $\omega = 270^\circ$ and $i_{cr} = 63.4^\circ$ demonstrates satellites moving together in a planar fashion. 51

21 This Planar Pattern, dubbed "Tre Lacci", is a 31-11-30 *Flower Constellation* with $F_n = 7, F_d = 10$, $i = 180^\circ$, $h_p = 9000\ km$, and $\omega = 270^\circ$. . . . 55

22 This pattern contains a helix with two intersections in the secondary closed path (i.e. $A = 1$ and $B = 2$). 56

23 This pattern contains 3 "Figure 8's" in it's base configuration and is represented here by a 37-18-57 *Flower Constellation* with $F_n = 6, F_d = 19$, $i = 63.4^\circ$, $h_p = 19702\ km$, and $\omega = 270^\circ$. 57

24 An 8-1-90-1-90 *Flower Constellation* with $i = 165^\circ$, $h_p = 3000\ km$, and $\omega = 270^\circ$. 58

25 A 4-1-5-1-5 *Flower Constellation* with $i = 174.8^\circ$, $h_p = 10354\ km$, and $\omega = 270^\circ$. 59

FIGURE Page

26 This pattern contains 2 intertwined spirals formed by a 15-7-49-23-49 *Flower Constellation* with $i = 63.4^\circ$, $h_p = 9000\ km$, and $\omega = 270^\circ$. 60

27 The Lone Star Constellation is shown here at two different instants of time. 61

28 This flowchart illustrates a basic FC design procedure. 63

29 The FC version of ESA's Galileo Constellation - a 17-10-30-1-3 *Flower Constellation* with $i = 56^\circ$, and $h_p = 22,913\ km$. 67

30 A 3-1-7-1-12 *Flower Constellation* is employed to re-create the 6+1 JOCOS constellation.[11] 69

31 A 3-4-12-11-12 *Flower Constellation* is employed to duplicate the example problem presented in Dondl's Section 5.2.[12] 70

32 A 2-1-3-1-3 *Flower Constellation* is employed to duplicate the example problem presented in Dondl's Section 6.[12] 71

33 Two 3-1-3-1-3 *Flower Constellations* are employed to re-create the basic 6-satellite COBRA Teardrop Array.[15] 73

34 Secondary closed paths can form on top of the relative orbit. 74

35 The Lone Star Constellation - a 38-23-77-23-77 *Flower Constellation* with $i = 0^\circ$, $\omega = 270^\circ$, and $h_p = 1300\ km$. 76

36 ECF View of a double 3-1-5 *Flower Constellation* with $i_{cr} = 63.4^\circ$ and either $\omega = 90^\circ$ or 270°. 77

37 3 ECF cardinal views (a,c,d) and an isometric view (b) of a 4-1-5 *Flower Constellation* with $\omega = 270^\circ$ and $i_{cr} = 116.6^\circ$. 80

38 A restricted *Flower Constellation* based upon a 3-1 *Flower Constellation*. 81

39 An "extreme" 2099-1571 *Flower Constellation* with 102 satellites. 82

40 A 5-2 *Flower Constellation* with $i = 63.4^\circ$, $\omega = 270^\circ$, and $h_p = 1500\ km$ that has been revolved about the ECI $\hat{\mathbf{K}}$ axis to form a surface. 84

41 The Earth Centered Inertial Frame and orbit parameters. 85

FIGURE Page

42 The Camera Placement Frame and the View Frame. 86

43 The vector $\mathbf{r}_c$ is defined in the $\hat{\mathbf{s}}$-$\hat{\mathbf{t}}$ plane such that it is a function of the angle β. 87

44 Here we see that each satellite is located by projecting the shape from the $\hat{\mathbf{s}}$-$\hat{\mathbf{t}}$ plane to the surface of the *Flower Constellation*. 89

45 This figure shows the relationship between the Camera Placement Frame and the Inertial Frame. 90

46 A 10-1 *Flower Constellation* surface with $i = 63.4^\circ$ and $\omega = 270^\circ$ was used to generate this triangle formation. 94

47 A 10-1 *Flower Constellation* surface with $i = 85.0^\circ$ and $\omega = 270^\circ$ was used to generate this circle formation. 99

48 For the parallel projection case, each of the satellites are positioned by projecting upwards from the surface of the Earth in a proscribed normal direction, $\hat{\mathbf{n}}$. 102

49 Two examples of other kinds of constellations and formations that can be created with this technique. 105

50 The 10 satellite triangle formation from Figure 46 on page 94 has been reoriented 90° from the original axis of symmetry. 108

51 A comparison of the resultant value of s for various values of N_p and N_d. . 113

52 Gedeon's resonance parameter can be used to determine whether or not resonance effects can be safely ignored. 114

53 The change in the RAAN over one year is plotted for various values of τ and eccentricity at the critical orbit inclination of 63.4°. Only the J_2 zonal term has been included. 126

54 The change in the argument of the perigee over one year is plotted for various values of τ and eccentricity at the critical orbit inclination of 63.4°. Only the J_2 zonal term has been included. 127

FIGURE Page

55 The change in the mean anomaly over one year is plotted for various values of τ and eccentricity at the critical orbit inclination of 63.4°. Only the J_2 zonal term has been included. 128

56 The change in the RAAN over one year is plotted for various values of τ and eccentricity at the critical orbit inclination of 63.4°. Zonal terms up to J_6 have been included. 129

57 The change in the argument of the perigee over one year is plotted for various values of τ and eccentricity at the critical orbit inclination of 63.4°. Zonal terms up to J_6 have been included. 130

58 The change in the mean anomaly over one year is plotted for various values of τ and eccentricity at the critical orbit inclination of 63.4°. Zonal terms up to J_6 have been included. 131

59 The change in the RAAN over one year is plotted for various values of τ and eccentricity at an orbit inclination of 27.5°. Zonal terms up to J_6 have been included along with Kozai's J_2^3 and J_2J_4 terms. 132

60 The change in the argument of the perigee over one year is plotted for various values of τ and eccentricity at an orbit inclination of 27.5°. Zonal terms up to J_6 have been included along with Kozai's J_2^3 and J_2J_4 terms. 133

61 The change in the mean anomaly over one year is plotted for various values of τ and eccentricity at an orbit inclination of 27.5°. Zonal terms up to J_6 have been included along with Kozai's J_2^3 and J_2J_4 terms. 134

CHAPTER I

THEORY OF THE *FLOWER CONSTELLATIONS*

In this research, constellations of satellites all having orbits compatible with rotating reference frames are considered. That is to say, no matter how many satellites are considered for the constellation, when viewed from an arbitrarily defined rotating reference frame of interest, they all follow a single, identical relative trajectory. In this regard, one could think of the relative trajectories as "space trajectories on a rotating reference frame."

In particular, this research concerns itself with reference frames constrained to rotate with the planet under consideration (e.g. the Earth Centered Earth Fixed (ECEF) frame, a frame rotating with the Earth). When the axis of symmetry of these constellations is aligned with the spin axis of the planet, then the ground track as projected onto the planet surface will be repeating.

It is important to emphasize here that the *Flower Constellations* can be made to be compatible with ANY arbitrary rotating reference frame. For instance, one could establish a *Flower Constellation* about the Earth, but synchronize the rotating reference frame such that it spins at a multiple of the Earth's rotation rate about the Sun. Therefore, keep in mind that while the equations presented herein are often written from an Earth centered point of view, they may be easily changed to other planets and other frames of reference with the appropriate choice of constants.

Also note that ground tracks for a *Flower Constellation* that has been synchronized with an arbitrary rotating reference frame will generally not be repeating as viewed by the planet-bound observer. This has a distinct advantage in that resonant perturbations stemming from oblateness effects will not be as much in evidence (See Chapter V). That

---

The journal model is the *AIAA Journal of Guidance, Control, and Dynamics*

being said, the concept of repeat ground track constellations has been around for a number of years. In the next section, a brief survey of those constellations is discussed on the way to their generalization as the *Flower Constellations*.

A. Survey of Similar Satellite Constellations

Dating back to 1967, first reported in 1981 as part of the University of Rome/NASA San Marco Project, Luigi Broglio conceptualized the *Sistema Quadrifoglio* (Four-Leaf Clover System)[1] as an equatorial constellation of four satellites, whose orbital parameters are given in Table I along with a graphical depiction of the ECI orbits and the relative orbit can be found in Figure 1. where T, Ω, ω, i, and M_0 represent the orbital period, the right

Table I. The *Sistema Quadrifoglio* (Four-Leaf Clover System) with $a = 20270.418\,km$ and $e = 0.655747$.

Satellite	T	$\Omega+\omega$	i (rad)	M_0 (rad)	ν_0 (rad)
#1	$T_s/3$	0	0	0	0
#2	$T_s/3$	$\pi/2$	0	$\pi/2$	2.64546
#3	$T_s/3$	π	0	π	π
#4	$T_s/3$	$3\pi/2$	0	$3\pi/2$	-2.64546

ascension of the ascending node (RAAN), the argument of perigee, the inclination, and the mean anomaly at the initial time, respectively. T_s is the sidereal rotation rate of the Earth.

This constellation was originally proposed to observe and to guarantee continuous measurement of the upper part of the atmosphere in the equatorial region. The purpose was to find out the relationships between the physical properties of the equatorial troposphere with the Solar and Geomagnetic activities. Broglio was interested in having continuous information at the perigee altitude. However, the beauty of the dynamics of this constellation

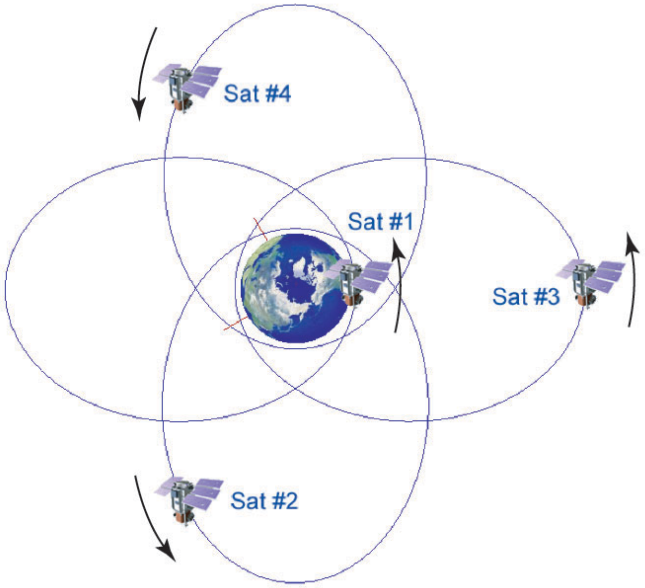

(a) Polar View showing ECI orbits

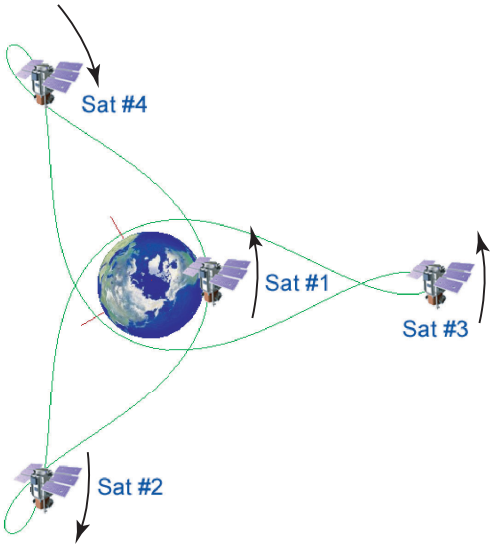

(b) Polar View showing the relative orbit

Fig. 1. A snapshot of the *Sistema Quadrifoglio* (Four-Leaf Clover System) at initial time.

can be better appreciated in an ECF system of coordinates by focusing the interest at the apogees. The satellites each spend about six hours near apogee and two hours in transition between successive apogees. Due to the phasing of the satellites in the orbits, three of the satellites are always near apogee and the other is in transition to replace the spacecraft with the largest mean anomaly (the one about to move quickly toward perigee). Finally, the three spacecraft near apogee (about 120° apart) have line of sight visibility of each other and each can observe well over 1/3 of the Earth's surface. At present knowledge, there exists only one known published paper dedicated to the *Sistema Quadrifoglio*,[2] which primarily analyzed the time history of the orbital parameters, and suggested that the perigee altitude be raised to $h_p = 600$ Km to reduce the atmospheric drag.

Since that time, a number of new constellation concepts similar in nature have been developed. These constellations are based upon the many categories of satellite orbits that exist today: Low Earth Orbits (LEO), Molniya [a subset of Highly Eccentric Orbits (HEO)], TUNDRA orbits, Geosynchronous/Geostationary Earth Orbits (GEO), Intermediate Circular Orbits (ICO), APTS (Apogee Always Pointing to the Sun) orbits,[3,4] and Multistationary Inclined Orbits (MIO). A number of the pertinent constellation concepts are: Walker Constellations,[5,6] Beste Constellations,[7] the "Gear array",[8] Ellipso,[9] Multi-regional Highly Eccentric Orbits (M-HEO),[10] Juggler Orbit COnStellation (JOCOS),[11] Loops in Orbit Occupied Permanently by Un-stationary Satellites (LOOPUS),[12] SYstem COmmunication MObile RElayed Satellite (SYCOMORES),[13] UK T-SAT,[14] and Communications Orbiting Broadband Repeating Arrays (COBRA).[15] Apparently, no one has yet undertaken a generalization of these types of constellations.

These constellations have generated considerable interest in the telecommunications industries for their ability to address certain specific needs, namely global and regional telecommunications coverage.[16,17] To that end, the European Space Agency (ESA) commissioned a study called *Archimedes* beginning in the late 80's and early 90's,[18] which

included the major space agencies in Western and Eastern Europe. This study searched for a constellation concept that would improve the poor reception from GEO satellites at higher latitudes. For instance, due to the low grazing angle between a point on the ground and a GEO satellite, buildings, terrain, and even trees often would disrupt cell phone use in Europe making it difficult to provide continuous service to users. The Archimedes effort studied many of the aforementioned constellation concepts and settled upon two basic designs based upon the Molniya (12 hour period) and TUNDRA (24 hour period) orbits.

Besides the *Sistema Quadrifoglio*, of particular interest are the HEO and MIO constellation concepts. Within these categories, the JOCOS, LOOPUS, and COBRA concepts have the most bearing, and we will consider the relative merits of these constellations. A brief description of these concepts are given below.

1. HEO/MIO

Highly Eccentric Orbits typically have a perigee altitude at or above 500 Km and apogee altitudes can be in excess of 7 Earth radii (refer to Table II). Often, as in the case of the Molniya orbits, the orbits are inclined at 63.4° or 116.6° in order to minimize the movement of the line of apsides and reduce orbit maintenance costs. Additionally, due to the high eccentricity of these orbits, an individual satellite will spend about two thirds of the orbital period near apogee, and, during that time, it appears to be almost stationary for an observer on the earth (this is often referred to as apogee dwell).

Multistationary Inclined Orbit (MIO) constellations are extensions of HEO constellations in that they generally refer to orbits which have repeating ground tracks. This, combined with the long apogee dwell time, create constellations where satellites spend up to two-thirds of their time over a particular region of the Earth.

Table II. Parameters of HEO orbits.

Parameters	MOLNIYA	TUNDRA	LOOPUS
Period (hour)	12	24	14.4
Eccentricity	0.65	0.2	0.6
Apogee height (Km)	39,400	44,220	41,700
Perigee height (Km)	2,900	27,350	5,642

2. JOCOS

The JOCOS concept involves the use of 8 hr, circular, inclined, repeating orbits. In that regard, the apogee location becomes irrelevant, and an orbit inclination of 75° was chosen to maximize Earth coverage. Six satellites are placed in orbits with nodes evenly arrayed. The mean anomalies of the satellites are chosen such that three satellites will be in the northern hemisphere and three will be in the southern. With only six satellites evenly arrayed along the relative path, as the top three simultaneously descend, the bottom three will simultaneously ascend to replace them. This is the special case of a *Flower Constellation* called *planar motion* as discussed in Chapter II. This particular arrangement was chosen in an attempt to ensure continued coverage of the Earth. However, this choice leaves gaps in coverage at the highest points of the orbits during the exchange at the equator, and an extra satellite must be placed into the mix to ensure complete coverage. For this reason, you will often see JOCOS referred to as the 6+1 JOCOS constellation. The JOCOS constellation is so named because it "juggles" 3 + 3 satellites simultaneously with three up and three down at any given time. The *Flower Constellation* theory easily creates a JOCOS constellation with appropriate choice of phasing parameters. Figure 2 graphically depicts a *Flower Constellation* version of the 6+1 JOCOS constellation while Chapter III demonstrates how to

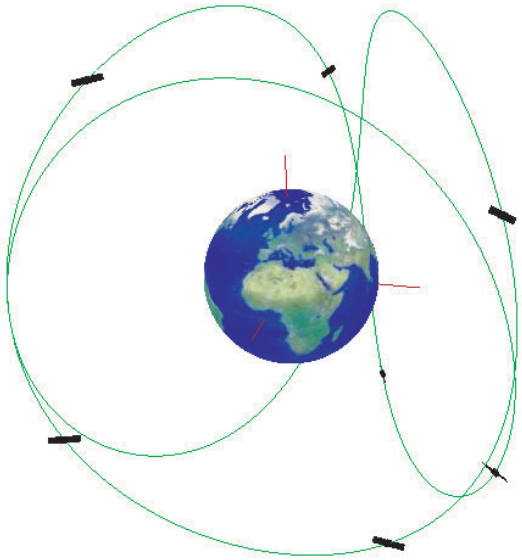

Fig. 2. The *Flower Constellation* representation of a JOCOS 6+1 constellation. See Chapter III for details.

re-create this constellation.

3. LOOPUS

LOOPUS (quasi-geostationary Loops in Orbit Occupied Permanently by Unstationary Satellites) is a constellation constructed from circular or HEO orbits. The LOOPUS concept focuses on solutions where loops are formed in the ground track. The satellites are arrayed such that two satellites will reach the intersection of the loop (one entering and one leaving) almost simultaneously where a communications hand-over is performed. As defined by Peter Dondl in 1984, a LOOPUS system is described by the following parameters: the number of LOOPUS positions n (i.e. the number of quasi-stationary points in the ECEF reference frame), the number of satellites m, the satellite orbit period T_o, and the dwelling time interval T_d (i.e. how long the satellites will spend near apogee inside the loop).

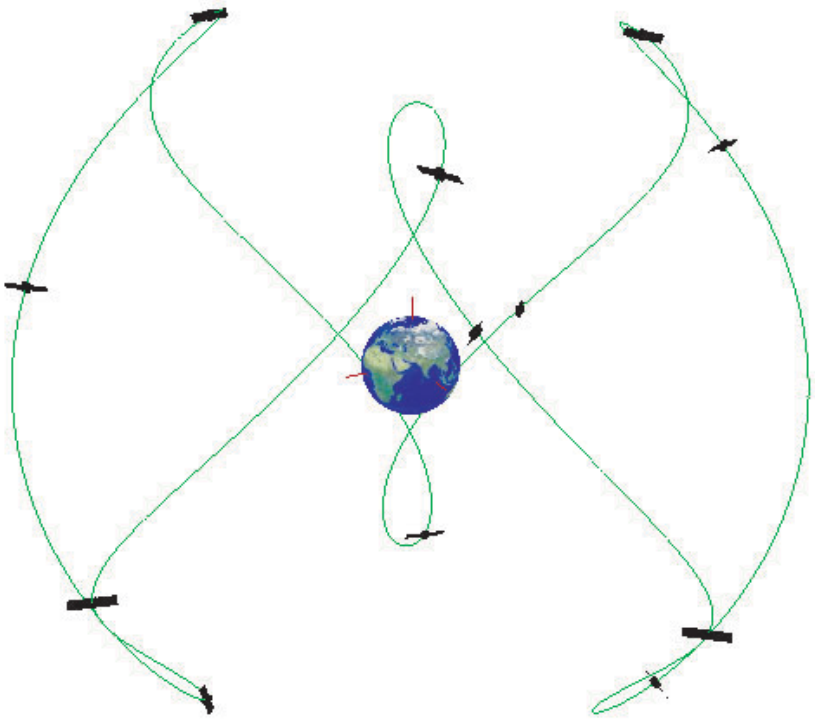

Fig. 3. The *Flower Constellation* representation of a LOOPUS constellation. See Chapter III for details.

In general, for the non-circular orbits, the inclination is chosen to be the 63.4° critical inclination. Thus, assuming values of $n = 2$, $m = 3$, $T_0 = 12$ hr and $T_d = 8$ hr, the LOOPUS concept will create a system of satellites which are in a Molniya orbit and have equally spaced nodes 120° apart. The name LOOPUS was chosen to recall the fact that the ground track creates a *loop* at apogee where the satellites spend up to two thirds of their time. Figure 3 graphically depicts a *Flower Constellation* version of one of Dondl's LOOPUS constellations.

As one reads the developments of this work, one will discover that the LOOPUS

constellation concept is a subset of the *Flower Constellation Set* that require very specific choices of FC design parameters. Chapter III covers in more detail about how to construct a LOOPUS constellation using the *Flower Constellations*. One important point to note is the vast opportunities provided in terms of satellite placement. Reading Dondl's paper, it is clear that there are severe limitations on the number of satellites that can be placed in any one LOOPUS constellation. In fact, the physical size of the constellation orbits directly affects the number of spots available in a LOOPUS constellation. In order to increase the number of satellites, it appears that Dondl proposes to duplicate the original LOOPUS constellation and either displace them about the Earth spin axis or appropriately shift the initial mean anomalies of the satellites along the relative path. The *Flower Constellation* theory has no such restriction as one will come to discover.

4. COBRA

The COBRA Teardrop concept involves two MIOs where the argument of perigee is not 90° or 270°, which would normally ensure that the location of the apogees is always over the southern or northern hemispheres, respectively. By choosing other values for the argument of perigee, a *lean* is created in the ground track. By combining two repeat track orbits, one with a right *lean* and the other with a left *lean*, a *tear drop* intersection is created. As in the LOOPUS concept, the intersection points between the two relative paths, which can be seen in Figure 4, are used to hand over communications responsibilities between satellites in the constellation. Once again, the COBRA concept is encompassed by the *Flower Constellation* theory. Chapter III demonstrates how to create a COBRA constellation using *Flower Constellations*. Note that this is really just a demonstration of combining multiple *Flower Constellations* to create a particular effect.

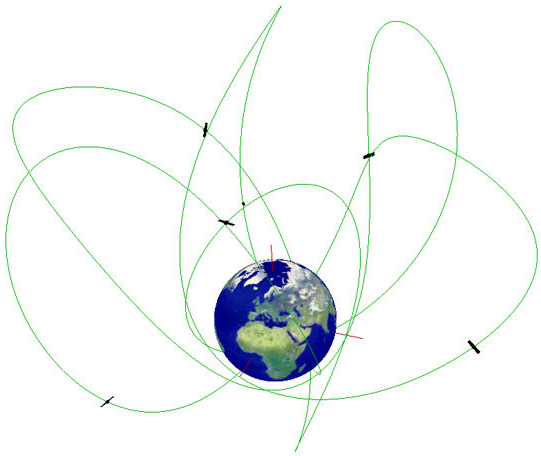

Fig. 4. A *Flower Constellation* representation of a COBRA constellation. See Chapter III for details.

B. Essential Theory of the *Flower Constellations*

This section introduces a methodology for generating the *Flower Constellation Set* that encompasses the Four-Leaf Clover System and other specific constellation types. Generally, all the orbits in a given *Flower Constellation*:

- Have identical orbit shape: anomalistic period, argument of perigee, height of perigee, and inclination.
- Are compatible: the orbital period is evaluated in such a way as to yield a perfectly repeated ground track.
- Have equally displaced node lines along the equatorial plane for each satellite in a complete *Flower Constellation*. Restricted or incomplete *Flower Constellations* have orbits whose RAANs are equally displaced within a limited right ascension range $\Delta\Omega$.

1. Compatible Orbits

To begin, consider an orbit that can be designed such that its ground track will repeat after one complete orbit around the Earth. Ideally, all that needs to be ensured is that the nodal period of the orbit, T_Ω, precisely matches the nodal period of Greenwich, $T_{\Omega G}$.

Not only can the nodal periods be set equal, but also this concept can be extended to a ground track that will repeat after the satellite completes N_p revolutions over N_d days. If T_r is the period of repetition, then

$$T_r = N_p T_\Omega = N_d T_{\Omega G} \tag{1.1}$$

Note here that the value of N_p, indicating the number of revolutions required to complete one period of repetition, corresponds to the number of *petals* that appear about the Earth in the ECF frame. Because of the flower petal-like shape of the orbits when viewed from a relative frame, we refer to a constellation of satellites which all have the exact same repeating ground track as a *Flower Constellation*. Clearly, N_p and N_d must be positive non-zero integer values (i.e. $N_p, N_d \in \mathbb{N}$, which can also written as $N_p, N_d \in \mathbb{Z}^+$. See Appendix A.).

At this point, it is necessary to write Equation (1.1) in terms of the anomalistic orbit period, T, of a satellite that belongs to the compatible orbit just defined. One can express the nodal crossing period, T_Ω, in terms of the anomalistic period (i.e. perigee to perigee). Once T has been established, the semi-major axis, a, can then be determined. The eccentricity, e, of the orbit can be determined from a and a specified perigee altitude h_p. Once a and e have been defined, the shape of the orbit is completely determined, and all that remains is to specify its orientation in space.

2. Finding the Nodal Period

To begin, examine the nodal period equations. Carter defines the nodal period of Greenwich as[19]

$$T_{\Omega G} = \frac{2\pi}{\omega_{\oplus} - \dot{\Omega}} \tag{1.2}$$

where $\omega_{\oplus} = 7.29211585530 \times 10^{-5}$ rad/sec is the rotation rate of the Earth and $\dot{\Omega}$ is the nodal regression of a satellite's orbit plane caused by perturbations such as the Earth's oblateness. By only considering orbits which repeat over a small fraction of a year, one can generally ignore the nodal regression of Greenwich due to luni-solar effects.

Following the development presented in Vallado, one can also determine the nodal period of the satellite as a function of its anomalistic period, T, as follows[20]

$$T_{\Omega} = \frac{2\pi}{\dot{M} + \dot{\omega}} = \frac{2\pi}{n + \dot{M}_0 + \dot{\omega}} \tag{1.3}$$

$$= \frac{2\pi}{n}\left(1 + \frac{\dot{M}_0 + \dot{\omega}}{n}\right)^{-1} = T\left(1 + \frac{\dot{M}_0 + \dot{\omega}}{n}\right)^{-1} \tag{1.4}$$

where $n^2 = \mu a^{-3}$ is the satellite's mean motion, $\dot{M}_0$ is the rate of change in the mean anomaly due to perturbations, and $\dot{\omega}$ is the rate of change in the argument of perigee due to perturbations. One can find expressions for $\dot{M}_0$, $\dot{\omega}$, and $\dot{\Omega}$ from geopotential perturbation theory. A more detailed discussion of the effect of perturbations can be found in Chapter V.

Considering only second order zonal effects, then the following expressions are valid[20]

$$\begin{cases} \dot{\omega} = \xi n\left(4 - 5\sin^2 i\right) \\ \dot{\Omega} = -2\xi n \cos i \\ \dot{M}_0 = -\xi n\sqrt{1-e^2}\left(3\sin^2 i - 2\right) \end{cases} \qquad \text{where} \qquad \xi = \frac{3R_{\oplus}^2 J_2}{4p^2} \tag{1.5}$$

where $R_{\oplus} = 6,378.1363$ Km is the mean radius of the Earth, $J_2 = 1.0826269 \times 10^{-3}$, p is the orbit semi-parameter, and i is the orbit inclination. Vallado continues on by assuming

circular orbits (i.e. $e \approx 0$). However, generally, the orbits under consideration in this research can range from circular to highly elliptic. Thus, the following development keeps the eccentricity terms. By substituting Equation (1.5) into Equation (1.3) and with some algebraic manipulation, one obtains

$$T_\Omega = T\left\{1+\xi\left[4+2\sqrt{1-e^2}-(5+3\sqrt{1-e^2})\sin^2 i\right]\right\}^{-1} \tag{1.6}$$

Substituting Equation (1.6) into Equation (1.1), obtain

$$T = \frac{N_d}{N_p} T_{\Omega G}\left\{1+\xi\left[4+2\sqrt{1-e^2}-(5+3\sqrt{1-e^2})\sin^2 i\right]\right\} \tag{1.7}$$

Before substituting for the nodal period of Greenwich, rearrange Equation (1.2)

$$T_{\Omega G} = \frac{2\pi}{\omega_\oplus - \dot{\Omega}} = \frac{2\pi}{\omega_\oplus}\left(1-\frac{\dot{\Omega}}{\omega_\oplus}\right)^{-1} \tag{1.8}$$

and, substituting $T_{\Omega G}$ into Equation (1.7), obtain

$$T = \frac{2\pi}{\omega_\oplus}\frac{N_d}{N_p}\left(1+2\xi\frac{n}{\omega_\oplus}\cos i\right)^{-1}\left\{1+\xi\left[4+2\sqrt{1-e^2}-(5+3\sqrt{1-e^2})\sin^2 i\right]\right\} \tag{1.9}$$

Equation (1.9) is the most general equation governing the anomalistic orbit period of the *Flower Constellation*. This equation shows that the orbit period (equal for all the satellites of the constellation) depends on the ratio

$$\tau = \frac{N_d}{N_p} \tag{1.10}$$

This implies that *Flower Constellations* characterized by the same τ are identical and that the parameters N_p and N_d must be relatively prime (See Appendix A). Note that the change in the node will cause a longitudinal shift in the orbit ground track. This shift in the node can be completely absorbed by the appropriate choice of the anomalistic orbit period (i.e. by solving Equation (1.9) including the J_2 effect).

3. Solving for a and e

Assuming that the orbit inclination has been specified, Equation (1.9) is essentially a single equation in terms of a single unknown, the semi-major axis. All of the other variables (n, ξ, p, T) can be resolved in terms of a. The eccentricity can be written as a function of a

$$e = 1 - \frac{R_\oplus + h_p}{a} \tag{1.11}$$

This allows us to write the semi-parameter only in terms of the unknown a

$$p = a(1-e^2) = 2(R_\oplus + h_p) - \frac{(R_\oplus + h_p)^2}{a} \tag{1.12}$$

The anomalistic period and mean motion are given by

$$T = \frac{2\pi}{n} = 2\pi\sqrt{\frac{a^3}{\mu}} \tag{1.13}$$

where $\mu = 398,600.4415$ Km^3/sec^2. Using any standard numerical solver, one can now solve for the semi-major axis. Once the semi-major axis has been established, we can obtain the required eccentricity and the anomalistic period.

4. Satellite Phasing

The phasing of the satellites in a *Flower Constellation* is critical to achieve the desired final effect. This is obtained by introducing a direct relationship between the right ascension of the ascending node Ω and the value of the mean anomaly at initial time $M(0)$. This relationship is equal for every satellite belonging to the constellation. Let us identify a given repeating ground track orbit, as observed in the ECI frame, which is characterized by the orbital parameters Ω, ω, i, a, and e as O^{I1}. Let O^{R1} be the relative orbit (as seen from an ECF frame) as produced with an initial orbital position characterized by the mean anomaly M_1 (see Fig. 5).

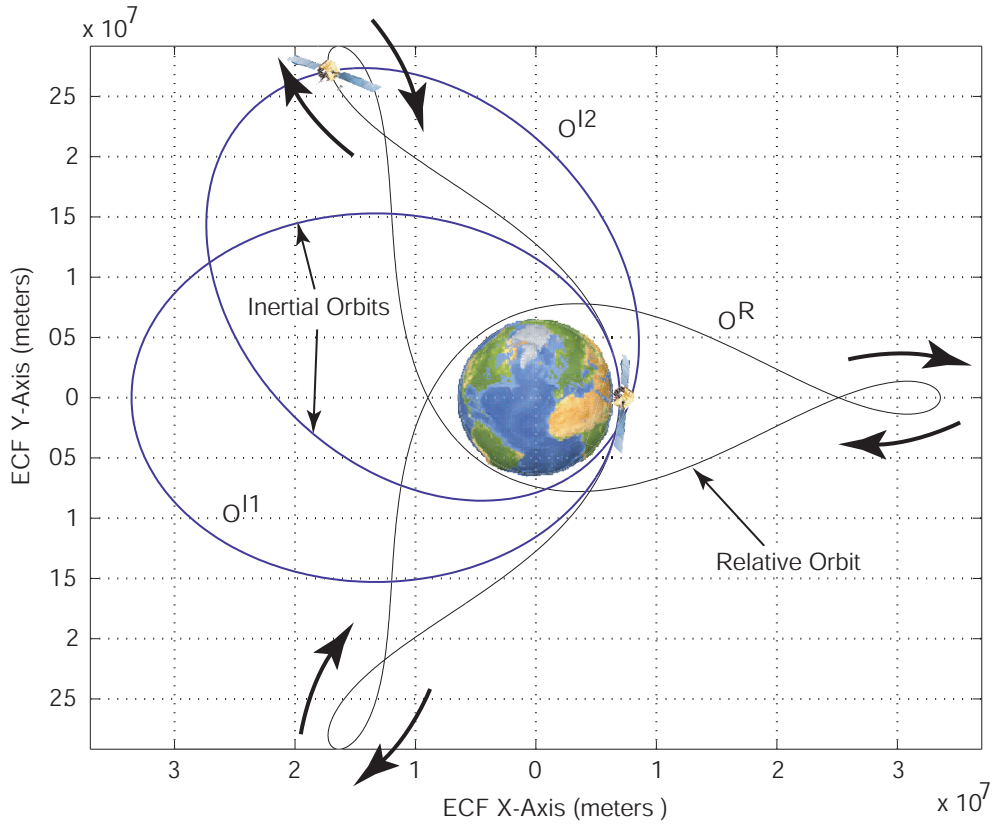

Fig. 5. Admissible locations for satellites in a 3-1 *Flower Constellation*.

Clearly, the orbiting satellite must belong to both the O^{I1} and the O^{R1} orbits. Therefore, this satellite must be at one of the intersections of these two curves. Note that, in the ECI frame, the O^{I1} orbit will appear fixed while the O^{R1} orbit will rotate in a counter-clockwise fashion at the Earth's angular spin rate. Looking at this motion in an ECF frame, then the dynamics will be reversed, with the O^{R1} orbit that appears fixed while the O^{I1} orbit is rotating, at the Earth's angular spin rate, in a clockwise fashion.

Now, let us consider an orbit O^{I2} which is *admissible* with respect to the O^{I1} orbit, where the word *admissible* means that the (ω, i, a, e) orbital parameters are identical for O^{I2} and O^{I1} orbits. When two orbits are not admissible, then there is no way that the

respective relative orbits can coincide. Two admissible orbits O^{I2} and O^{I1} differ only in that they have different values of Ω (in particular, the orbit O^{I2} is associated with an Ω_2 less than Ω_1 of the O^{I1} orbit).

The problem then is to find the initial position $M_2(0)$ of a satellite belonging to O^{I2} that produces the same relative orbit ($O^{R2} = O^{R1}$) of a satellite belonging to O^{I1} with initial position $M_1(0)$. This is identical to the problem of finding the position of the first satellite, in the ECF, when the orbit $O^{I1}(t)$ will coincide with the orbit $O^{I2}(0)$. Let Ω_1 and Ω_2 be the RAANs of the two orbits. Then $O^{I1}(\Delta t)$ will reach $O^{I2}(0)$ after a time interval

$$\Delta t = \frac{\Omega_1 - \Omega_2}{\omega_\oplus + \dot{\Omega}} \tag{1.14}$$

where $\omega_\oplus$ is the Earth spin rate and $\dot{\Omega}$ is the nodal precession rate of change due to perturbations. Therefore, after a Δt time the mean anomaly has increased its value by

$$\Delta M = (n + \dot{M}_0)\,\Delta t \tag{1.15}$$

Therefore, in order for O^{I2} to be admissible with O^{I1}, the satellite #2 should be located with an initial mean anomaly

$$M_2(0) = M_1(0) + (n + \dot{M}_0)\,\Delta t = M_1(0) + (n + \dot{M}_0)\,\frac{\Omega_1 - \Omega_2}{\omega_\oplus + \dot{\Omega}} \tag{1.16}$$

Interestingly, one can examine the dynamics of a satellite placed at the various intersections of the inertial and relative orbit. By rotating the O^{R1} orbit around the O^{I1} orbit, each intersecting point has its own set of dynamics that may or may not be physically realizable. It is possible to demonstrate that, for a one day repeat ground track, only one among all the intersecting points has the *correct* dynamics. That is to say, the angular momentum ($\vec{r} \times \vec{v}$) is preserved at that point as required by the two-body problem.

However, when one examines multiple day repeat ground tracks, one finds additional valid intersecting points. In point of fact, for each day it takes to repeat a ground track there

is one valid intersection which a satellite could be located. Figure 6 shows a 5-2 *Flower Constellation* where two satellites have been placed in a single orbit. Yet, both satellites also belong to the same relative orbit. By extension, if one places a number of satellites that is an integer multiple of the number of days to repeat, then there will be one orbit for every N_d satellites. In other words, for a *Flower Constellation* that repeats in N_d days, you can not have more than N_d satellites per orbit. In this case, the N_d different initial locations array on a single orbit, provided in terms of mean anomaly, are given by the relationship

$$M_{k+1}(0) = M_k(0) + 2\pi \frac{(n + \dot{M}_0)}{\omega_\oplus + \dot{\Omega}} \qquad k = 1, \cdots, N_d - 1 \tag{1.17}$$

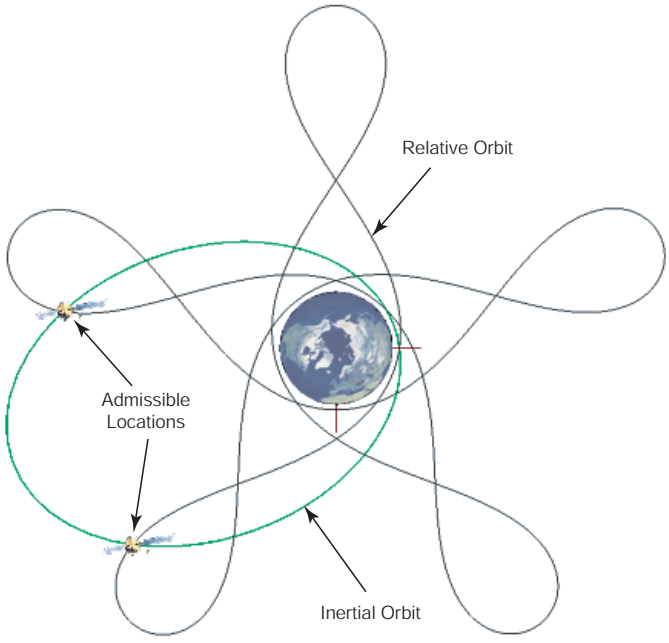

Fig. 6. A 5-2 *Flower Constellation* can accept two satellites per orbit.

a. Symmetric Schemes

The symmetric phasing scheme that has been adopted for use in the *Flower Constellations*, characterized by N_s satellites, is obtained by the phasing rule

$$\Omega_{k+1} = \Omega_k - 2\pi \frac{F_n}{F_d} \tag{1.18}$$

$$M_{k+1}(0) = M_k(0) + 2\pi \frac{F_n}{F_d} \left(\frac{n + \dot{M}_0}{\omega_\oplus + \dot{\Omega}} \right) \tag{1.19}$$

where $k = 1, \cdots, N_s - 1$, where F_n and F_d are two integer parameters that can be freely chosen provided that $F_n \in \mathbb{Z}$ and $F_d \in \mathbb{N}$, and where $M_1(0)$ and Ω_1 (which are assigned) dictate the initial position of the first satellite and the angular shifting of the O^R relative orbit, respectively.[1]

However, Equation (1.19) has a more simplified form that allows for more extensive analysis. To find this form, one must first solve Eq. (1.9) on page 13 for the mean motion, n, in terms of the known parameters. To accomplish this, the mean motion must be isolated on the left hand side of the equation, which leads to an equation of the following form:

$$n = \frac{\omega_\oplus [1 + A(\xi)]^{-1}}{\tau - 2\xi [1 + A(\xi)]^{-1} \cos i} \approx \frac{\omega_\oplus [1 - A(\xi)]}{\tau - 2\xi \cos i} \tag{1.20}$$

where

$$A(\xi) = \xi \left[4 + 2\sqrt{1 - e^2} - (5 + 3\sqrt{1 - e^2}) \sin^2 i \right] \tag{1.21}$$

Note that the approximation given in Equation (1.20) results from two simplifications. Terms that are O(ξ^2) have been ignored, and the approximation, $(1 + x)^n = 1 + nx$ for sufficiently small x, has been utilized. However, if one will consider higher order perturbations,

[1] Note that this choice can be somewhat limiting in that irrational numbers are excluded. To avoid this limitation, F_n/F_d should be substituted by a single decimal parameter, F, where $F \in \mathbb{R}$. With this choice, all the currently known possible types of symmetric phasing are encompassed. As more investigation is completed, additional symmetric schemes may become apparent.

such as J_3 and J_4 that are generally O(ξ^2), then this simplification can not be made.

Next, the perturbative quantities $\dot{\Omega}$ and $\dot{M}_0$ can be expressed as a function of the J_2 perturbation and known parameters by incorporating Equation (1.20):

$$\dot{\Omega} = -2\xi n \cos i \approx \frac{-2\xi\omega_{\oplus}[1-A(\xi)]\cos i}{\tau - 2\xi\cos i} \tag{1.22}$$

$$\dot{M}_0 = -\xi n\sqrt{1-e^2}(3\sin^2 i - 2) \approx \frac{-\xi\omega_{\oplus}[1-A(\xi)]\sqrt{1-e^2}(3\sin^2 i - 2)}{\tau - 2\xi\cos i} \tag{1.23}$$

Note that the simplified form of Equation (1.20) has been used because only the J_2 effect is being considered at this point.

By substituting Equation (1.22), Equation (1.23), and Equation (1.20) into Eq. (1.19) on page 18, we obtain:

$$M_{k+1}(0) = M_k(0) + \frac{2\pi F_n}{\tau F_d}\left\{\frac{[1-A(\xi)][1-\xi\sqrt{1-e^2}(3\sin^2 i - 2)]}{1-4\xi\cos i/\tau}\right\} \tag{1.24}$$

or

$$M_{k+1}(0) = M_k(0) + \frac{2\pi F_n N_p}{F_d N_d}\left\{\frac{1-A(\xi)-\xi\sqrt{1-e^2}(3\sin^2 i - 2)}{1-4\xi\cos i/\tau}\right\} \tag{1.25}$$

where in Equation (1.25) terms of O(ξ^2) have been ignored. If perturbations are ignored, then the most simplified version of the phasing relationships are given by

$$\Delta\Omega = -2\pi\frac{F_n}{F_d} \tag{1.26}$$

$$\Delta M_0 = 2\pi\frac{F_n}{F_d}\frac{N_p}{N_d} = -\Delta\Omega\frac{N_p}{N_d} \tag{1.27}$$

Note that $\Delta\Omega$ and ΔM as expressed in Equation (1.26) and Equation (1.27) are both rational, constructible numbers (See Appendix A.). It becomes clear here that the maximum number of satellites in a given *Flower Constellation* is

$$N_{s,max} = F_d N_d \tag{1.28}$$

and that the right ascension of the ascending node will repeat N_d times. This is due to the

fact that a single RAAN and mean anomaly value will be assigned in sequence to each satellite in a unique pairing. Since the mean anomaly steps by $F_d N_d$, then it will take a total of $F_d N_d$ steps in order to complete the assignments. It follows from $\Delta\Omega F_d N_d$ that the unique values of $\Delta\Omega$ will repeat N_d times. Note the Equation (1.28) is an upper bound on the number of satellites. One is not required to completely fill out a *Flower Constellation* but rather can selectively choose where to place satellites once the phasing scheme has been established. Therefore,

$$N_s \leq F_d N_d \tag{1.29}$$

b. Restricted Schemes

Consider now that, for some mission design reason, the RAAN angle is constrained to fall within a certain range. These constellations are built with orbit node lines uniformly distributed in a limited $\Delta\Omega \frac{F_n}{F_d}$ range instead of $2\pi \frac{F_n}{F_d}$. In this case, the phasing rules given in Eqs. (1.18) and (1.19) are specialized as follows

$$\Omega_{k+1} = \Omega_k - \Delta\Omega \frac{F_n}{F_d} \tag{1.30}$$

$$M_{k+1}(0) = M_k(0) + \Delta\Omega \frac{F_n}{F_d} \left(\frac{n + \dot{M}_0}{\omega_\oplus + \dot{\Omega}} \right) \tag{1.31}$$

c. Non-symmetric Schemes

Building upon the concept of the restricted phasing scheme, the phasing relationships can also be expressed as

$$\Omega_{k+1} = \Omega_k - \Delta\Omega_k \tag{1.32}$$

$$M_{k+1}(0) = M_k(0) + \Delta\Omega_k \left(\frac{n + \dot{M}_0}{\omega_\oplus + \dot{\Omega}} \right) \tag{1.33}$$

This implies that the difference in node value between any two satellites in the placement sequence can be arbitrary provided that the mean anomaly is selected appropriately.

d. Incomplete Schemes

Based upon the developments of the previous section, it is clear that changing the number of satellites in the constellation does not have any dramatic effect on the overall dynamics of the *Flower Constellation*, which, in turn, is dictated by the overall structure (parameters N_p and N_d) and the phasing rules (parameters F_n and F_d). Once a desired dynamic is achieved by a proper choice of the constellation parameters, then it becomes an easy task to find out the minimum number of satellites required to accomplish a specific mission objective. If it is desirable to remove a portion of the satellites but maintain the overall dynamics, one must generate the *Flower Constellation* as if the complete number of satellites were going to be placed and then selectively remove the undesirable number of satellites. That is to say, once the orbit elements have been generated for all possible satellites, the mission designer can selectively choose sets of parameters from the list. This procedure is necessary because of the way that the phasing rules are mathematically constructed. Doing this leads to an incomplete *Flower Constellation.*

5. Switched *Flower Constellations*

Any constellation can be characterized by the knowledge of the initial position and velocity of each satellite. By switching the signs of all the initial velocities, a mirror-image constellation can be built. However, this resulting *switched* constellation will be characterized by prograde orbits (toward East) if the original orbits are retrograde (toward West), and vice versa. The switched constellation idea allows one to keep the overall relative dynamics but in a reverse mode.

6. Re-Orientation of a *Flower Constellation*

The *Flower Constellation Set* has a characteristic property that the axis of symmetry is coincident with the Earth spin axis. Obviously, this is intimately related to the desire of obtaining repeating ground tracks. However, if there is a particular *Flower Constellation* that has a useful interplay between the satellites, then one can rigidly rotate all the satellite orbits that will, in turn, move the axis of symmetry to some other desired direction. Note that this is not a reconfiguration technique, but rather a mathematical technique to reorient the *Flower Constellation* for placement at initial time. Keep in mind though that this procedure will generally result in each satellite having different inclinations, nodes, and arguments of the perigee. The fuel cost for maintaining a reoriented *Flower Constellation* is generally prohibitive but is presented for completeness.

There are two consequences of re-orienting a *Flower Constellation*. First, the repeating ground track property is, in general, destroyed. Second, because all the orbits which construct a *Flower Constellation* are identical except for a varying RAAN, each orbit is subjected to identical perturbations due to the Earth's oblateness. By re-orienting the *Flower Constellation*, this dynamical symmetry with respect to the Earth is, in general, completely lost. This implies that active control is then required to maintain the constellation dynamics because the Earth gravitational perturbations now affect each orbit differently.

To re-orient a *Flower Constellation*, let $\mathbf{r}_n$ and $\mathbf{r}_p$ be unit vectors identifying the normal and the perigee directions associated with a given orbit of the constellation. In particular,

$\mathbf{r}_n$ and $\mathbf{r}_p$ can be expressed in terms of orbital parameters

$$\mathbf{r}_n = \left\{ \begin{array}{c} \sin i \sin \Omega \\ -\sin i \cos \Omega \\ \cos i \end{array} \right\}$$

$$\mathbf{r}_p = \left\{ \begin{array}{c} \cos \omega \cos \Omega - \sin \omega \sin \Omega \cos i \\ \cos \omega \sin \Omega + \sin \omega \cos \Omega \cos i \\ \sin \omega \sin i \end{array} \right\} \tag{1.34}$$

Now, let

$$\mathbf{r} = \left\{ \begin{array}{c} \sin \vartheta \cos \varphi \\ \sin \vartheta \sin \varphi \\ \cos \vartheta \end{array} \right\} \tag{1.35}$$

be the new desired *Flower Constellation* axis. This implies that all the orbits of the *Flower Constellation* must be rotated by the angle ϑ about the axis

$$\mathbf{r}_a = \left\{ \begin{array}{c} -\sin \varphi \\ \cos \varphi \\ 0 \end{array} \right\} \tag{1.36}$$

The matrix performing such a rigid rotation is

$$R(\mathbf{r}_a, \vartheta) = \left[\begin{array}{ccc} \cos \vartheta \cos^2 \varphi + \sin^2 \varphi & (\cos \vartheta - 1) \sin \varphi \cos \varphi & \cos \varphi \sin \vartheta \\ (\cos \vartheta - 1) \sin \varphi \cos \varphi & \cos \vartheta \sin^2 \varphi + \cos^2 \varphi & \sin \varphi \sin \vartheta \\ -\cos \varphi \sin \vartheta & -\sin \varphi \sin \vartheta & \cos \vartheta \end{array} \right] \tag{1.37}$$

Now, the rotated orbit will have new values for inclination, argument of perigee, and right

ascension of ascending node that can be evaluated from the vectors

$$\mathbf{r}_n^* = \left\{ \begin{array}{c} \sin i^* \sin \Omega^* \\ -\sin i^* \cos \Omega^* \\ \cos i^* \end{array} \right\} = R(\mathbf{r}_a, \vartheta)\, \mathbf{r}_n \qquad \text{and}$$

$$\mathbf{r}_p^* = \left\{ \begin{array}{c} \cos \omega^* \cos \Omega^* - \sin \omega^* \sin \Omega^* \cos i^* \\ \cos \omega^* \sin \Omega^* + \sin \omega^* \cos \Omega^* \cos i^* \\ \sin \omega^* \sin i^* \end{array} \right\} = R(\mathbf{r}_a, \vartheta)\, \mathbf{r}_p \tag{1.38}$$

which are written in terms of the new orbital parameters similar to Eq. (1.34).

By substituting Eqs. (1.34), and (1.37) into Eq. (1.38), we obtain two equations that allows us to unambiguously solve for ω^*, Ω^*, and i^*. First, for each satellite, find its new inclination.

$$\cos i^* = \mathbf{r}_n^*(3) \tag{1.39}$$

We can now solve for the new right ascension of the ascending node for each satellite using the `atan2` function, where

$$\sin \Omega^* = \frac{\mathbf{r}_n^*(1)}{\sin i^*} \qquad \text{and} \qquad \cos \Omega^* = -\frac{\mathbf{r}_n^*(2)}{\sin i^*} \tag{1.40}$$

Finally, we can solve for the argument of the perigee, also using `atan2`, for each satellite

$$\sin \omega^* = \frac{\mathbf{r}_p^*(3)}{\sin i^*} \qquad \text{and} \qquad \cos \omega^* = \mathbf{r}_p^*(1) \cos \Omega^* + \mathbf{r}_p^*(2) \sin \Omega^* \tag{1.41}$$

7. *Flower Constellations* about Other Planets and Frames of Reference

If one desires to build a *Flower Constellation* about another planet, all that is required is to choose the appropriate values for the planet's rate of spin, mean equatorial radius, and gravitational constant. Table III provides these constants for the nine planets of our solar

system. Note that if one desires to generate a *Flower Constellation* about an arbitrary rotating frame of reference, then the choice of values for these parameters is largely up to the mission designer.

Table III. Planetary constants.[20]

Planet	$2\pi/\omega_p$ (Earth days)	$r_p\ (km)$	$\mu_p\ (km^3/s^2)$
Mercury	58.6462	2439.	2.2032×10^4
Venus	-243.01	6052.	3.257×10^5
Earth	0.99726968	6378.1363	3.986004415×10^5
Mars	1.02595675	3397.2	4.305×10^4
Jupiter	0.41354	71492.	1.268×10^8
Saturn	0.4375	60268.	3.794×10^7
Uranus	-0.65	25559.	5.794×10^6
Neptune	0.768	24764.	6.809×10^6
Pluto	-6.3867	1151.	9.00×10^2
Sun	25.38 (Solar Days)	696,000.000	$1.32712428 \times 10^{11}$

C. Secondary Closed Paths - Existence and Uniqueness

In the previous sections, a method for generating a single closed path - the relative path - is described. All the satellites belonging to a particular *Flower Constellation* belong to that single relative path. In order for this to occur, each satellite is assigned a unique pairing of RAAN and mean anomaly angles $(\Omega_i, M_i(0))$ while their remaining orbit parameters are

identical ($a, e, i,$ and ω). Ignoring perturbations, Equation (1.26) and Equation (1.27) define the allowable values for these pairs.

Considering Equation (1.27), the maximum value of $M(0)$ is $M_f(0) = 2\pi F_n N_p$. One can also see that there are a maximum of $F_d N_d$ unique mean anomaly angles. This is graphically illustrated in Figure 7. Furthermore, examining Equation (1.26), one can see that the maximum value of RAAN is $2\pi F_n$. However, since there are more available mean anomaly angles to assign, the RAAN must cycle until a value has been assigned to each corresponding value of the mean anomaly. Therefore, the final value of RAAN will be $\Omega_f = \Delta\Omega F_d N_d = -2\pi F_n N_d$.

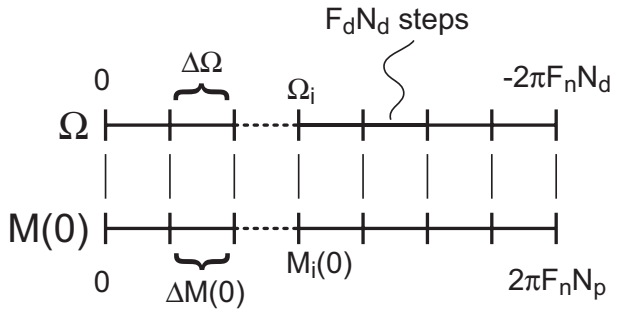

Fig. 7. Comparison of the sequence of allowable values for the RAAN and mean anomaly angles. Each mark on the number line corresponds to a unique pair of RAAN and mean anomaly angles that specifies a location for the i^{th} satellite to be placed in an orbit. All other orbit parameters have been specified by the design of the *Flower Constellation*.

Now consider the possibility that the pairs of RAAN and mean anomaly angles will repeat before (Ω_f,$M_f(0)$) is reached. In this case, there exists only a subset of angle pairs that are unique. This subset of unique angle pairs is what is termed a *secondary closed path*. If one were to continue placing satellites in the standard fashion, they would be placed physically on top of one another. While this might be a mathematical possibility, it is a physically unrealizable condition! Thus, the secondary closed path is a unique pattern

of satellites that lies *on top of* the original relative path. A satellite belonging to a secondary closed path also belongs to the original relative path.

A question is now posed. What values of the *Flower Constellation* design parameters will cause a secondary closed path to occur?

Theorem C.1. *For N_p sufficiently large, a* Flower Constellation *secondary closed path occurs when $N_d = 1$ or $F_n = kN_d$ for $k \in \mathbb{N}$.*

Remark C.2 *(Theorem C.1).* N_p is the number of "petals" in the relative path of a *Flower Constellation*. In order for a secondary closed path to be distinguishable, the number of petals must be large enough that they overlap sufficiently to allow for the closed path to be obvious. The choice of N_p and the relative merit of "sufficiently large" is left up to the mission designer.

Proof. In order for the $(\Omega_i, M_i(0))$ pairs to repeat and form a unique subset, the mean anomaly angle must be an integer multiple of 2π less than $M_f(0)$. Assume that there are a maximum of $N^*_{s,max}$ satellites in this subset. This leads to

$$\Delta M m = 2\pi n_2 \tag{1.42}$$

Likewise, for the RAAN, one can write

$$\Delta \Omega m = 2\pi n_1 \tag{1.43}$$

where m, n_1 and n_2 are unknown integers.

This can be written out in equation form as

$$-2\pi m \frac{F_n}{F_d} = 2\pi n_1 \tag{1.44}$$

$$2\pi m \frac{F_n}{F_d}\frac{N_p}{N_d} = 2\pi n_2 \tag{1.45}$$

which reduces to

$$-m\frac{F_n}{F_d} = n_1 \tag{1.46}$$

$$m\frac{F_n}{F_d}\frac{N_p}{N_d} = n_2 \tag{1.47}$$

It has already been established that F_n and F_d must be relatively prime for a unique *Flower Constellation* as must be N_p and N_d. Examining Equation (1.46), one can immediately say by the division lemma that, since $F_n \perp F_d$, $F_d \mid m$ for n_1 to be an integer (i.e. $m = jF_d$ for $j \in \mathbb{N}$). The smallest integer value of F_d that divides m is required for a unique base pattern due to the simple fact that multiples of m will only result in multiples of the base secondary closed path. Therefore, $m = F_d$, and, consequently, $n_1 = -F_n$.

Equation (1.47) can be analyzed in a similar way. Here, $(F_d N_d) \mid (mF_n N_p)$. However, since it was just established that $m = F_d$, this reduces to $N_d \mid (F_n N_p)$. From this condition and the division lemma, one can easily see that either $N_d = 1$ or $N_d \mid F_n$. In other words, a unique secondary closed path is formed when F_n is an integer multiple of N_d (i.e. $F_n = kN_d$ for $k \in \mathbb{N}$). When $k > 1$, then a unique set of multiple base paths will form. These requirements are graphically depicted in Figure 8. Note that when $F_n = N_d$, then $n_1 = -F_n = -N_d$ and $n_2 = N_p$. Likewise, when $N_d = 1$, $n_2 = F_n N_p$. □

Corollary C.3 (Theorem C.1). *For N_p sufficiently large, a* Flower Constellation *secondary closed path can also occur when $F_n \mid N_d$ (i.e. $N_d = rF_n$ where $r \in \mathbb{N}$) for $r \in \mathbb{N}$.*

Proof. In Theorem C.1, it was shown that a secondary closed path occurs when $N_d \mid F_n$ which is equivalent to saying that F_n is an integer multiple of N_d. If one rearranges this requirement to show that $F_n/k = N_d$, one can see immediately that N_d can only be an integer when $k \mid F_n$. Therefore, a secondary closed path can also occur when $N_d = rF_n$ where $r \in \mathbb{N}$. □

One can see clearly now that the secondary closed path subset of RAAN and mean

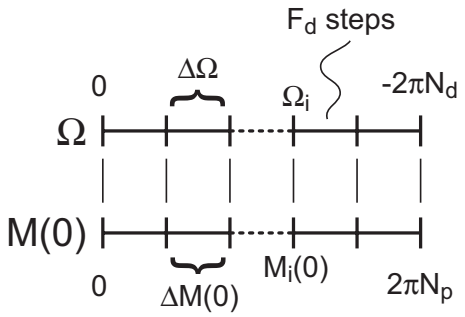

(a) $F_n = N_d$

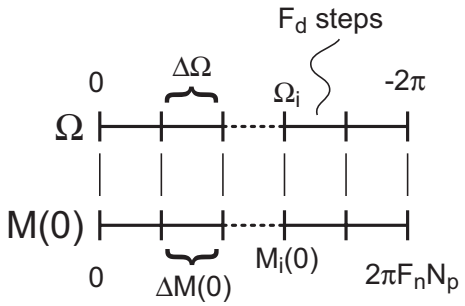

(b) $N_d = 1$

Fig. 8. When specific choices of parameters are made, then the pattern of pairs of RAAN and mean anomaly angles will repeat before the complete range is filled.

anomaly pairs will repeat after F_d pairs. Thus, the maximum number of satellites in a secondary closed path is

$$N^*_{s,max} = F_d \tag{1.48}$$

Note that $N_s \leq F_d$ with $N_s = F_d$ in order to completely visualize the entire secondary closed path. At this point, not much has been said about the actual values of N_p, N_d, or F_d. From previous developments, N_p and N_d determine the anomalistic orbit period of the satellites. Thus, these values would generally be established by mission design requirements.

F_d, however, has no such constraints and, in general, can be any non-zero positive

integer (i.e. $F_d \in \mathbb{N}$). Furthermore, the value of F_d can be chosen in a specific way that allows one to predict the resultant secondary path shape.

Theorem C.4. *For N_p sufficiently large, and assuming that Theorem C.1 has been satisfied, the phasing denominator can be expressed as $F_d = AN_d + BN_p$ where $F_d \in \mathbb{N}$, N_p and N_d are specified according to* Flower Constellation *theory and given arbitrary $A, B \in \mathbb{Z}$ such that A and B have the physical meaning of the integer number of times the mean anomaly and the RAAN are divisible by* 2π.

Proof. Examine Equation (1.26) and Equation (1.27) now written for the specific case of the secondary closed path:

$$\Delta\Omega = -\frac{2\pi N_d}{F_d} \tag{1.49}$$

$$\Delta M_0 = \frac{2\pi N_p}{F_d} \tag{1.50}$$

In order to determine the form of F_d, it is sufficient to demonstrate the form of either Equation (1.49) or Equation (1.50) can be constructed. First consider

$$\Delta M_0 \equiv C \bmod 2\pi \tag{1.51}$$

$$|\Delta\Omega| \equiv D \bmod 2\pi \tag{1.52}$$

where the symbol $\equiv$ means *congruent*. According to the definition of congruency,

$$a \equiv c \bmod b \Leftrightarrow b \mid (a-c). \tag{1.53}$$

Therefore, one can write that

$$2\pi \mid (\Delta M_0 - C) = A \tag{1.54}$$

$$2\pi \mid (|\Delta\Omega| - D) = B \tag{1.55}$$

where A and B are integers.

From Equation (1.27), one can express ΔM in terms of $\Delta\Omega$. This leads to

$$2\pi \mid \left(-\Delta\Omega \frac{N_p}{N_d} - C \right) = A \tag{1.56}$$

$$2\pi \mid (|\Delta\Omega| - D) = B \tag{1.57}$$

which can also be written as

$$2\pi A = \left(-\Delta\Omega \frac{N_p}{N_d} - C \right) \tag{1.58}$$

$$2\pi B = (\Delta\Omega - D) \tag{1.59}$$

where the absolute value of $\Delta\Omega$ in Equation (1.59) has been dropped. Solving for 2π and then equating to the two equations results in

$$\frac{A}{B}(\Delta\Omega - D) = -\Delta\Omega \frac{N_p}{N_d} - C \tag{1.60}$$

Collecting terms,

$$\Delta\Omega \left(\frac{A}{B} + \frac{N_p}{N_d} \right) = \frac{A}{B} D - C \tag{1.61}$$

Finding the common denominator of the term in parentheses,

$$\Delta\Omega \left(\frac{AN_d + BN_p}{BN_d} \right) = \frac{A}{B} D - C \tag{1.62}$$

Multiplying through,

$$\Delta\Omega(AN_d + BN_p) = ADN_d - BCN_d = (AD - BC)N_d \tag{1.63}$$

which leads to

$$\Delta\Omega = \frac{(AD - BC)N_d}{AN_d + BN_p} \tag{1.64}$$

where it is now clear comparing Equation (1.64) to Equation (1.49) that $F_d = AN_d + BN_p$ and A and B represent the integer number of times that the RAAN and the mean anomaly

are divisible by 2π. □

What is most interesting is that the values selected for A and B have physical meaning. One can think of B as the number of times the secondary closed path will intersect itself or twist over onto itself. A is the whole number of times that the node angle will be swept through 2π. One can see this clearly by plotting the RAAN (Ω) versus the mean anomaly (M) in cartesian coordinates for various values of A and B. Figure 9 on page 33 shows 6 cases where $(A,B) \in \{(0,3)\,(3,0)\,(2,3)\,(3,2)\,(-1,3)\,(3,-1)\}$.

For an arbitrary choice of F_d, the plot of RAAN and mean anomaly can have a sparse scatter-plot appearance. This is in large part due to the fact that the maximum number of satellites is controlled by F_d (assuming N_d is a defined mission parameter). However, when F_d is chosen to have the form given in Theorem C.4, then the scattered points will coalesce into distinct bands. Therefore, it is important to consider that while Theorem C.1 guarantees a secondary closed path will exist, Theorem C.4 determines in large part if the secondary closed path is *distinguishable* to the human eye. The categories of *Flower Constellations* given in Chapter II are merely human interpretations of a mathematical phenomena.

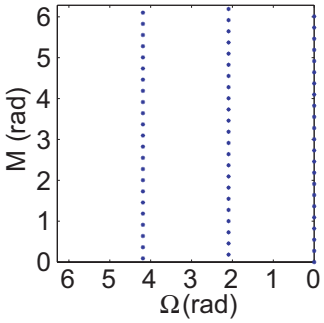

(a) $A = 3, B = 0, F_d = 69$

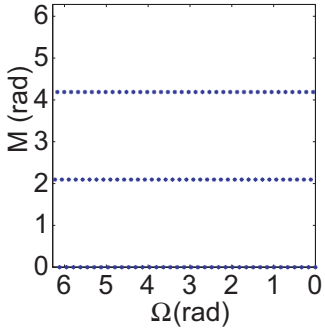

(b) $A = 0, B = 3, F_d = 114$

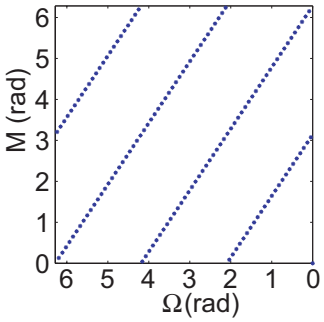

(c) $A = 3, B = 2, F_d = 145$

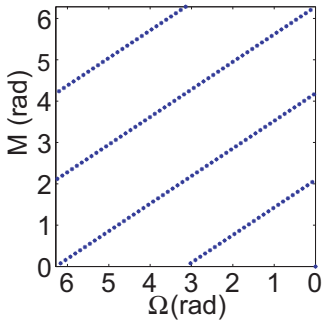

(d) $A = 2, B = 3, F_d = 160$

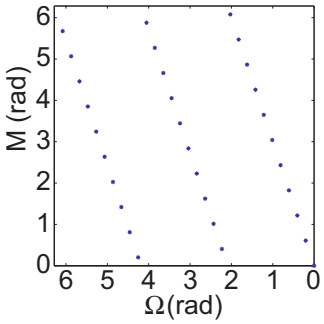

(e) $A = 3, B = -1, F_d = 31$

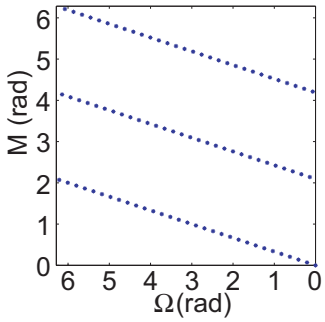

(f) $A = -1, B = 3, F_d = 91$

Fig. 9. By graphing the RAAN versus mean anomaly over mod(2π), one can see that as the satellites are placed, distinct banding can appear depending upon the values of *A* and *B*. A 38-23-F_d-23-F_d *Flower Constellation* is used for each plot where the naming convention follows N_p-N_d-N_s-F_n-F_d for the sake of brevity.

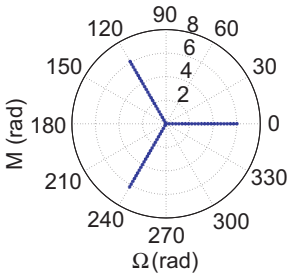

(a) $A = 3, B = 0, F_d = 69$

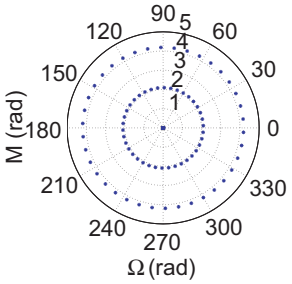

(b) $A = 0, B = 3, F_d = 114$

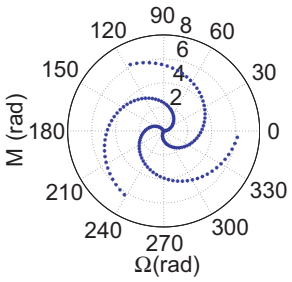

(c) $A = 3, B = 2, F_d = 145$

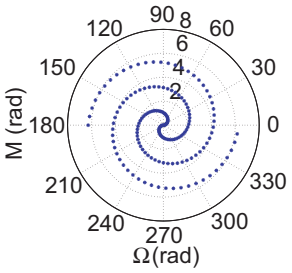

(d) $A = 2, B = 3, F_d = 160$

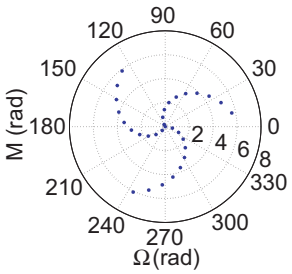

(e) $A = 3, B = -1, F_d = 31$

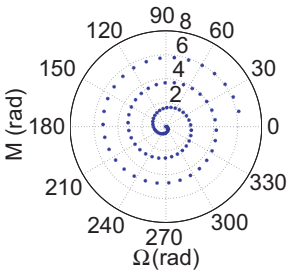

(f) $A = -1, B = 3, F_d = 91$

Fig. 10. Here the RAAN is plotted versus mean anomaly over mod(2π) in a polar plot. Ω is the angle and M is the radius on the polar plot. Notice the distinct branches that appear for specific values of A and B as well as the direction of the branches according the sign of A and B. A 38-23-F_d-23-F_d *Flower Constellation* is used for each plot.

CHAPTER II

THE FORWARD DESIGN PROCESS

Consider briefly that, if one had two satellites in arbitrary orbits, one would need to specify twelve separate parameters to completely locate the satellites in space. In particular, for the satellites to have a common relative path, one would need to specify a common semi-major axis, eccentricity, argument of the perigee, and inclination along with individual RAAN and mean anomaly. Because the mean anomaly is specified through a phasing relationship as a function of RAAN, there are five total parameters that must be set to establish the orbits.

Using the *Flower Constellation* parameter set, one will also find that six parameters are needed among the two satellites: N_p and N_d specify the common semi-major axis, h_p specifies the eccentricity in conjunction with N_p and N_d, ω and i orient the orbit planes, and Ω is specified for each satellite, which, in turn, specifies M through a functional relationship. The difference here is that the semi-major axis is specified using two integer parameters. Note that $N_s, F_n,$ and F_d do not play a roll in positioning the satellites for the *Flower Constellations*. Also note that a particular *Flower Constellation* is referred to as a N_p-N_d-N_s *Flower Constellation* or N_p-N_d-N_s-F_n-F_d *Flower Constellation* for the sake of brevity.

In summary, *Flower Constellations* are identified by eight parameters in total. Five are integer parameters: the number of *petals* (N_p), the number of sidereal days to repeat the ground track (N_d), the number of satellites (N_s), and two integers that govern the phasing (F_n and F_d). Three are orbit parameters which are equivalent for all satellites: the argument of perigee (ω), the orbit inclination (i), and the perigee altitude (h_p). However, keep in mind that if a *Flower Constellation* has been reoriented, the orbit parameters $\omega, \Omega,$ and i will be different for each orbit. Therefore it is desirable in many cases to design a *Flower*

Constellation such that its spin axis is aligned with the planet spin axis to obtain a useful phasing arrangement that can then be reoriented as a final step.

Having laid the foundation of the *Flower Constellations*, this chapter provides some guidelines for utilizing *Flower Constellations* as a design tool. There are some explicit consequences of parameter selection on the resultant design of a *Flower Constellation* that must be understood. In that regard, there are three groupings of parameters that will be discussed: (i, ω, h_p), (N_p, N_d), and (F_n, F_d).

When reading this chapter, keep in mind that a large number of satellites is used to completely visualize some of these constellations. Thus, many *Flower Constellations* lend themselves easily to micro- and nano-satellite constellations. However, *Flower Constellations* are readily scalable to any mission size and scope after the phasing scheme has been established. That is to say, the mathematical formulation presented in this research fills out complete constellations. One can arbitrarily choose to omit any satellite from the scheme.

Also keep in mind that *Flower Constellations* are characterized by an axis of symmetry that can be arbitrarily oriented. While the relative geometry and phasing of all the satellites is preserved in a reoriented *Flower Constellation*, the identical repeat ground track property is only present when aligned with the Earth spin axis. Thus, once a fundamental design has been chosen, any FC can be reoriented as necessary.

Additionally, the *Flower Constellations* presented in this chapter were designed using an ideal Earth. In general, incorporating geopotential perturbations result in a slight shift of the mean anomaly angles and do not dramatically affect the overall design. For a discussion of the impact of perturbations on phasing, consult Chapter V.

A. Choosing a *Flower Constellation*

There are four basic steps to selecting a *Flower Constellation*. First, the orbit inclination, argument of the perigee, and the height of perigee (i, ω, h_p) must be specified. Second, one must decide on an overall shape. Third, one must decide on the desired phasing of the constellation. Lastly, to orient the *Flower Constellation*, an axis of symmetry must be specified relative to the Earth's spin axis.

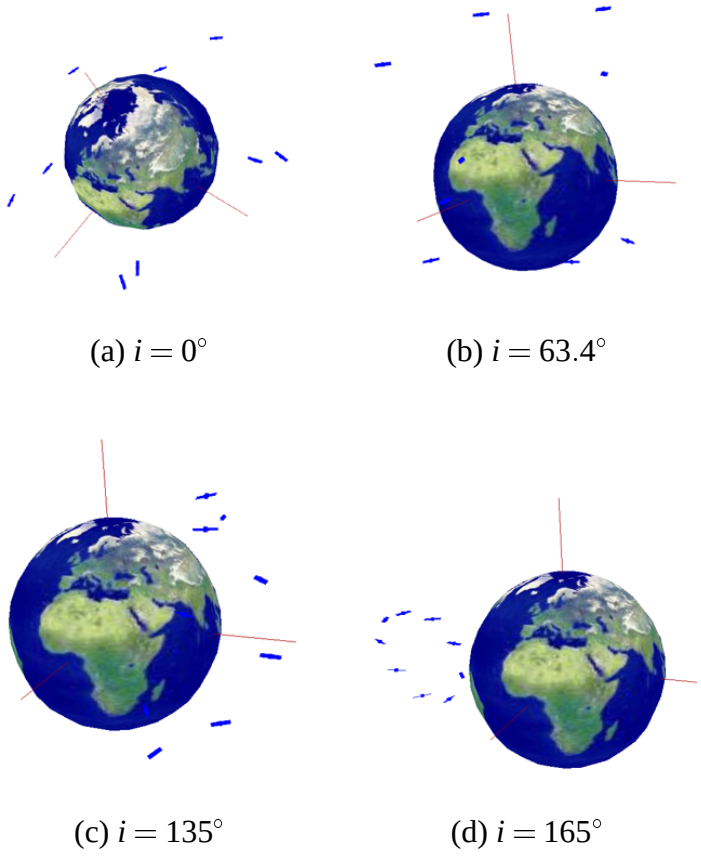

(a) $i = 0^\circ$ (b) $i = 63.4^\circ$

(c) $i = 135^\circ$ (d) $i = 165^\circ$

Fig. 11. A 8-1-9 *Flower Constellation* with various choices of inclination. Refer to Table XI on page 154 for phasing details.

1. Shape Considerations

One of the first tasks in designing a *Flower Constellation* is to select the orbit inclination, argument of perigee, and the height of perigee.

a. Inclination

In many cases, it is desirable to select the orbit inclination to be one of the critical inclinations in an effort to *freeze* the *Flower Constellation*, which will prevent the line of apsides from shifting over time. However, through experimentation, a number of unique constellations have been discovered that only occur at specific inclinations. Figure 11 shows several cases of a 8-1-9 *Flower Constellation* for varying inclinations. In each of these cases, the only parameter that has been changed is the inclination.

Figure 11(a) depicts the 8-1-9 *Flower Constellation* in the equatorial plane. Whenever the inclination is set to 0°, patterns are formed, which, in this case, is a five pointed star. Each of the satellites moves in such a way that the star spins about the constellation axis of symmetry while maintaining the overall configuration. Figure 11(b) depicts the 8-1-9 *Flower Constellation* with an inclination of 63.4°. As one can see, the pattern of satellites is somewhat sparse and forms a rough figure eight. When the inclination is increased to 135°, a tear-drop like constellation, shown in Figure 11(c), is formed. Finally, as the inclination is increased even further to 165°, a roughly circular constellation is formed, which is depicted in Figure 11(d). Unless otherwise stated, the default inclination that is used for figures in this work is 63.4°.

b. Argument of the Perigee

Another important parameter is the argument of perigee. The constellations depicted in Figure 11 all have ω set to 270°. If one were to set $\omega = 90^\circ$, then the constellations would

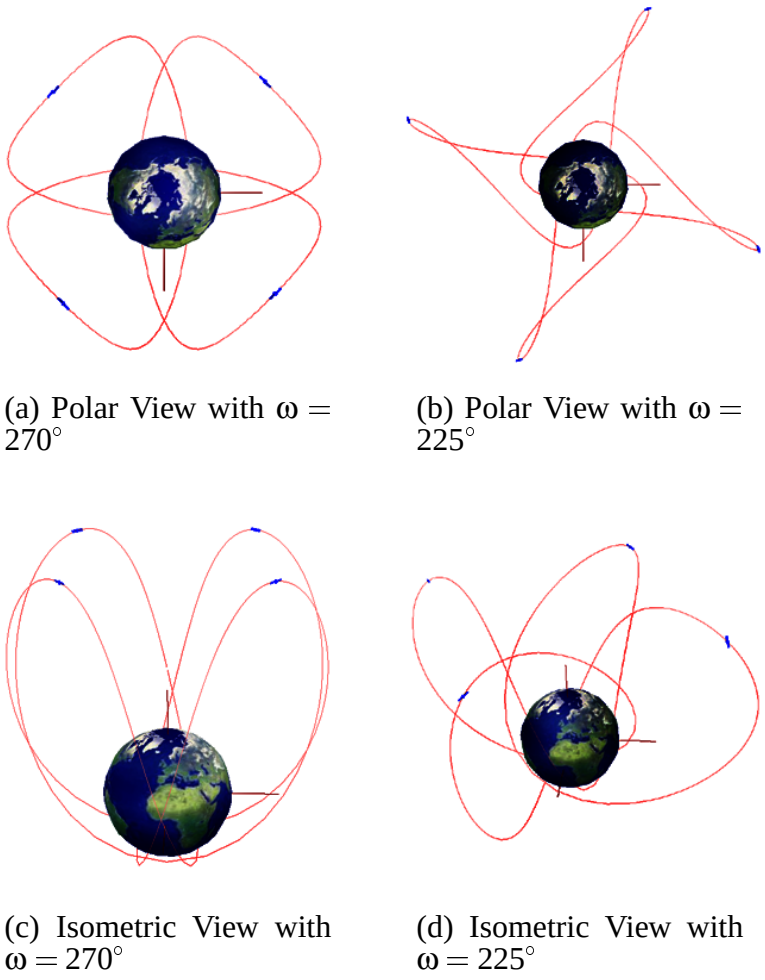

(a) Polar View with $\omega = 270^\circ$

(b) Polar View with $\omega = 225^\circ$

(c) Isometric View with $\omega = 270^\circ$

(d) Isometric View with $\omega = 225^\circ$

Fig. 12. Two cases of a 4-1-4 *Flower Constellation* with the argument of perigee equal to 270° or 225°. Refer to Table XII on page 154 for phasing details.

be mirror images with respect to the Earth's equator. Adjusting the argument of perigee is one way of reorienting a *Flower Constellation* except that the axis of symmetry is still coincident with the Earth's spin axis.

Setting $\omega = 45^\circ, 135^\circ, 225^\circ$, or 315° results in a constellation that looks more like a fan blade than a flower (See Figure 12). Thus, all other things being equal, one will notice that adjusting ω has several "critical" points: 90° and 270° create *Flower Constellations* with the highest apogee altitudes, 0° and 180° create *Flower Constellations* that are sym-

metric with respect to the plane perpendicular to the axis of symmetry (the equator in this case) resulting in the lowest apogee altitudes, and $45^\circ, 135^\circ, 225^\circ$, or 315° result in a blend between the two extremes. Unless otherwise stated, the default argument of perigee that is used for figures in this work is 270°.

c. Height of Perigee

The last of the three orbit parameters, the height of perigee (h_p), is intimately tied into the determination of the orbit eccentricity. Recall from the *Flower Constellation* Theory that, once we have determined the semi-major axis of the orbits, knowing the height of perigee, we can solve for the eccentricity.

$$e = 1 - \frac{R_\oplus + h_p}{a}$$

Essentially, for a fixed a, decreasing h_p yields a more eccentric orbit while increasing h_p

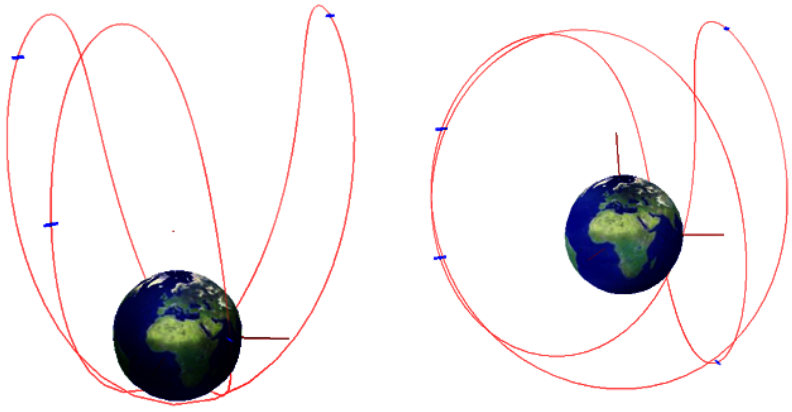

(a) Isometric View with $h_p = 400\ km$

(b) Isometric View with $h_p = 13892\ km$

Fig. 13. Two cases of a 3-1 *Flower Constellation* with different heights of perigee (h_p). Refer to Table XVI on page 156 for phasing details.

yields a more circular orbit. What this implies is that there are constraints on the overall

size of a given *Flower Constellation*. *Flower Constellations* created with circular orbits will have a relative orbit that is equidistant from the surface of the Earth, while *Flower Constellations* created with highly eccentric orbits will tend to be more slender and narrow with parts of the relative orbit extending far above the Earth. Figure 13 illustrates a 3-1 *Flower Constellation* with (a) a relatively low value for h_p and (b) the maximum value of h_p for this case, which corresponds to circular orbits.

Additionally, h_p has an impact on the maintenance of *Flower Constellations*. If h_p is set too low, the atmospheric drag will become a major concern in maintaining the overall design of a given *Flower Constellation*. Castronuovo, Bardone and Di Ruscio[2] have shown that h_p should be kept above 600 *km* to reduce drag effects. Therefore, unless otherwise stated, the default value for the h_p is 600 *km*.

2. Selecting N_p and N_d

Referring back to Equation (1.10), recall that there is a ratio, τ, between two of the integer parameters that roughly governs the overall size of a *Flower Constellation*.

$$\tau \equiv \frac{N_d}{N_p} \tag{2.1}$$

Referring back to Equation (1.9), one can see that if $\tau = 1$, for instance, then the anomalistic

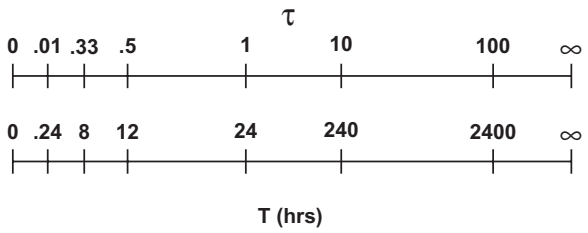

Fig. 14. Varying τ has a direct impact on the anomalistic orbit period. A 3-1 *Flower Constellation* has an 8 *hr* orbit period corresponding to $\tau = 0.3333$.

orbit period will be 24 hours (not including perturbative effects).

Note that it is important to keep the values of N_p and N_d in proportion to one another. For a given value of N_d, as $N_p \to \infty$, $\tau \to 0$, which means that the anomalistic orbit period also goes to zero (which is physically unrealizable). Conversely, for a given value of N_p, as $N_d \to \infty$, $\tau \to \infty$, which means that the anomalistic orbit period goes to infinity. This is also generally unacceptable. Therefore, even though N_p and N_d may individually be quite large, provided that the overall ratio, τ is kept in a reasonable range (See Figure 14), the resultant *Flower Constellation* will be plausible.

Table IV. Lower bound on τ as a function of minimum altitude.

$h_{min}(km)$	τ_{min}
90	6.0083×10^{-2}
400	6.4454×10^{-2}
600	6.7328×10^{-2}
800	7.0243×10^{-2}
1000	7.3050×10^{-2}
10000	2.4209×10^{-1}

Note that a lower bound for τ can be found as a function of some minimum allowable perigee altitude. This lower bound can be expressed as

$$\tau \geq \omega_{\oplus} \sqrt{\frac{(R_{\oplus} + h_{min})^3}{\mu_{\oplus}}} \tag{2.2}$$

where h_{min} is the minimum altitude about the earth expressed in the same units as the mean equatorial radius of the Earth, $R_{\oplus}$. Table IV shows the resultant minimum value for τ for some specific values of the minimum altitude h_{min}.

Because *Flower Constellations* are geometrically symmetrical about the axis of symmetry, as the number of petals increases while the number of days to repeat the pattern

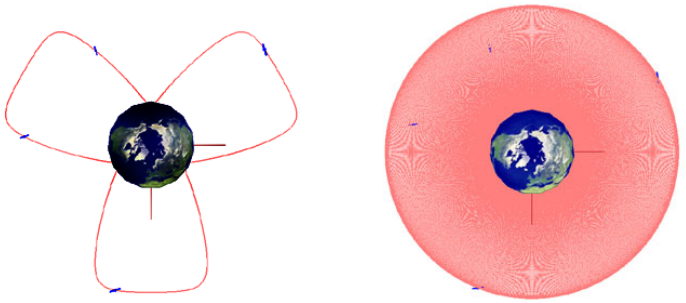

(a) Case 1 Polar View

(b) Case 2 Polar View

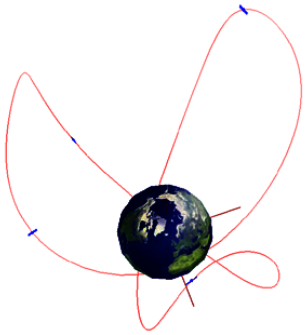

(c) Case 1 Isometric View

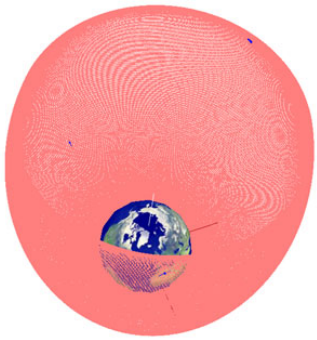

(d) Case 2 Isometric View

Fig. 15. Case 1: A 3-1 *Flower Constellation*, Case 2: A 769-257 *Flower Constellation*. Refer to Table XVI on page 156 and Table XIII on page 155 for phasing details.

stays the same, the petals begin to overlap each other. As N_p grows large, the relative orbit begins to look less like distinct flower petals and more like a surface. Figure 16 shows two cases to illustrate this point. The first case shows a $N_p = 3$, $N_d = 1$ *Flower Constellation* ($\tau = 0.3333$) while the second case has $N_p = 769$, $N_d = 257$ ($\tau = 0.3342$).

Now, remove the relative orbits that are depicted in Figure 15 and, instead, increase the number of satellites to fill out the pattern. When one views both of these cases from the North pole of the Earth without the relative orbits (Figure 16), one will see something rather unexpected. Both constellations look almost identical.

In fact, there is only one subtle difference between the two patterns of satellites. In

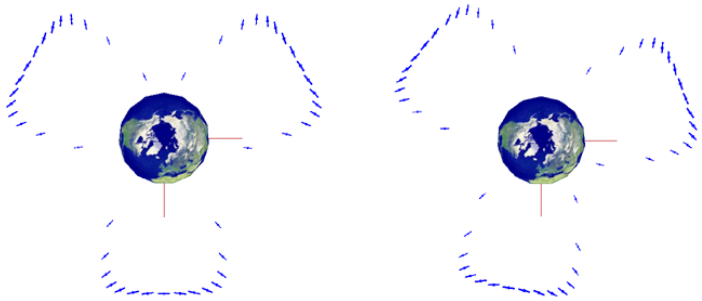

(a) Case 1 Polar View (b) Case 2 Polar View

Fig. 16. Case 1: A 3-1 *Flower Constellation*with 50 satellites, Case 2: A 769-257 *Flower Constellation*with 50 satellites. For both cases, each satellite has been placed into its own orbit (i.e. $F_n/F_d = 1/N_s$).

Case 1, the pattern fits exactly on the relative path and, thus, is a closed path. In Case 2, there are two ”paths” for the satellites to follow. The first ”path” is the relative orbit depicted in Figure 15. The secondary path is generated by the pattern that you see in Figure 16. The secondary path, for this particular case, is open ended. That is, if you follow a particular satellite from the starting point to the end point of the pattern, those points do not coincide. As the number of petals is decreased (while maintaining the appropriate τ ratio), this disconnect will become more and more pronounced.

Note that, in general, secondary paths can be closed or open. Part of the constellation design process will focus on selecting patterns of satellites that are either on closed or open secondary paths. Secondary open paths are formed when τ is perturbed slightly and all other design parameters remain constant. Secondary closed paths result from a combination of both the shape of the *Flower Constellation* and the selected phasing.

3. Phasing Considerations

There are two parameters which govern the phasing scheme of a *Flower Constellation*: F_n and F_d. Before embarking upon a phasing analysis of a particular *Flower Constellation*,

there are a couple things to keep in mind.

Recall from Section I.B.4 that the number of available slots for satellites was limited by the relationship

$$N_s \leq F_d N_d$$

What this implies is that as the number of days to repeat a given *Flower Constellation* increases or as the phasing denominator increases, there are more slots open for satellites to fill. Therefore, the potential number and kind of *Flower Constellation* types correspondingly increases. Recall in the previous section that one could search for integer values of N_p and N_d given a decimal value for τ. Now, it becomes apparent that, if one perturbs τ slightly, one can identify alternative *Flower Constellations* that might offer additional phasing possibilities. The consequence of this is that the alternative patterns might be a secondary path that is rotating relative to the relative orbit, which may or may not be desirable.

Also recall that the number of satellites that could be placed into a single orbit belonging to a *Flower Constellation* is equivalent to the number of days to repeat, N_d. If one starts out with a base *Flower Constellation* design that has fewer available slots for satellites than what you need, then perturb τ slightly to obtain a similar solution which allows for larger values of N_p and N_d. For example, if one desires to place four satellites per orbit, then search for solutions where $N_d \geq 4$.

F_n and F_d are intimately related to the distribution of the right ascension of the ascending node, which leads to an interesting consequence that occurs for certain choices of said parameters. Note that the ratio of F_n to F_d must be relatively prime for analysis purposes (see Appendix A). By examining Eq. (1.26) on page 19, one can see that F_d determines the number of physical orbits available to place satellites into. In other words, if one desires to place satellites into four separate orbits, then $F_d = 4$. This holds for any value of N_d. Figure 17 illustrates the effect of various values of F_d for given *Flower Constellations*.

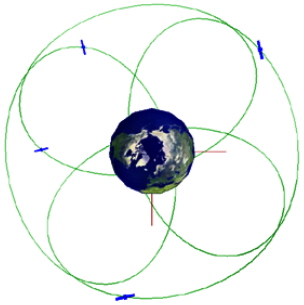

(a) A 3-1-4 FC with $F_n = 1, F_d = 4$

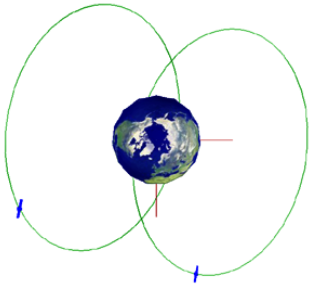

(b) A 3-1-4 FC with $F_n = 1, F_d = 2$

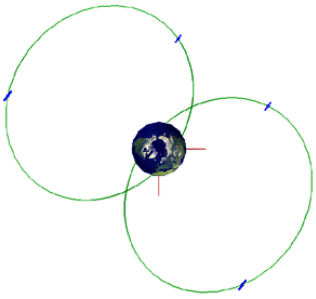

(c) A 3-2-4 FC with $F_n = 1, F_d = 2$

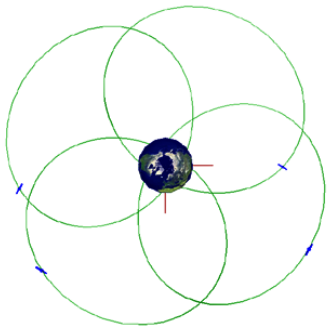

(d) A 3-2-4 FC with $F_n = 1, F_d = 4$

Fig. 17. This figure illustrates a polar view of ECI orbits and the effect of various choices of F_n and F_d for a 3-1-4 and a 3-2-4 *Flower Constellation* with $i = 63.4^\circ$ and $\omega = 270^\circ$. Refer to Table XVI on page 156 for phasing details.

Now consider that $N_d = 1$, what happens when $F_d \geq N_s$. The answer is that Eq. (1.18) on page 18 will generate available orbit planes based upon the value of F_d regardless of the number of satellites. For example, if one selects $F_n = 1, F_d = 7$ for a 3-1-4 *Flower Constellation*, then one will get four satellites in four separate orbits that are arrayed as if there were actually seven orbits (See Figure 18). An additional consideration is the multiplicity of patterns. A particular pattern is considered to be unique provided that the ratios of N_p to N_d and F_n to F_d are relatively prime (See Appendix A). To create multiple

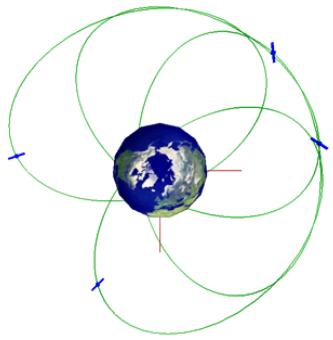

Fig. 18. Increasing the value of F_d beyond N_s causes the spacing between ECI orbits to shrink. When $F_n = 1$, F_d is the number of available orbit planes. Thus, empty orbit planes are left when $F_d > N_s$. A polar view of a 3-1-4 *Flower Constellation* is shown here with $F_n = 1, F_d = 7$.

instances of a unique pattern is very simple. By multiplying both the number of satellites (N_s) and the phasing denominator (F_d) by a factor of k while keeping all other things equal, then the resulting *Flower Constellation* will have precisely k equally spaced patterns about the axis of symmetry. As k becomes large, then the duplicate patterns will begin to overlap. Figure 19 demonstrates this procedure on a basic "Figure 8" shaped *Flower Constellation*.

4. Some Consequences of Parameter Selection

In the *Flower Constellation* concept, there are two primary parameters which affect overall shape and size of the constellation: the number of petals, N_p, and the number of days to repeat, N_d. Note that the number of satellites, N_s, is generally independent of these parameters and does not affect the design of the *Flower Constellation* other than to make a constellation complete or not (See Section d). That being said, there is an interplay between these parameters and the phasing parameters F_n and F_d that have very interesting consequences. These consequences can best be described by examining four defined relationships, τ, η_o, $\eta_{s/o}$, and ϕ. Previously, the parameter τ, introduced in Equation (1.10), was discussed. This section looks a little closer at τ. Next, the parameter $\eta_{s/o}$ is defined

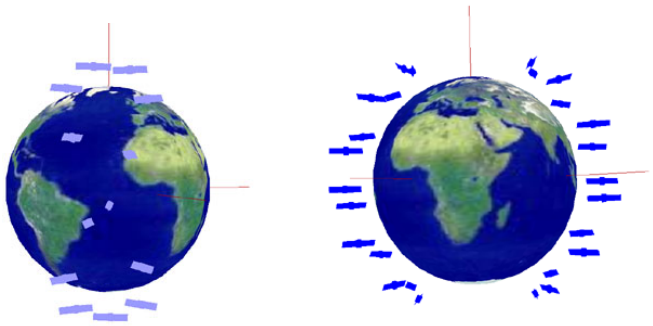

(a) $N_s = 13$ and $F_d = 13$

(b) $N_s = 26$ and $F_d = 26$

Fig. 19. The basic "Figure 8" configuration is represented here by a 12-1-13 *Flower Constellation*with $F_n = 1, F_d = 13$, $i = 116.6°$,$h_p = 1666\ km$, and $\omega = 270°$. By doubling the number of satellites and the phasing denominator, we double the pattern as seen in (b). Note that they are equally spaced about the axis of symmetry. Refer to Table XVII on page 156 and Table XVIII on page 157 for phasing details.

that relates F_d to N_s followed by the parameter η_o that relates N_d to N_s. Lastly, the parameter ϕ is introduced that relates the four primary parameters $N_p, N_d, F_n,$ and F_d. Note that τ is independent of the phasing parameters F_n and F_d and is solely related to the period of the *Flower Constellation*.

a. Similitude of *Flower Constellations*

The complete set of *Flower Constellations* includes all positive integer values of N_p and N_d. However, in reality, there exists only a reduced set of unique *Flower Constellations*. To determine which set of constellations is unique, one must look to the parameter τ. Recall that

$$\tau \equiv \frac{N_d}{N_p}$$

If τ is identical for any two given N_p-N_d *Flower Constellations*, then there is only one unique relative orbit between them because the resultant orbit period is identical (see Eq.

(1.9) on page 13). Therefore, the *Flower Constellation* with the lowest common denominator is the only unique constellation. For example, a 6-2 *Flower Constellation* will produce an identical relative path as a 3-1 *Flower Constellation*. Likewise, a 9-6 *Flower Constellation* is equivalent to a 3-2 *Flower Constellation*. In other words, N_p and N_d must be relatively prime in order for a *Flower Constellation* to be unique. In order for a proper analysis of a *Flower Constellation* design to move forward, one must first ensure that this condition is met.

b. Specifying the number of satellites per orbit

In determining the number of satellites per orbit, a relationship between the number of satellites and the number of days to repeat is evident. It has already been established that N_d specifies the number of allowable slots to place a satellite on any one given orbit (i.e. the maximum number of satellites per orbit). It follows that if one multiplies the number of orbits by the maximum number of satellites per orbit, one can write

$$\eta_{s/o} \equiv \left\lfloor \frac{N_s}{F_d} \right\rfloor = \left\lfloor \frac{N_s}{\eta_o} \right\rfloor \tag{2.3}$$

where η_o is the number of orbit planes and there will be exactly $\eta_{s/o}$ satellites per orbit. The floor function $\lfloor \cdot \rfloor$ is required here because there cannot be a fractional number of satellites per orbit, only whole integer values. Note that Equation (1.29) must still be satisfied, which leads to the lower bound on $\eta_{s/o}$, $\eta_{s/o} \geq 1$. As mentioned, the maximum number of satellites per orbit is N_d. Therefore, $1 \leq \eta_{s/o} \leq N_d$.

c. Specifying the number of orbits

Eq. (1.26) on page 19 specifies how the RAAN is arrayed about 2π for a complete symmetric *Flower Constellation*. Provided that F_n and F_d are relatively prime, then F_d specifies the number of allowable orbit planes. That is to say, if $N_s \geq F_d$, then there will be at least

one satellite per allowable orbit plane. However, if $N_s < F_d$, there will only be N_s orbit planes arrayed as if there were actually F_d orbit planes. The number of orbit planes can be expressed as

$$\eta_o \equiv \left\lfloor \frac{N_s}{N_d} \right\rfloor = \left\lfloor \frac{N_s}{\eta_{s/o}} \right\rfloor \tag{2.4}$$

where $\eta_{s/o}$ is the number of satellites per orbit. Once again, the floor function is utilized to ensure a whole integer value for the number of orbit planes. This consequence can be utilized, for example, to minimize launch costs by restricting the number of orbits into which satellites must be placed.

d. Planes of Satellites

The number of satellites selected for a particular flower constellation has some interesting consequences due to the phasing requirements described previously. When the phasing denominator exactly equals or is an integer multiple of the number of petals, then what we call *planar motion* results. In this configuration, the sequential juggling effect disappears (See Section Bchap:examples for a complete description of the sequential juggling effect).

Consider Figure 20. In this case, a 3-1-6-1-6 *Flower Constellation* with $\omega = 270^\circ$ and $i_{cr} = 63.4^\circ$ is utilized. By selecting $F_d = 2N_p$, two *planes* of satellites were created in groups equivalent to the number of petals.

This leads to another interesting parameter

$$\phi \equiv \frac{F_d N_d}{F_n N_p} \tag{2.5}$$

If ϕ is an integer (i.e. if $F_n N_p | F_d N_d$), then ϕ planes containing N_p satellites per plane will result. As $F_d \to \infty$ (or the desirable separation between any two satellites reaches a limit), then the constellation appears to be one continuous line of satellites moving about the relative orbit. However, if one looks closely, one will still see distinct groups of N_p satellites

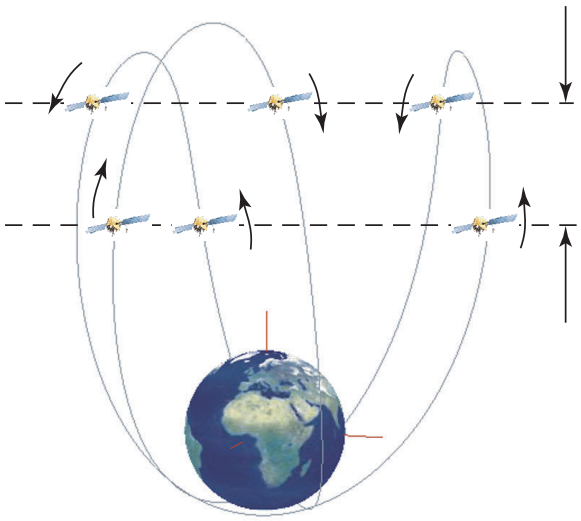

Fig. 20. In this case, an equatorial view of a 3-1-6-1-6 *Flower Constellation* with $\omega = 270^\circ$ and $i_{cr} = 63.4^\circ$ demonstrates satellites moving together in a planar fashion.

moving together in a plane. Note that this case is essentially an extension of the JOCOS concept. If ϕ is not an integer, then planar motion will not result and the sequential juggling effect will be evident again. Also note that $\eta = 1$ is required to completely visualize each plane of satellites. $\eta > 1$ will result in satellites missing from the plane of motion.

B. Categories of *Flower Constellations*

This section describes some of the broad categories of *Flower Constellations* and gives some insight into how to choose the *Flower Constellation* parameters to create these kinds of constellations. These concepts provide a basic understanding of what can be done with a single *Flower Constellation*. However, any one *Flower Constellation* can be combined in a myriad of fashions with other *Flower Constellations* to create very dynamic constellation types. Additionally, the satellites in a given *Flower Constellation* can be distributed around the allowable orbit positions in a multitude of different ways. In essence, one is not con-

strained to fill out every available slot nor is one constrained to fill them out in an evenly distributed fashion.

1. Basic Flowers

The original foray into the *Flower Constellation* concept focused on what is now termed ”Basic Flowers.” These *Flower Constellations* generally are constellations of satellites whose patterns are constructed by the relative orbit itself. Figure 12 on page 39 shows an example of a Basic Flower. These relative orbits can be quite complicated, however. Figure 2 on page 44 shows a relative orbit whose petals overlap to the point where it almost appears to be a surface.

2. Secondary Open Paths

As mentioned in the previous section, one can begin to choose the number of petals and the number of days to repeat by choosing τ such that a desired anomalistic orbit period is generated. Particular values of N_p and N_d might also be desirable while maintaining an overall value of τ within some tolerance. Therefore, if one finds a *basic flower*, for instance, that has all the desired phasing but the orbit period needs to be adjusted to account say for perturbations, then a secondary open path can be created that is almost identical to the original *basic flower*. This is done by choosing values of N_p and N_d that closely approximate the original value of τ that was used to generate the original constellation. Figure 15 on page 43 shows an example where N_p and N_d were adjusted while maintaining a similar value of τ.

The following simple Matlab code allows one to specify the value of τ, will search through k (N_p, N_d) pairs, and then output up to *kmax* of the best pairs that approximate τ.

Matlab v. 6.0 Code

```
function [ num, den ] = f2i( F, k, kmax ),
```

```
% This function provides k approximate solutions of F=num/den
% where ”F” is any decimal number and ”num” and ”den” are two
% integer arrays of length k. Texas A&M, Mortari and Wilkins, 8-30-03
nmin = floor( 1 / F );
if ( nmin == 0 ), nmin = 1; end
den = nmin + [ 0 : k-1 ]';
num = round( F * den );
X = abs( F - num./den );
[ Y, I ] = sort(X);
num = num(I); num = num( 1 : kmax );
den = den(I); den = den( 1 : kmax );
```

End Matlab v. 6.0 Code

This code can be used to solve for the numerator and denominator of any of the integer ratios presented in this work. For example, if one desires an 8 *hr* orbit, then $\tau = 0.3342$ based upon a sidereal period of 23 *hr* 56 *min* 4.09 *s*. The Matlab output is the following:

Matlab v. 6.0 Code

```
>> [Nd,Np] = f2i(.3342,1000,10);
>> [Nd Np Nd./Np]
ans =
   257   769   3.3420e-001
   129   386   3.3420e-001
   258   772   3.3420e-001
   128   383   3.3420e-001
   256   766   3.3420e-001
   259   775   3.3419e-001
   255   763   3.3421e-001
   130   389   3.3419e-001
   260   778   3.3419e-001
   127   380   3.3421e-001
```

End Matlab v. 6.0 Code

The results are sorted such that the best results are presented first. If one were to limit the scope of the search to the first 100 integers, the code will find the more obvious, but not as accurate, guesses such as (1,3), (2,6), (3,9), etc.

3. Planar Patterns

When the orbit inclination is 0° or 180°, then what is termed *Flower Constellation* "Planar Patterns" results. These patterns tend to spin the most rapidly of all the categories of *Flower Constellations*. In some cases, these patterns are of a fixed shape (i.e. they are secondary closed paths) and merely rotate about the axis of symmetry. In other cases, the patterns start out in one shape but then reform themselves into another in a never-ending cyclical process. This is typical of secondary open paths or incomplete schemes. No specific method other than that described for a secondary closed path is available for generating a planar pattern. While practical applications of these patterns have yet to be found, they are very interesting in their own right. Figure 21 shows four intermediate stages of a transforming pattern.

4. Helixes

Helical constellations are another interesting category of *Flower Constellations*. Helixes are actually a general secondary closed path that is typically formed by one or more intersections of the secondary path with itself. Generating a helix requires the appropriate selection of the value of F_d. Recall that a secondary closed path is formed when $F_n = N_d$ and $F_d = AN_d + BN_p$. Helixes are formed when $A = \pm 1$ and B represents the number of intersections or "twists" in the secondary closed path. Figure 22 shows a 31-18-80-18-80 *Flower Constellation* where $A = 1$ and $B = 2$.

5. Figure 8's

Another basic pattern that has been discovered is the "Figure 8." Figure 8's are in reality a helix with a single point of intersection in the closed path. Therefore, a Figure 8 is created when $A = \pm 1$ and $B = 1$. The uniform double lobes that one associates with a Figure 8 is created using circular orbits. Eccentric orbits combined with varying the argument of

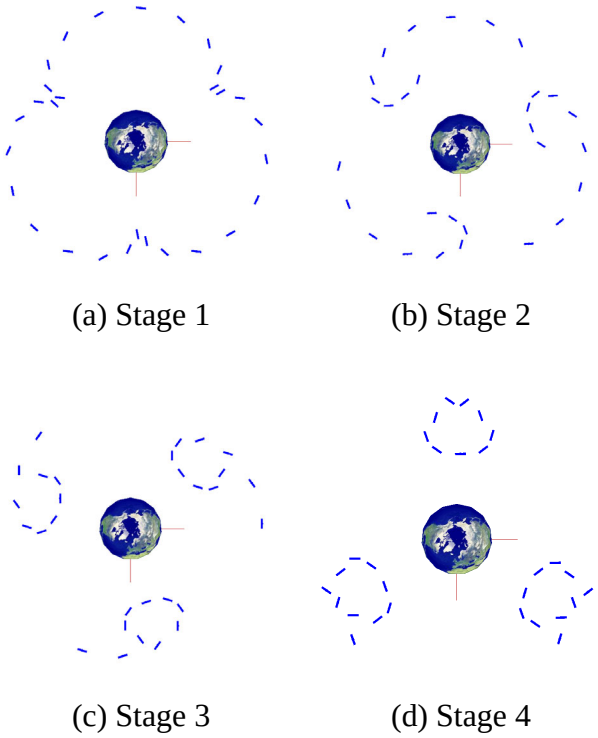

(a) Stage 1 (b) Stage 2

(c) Stage 3 (d) Stage 4

Fig. 21. This Planar Pattern, dubbed "Tre Lacci", is a 31-11-30 *Flower Constellation* with $F_n = 7, F_d = 10$, $i = 180^\circ$, $h_p = 9000$ *km*, and $\omega = 270^\circ$. As time progresses, the three groups of satellites curl in on themselves to form a ball before un-curling back into the original formation depicted in (a). Refer to Table XIX on page 158 for phasing details.

perigee will create lobes that are larger on one half than the other.

Figure 19(a) on page 48 shows an example of a single Figure 8 that is very close to the Earth's surface. One can also design Figure 8's that are much larger in scale. In addition to single Figure 8's, there are unique sets of parameters that generate multiple Figure 8's as a base configuration. Figure 23 shows an example with 3 Figure 8's created by a 37-18-57-6-19 *Flower Constellation*. Removing one third of the satellites from a base configuration such as this will not remove a whole Figure 8. Instead, the satellites will be removed in a distributed fashion from all of the Figure 8's. One can double a pattern such as this to

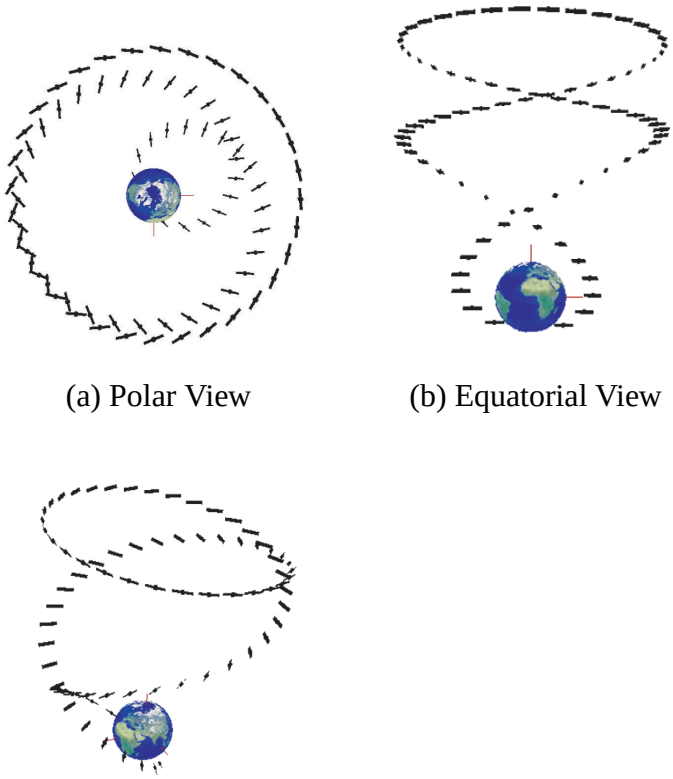

(a) Polar View (b) Equatorial View

(c) Isometric View

Fig. 22. This pattern contains a helix with two intersections in the secondary closed path (i.e. $A = 1$ and $B = 2$). This constellation is generated with a 31-18-80-18-80 *Flower Constellation* with $i = 63.4^\circ$, $h_p = 600$ *km*, and $\omega = 270^\circ$.

obtain 6 equally spaced Figure 8's.

6. Rings

One can also create rings of satellites. Figure 11(d) on page 37 depicts one such ring of satellites. These rings are not necessarily perfect circles and their size and orientation can be adjusted by tuning the various *Flower Constellation* parameters. An effort to produce perfect circles will be the focus of future work. As mentioned earlier, *Flower Constellations* can be multiplied. In Figure 24, the single inclined ring from Figure 11(d) on page 37

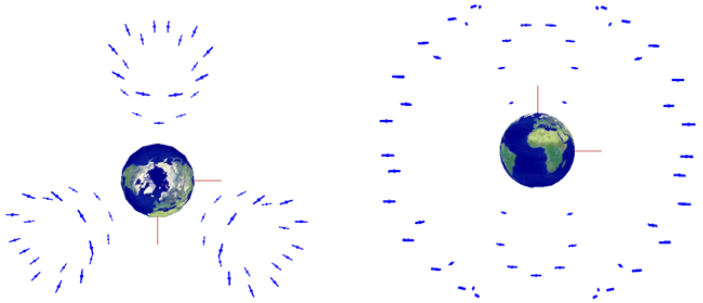

(a) Polar View, $N_s = 13$ and $F_d = 13$

(b) Equatorial View, $N_s = 26$ and $F_d = 26$

Fig. 23. This pattern contains 3 "Figure 8's" in it's base configuration and is represented here by a 37-18-57 *Flower Constellation* with $F_n = 6, F_d = 19$, $i = 63.4^\circ$, $h_p = 19702\ km$, and $\omega = 270^\circ$. Note that by doubling this pattern, we will get 6 "Figure 8's" that are equally spaced about the axis of symmetry. Refer to Table XX on page 159 for phasing details.

has been multiplied into 10 rings rigidly rotating about the axis of symmetry. Rings such as this are generated with $F_d = N_p + N_d$ (i.e. $A = B = 1$).

7. Nearly Straight Lines of Satellites

While not physically realizable due to the intersecting relative orbit path that ultimately leads to this type of *Flower Constellation*, it is still mathematically possible to generate a nearly straight line of satellites that rigidly rotates about the axis of symmetry. Figure 25 depicts one such line of satellites. Due to the very precise choice of inclination, the satellites regularly meet at the intersections of the relative orbit as they rotate about the Earth. This is what generates the appearance of a straight line of satellites but also makes it physically impossible to put into practice.

These lines are formed basically by collapsing the ring formation in upon itself. By making the inclination of a ring formation almost 180° and setting the height of perigee

Fig. 24. An 8-1-90-1-90 *Flower Constellation* with $i = 165^\circ$, $h_p = 3000\ km$, and $\omega = 270^\circ$. These rings spin about their own axis of symmetry while rigidly rotating about the *Flower Constellation* axis of symmetry.

such that circular orbits result, then one will get a straight line formation.

8. Spirals

One can also generate a single spiral that resemble a ”Slinky” toy as it collapses and expands about the Earth. Furthermore, one can generate multiple spirals that are either intertwined or separate. These spirals are not closed paths. Figure 26 depicts a case where two spirals are intertwined about the axis of symmetry. At perigee, the spirals will collapse down into a flat ring before expanding back up towards apogee where they will once again collapse into a flat ring in a cyclical process.

C. Spin Rate of Secondary Paths

It is important to note that only the relative path is fixed with respect to the Earth. The secondary path depicted for Figure 2 on page 44, for instance and regardless of whether or not the secondary path is closed or open, continuously spins about the axis of symmetry

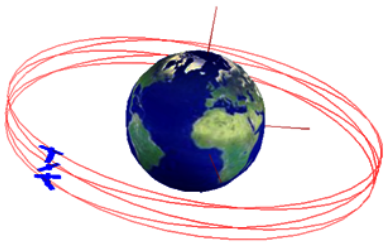

Fig. 25. A 4-1-5-1-5 *Flower Constellation* with $i = 174.8°$, $h_p = 10354\,km$, and $\omega = 270°$. A straight line of satellites rigidly rotates about the Earth. Due to a high collision probability, this type of *Flower Constellation* is physically unrealisable. Refer to Table XV on page 155 for phasing details.

while overlaid upon the fixed relative path. In general, the entire secondary path rotates about the axis of symmetry at a constant rate. Consider the *Lone Star Constellation* once again at two different instants of time. One would obtain something similar to that depicted in Figure 27. The spin rate of the secondary path can be quantified by considering that the path "moves" because individual satellites are approaching apogee in their individual orbits in succession. Therefore, the apparent amount of time that it takes for the path to move is

$$\omega_s^I = \frac{\Delta\Omega}{\Delta t} \tag{2.6}$$

where $\Delta\Omega$ is the angular spacing in radians between two successive orbit nodes, Δt is the amount of time between two satellites along the secondary path, and the superscript I means that this angular velocity is expressed in the ECI frame. $\Delta\Omega$ is already defined in Eq. (1.26) on page 19. On initial inspection, one could use Kepler's equation and write $\Delta t = \frac{\Delta M_0}{n}$ where ΔM_0 is defined in Eq. (1.27) on page 19. This leads to

$$\omega_s^I = -n\tau \tag{2.7}$$

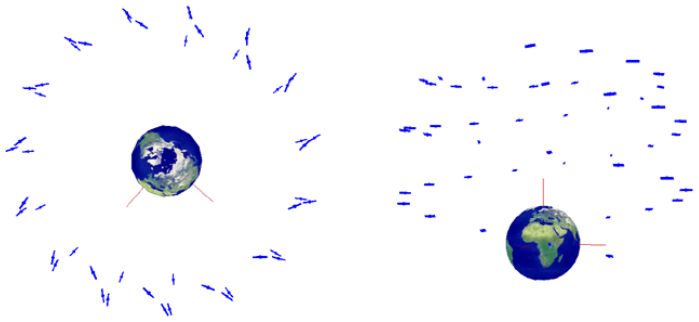

(a) Polar View (b) Equatorial View

Fig. 26. This pattern contains 2 intertwined spirals formed by a 15-7-49-23-49 *Flower Constellation* with $i = 63.4°$, $h_p = 9000\ km$, and $\omega = 270°$. These two spirals descend from apogee and collapse in on themselves at perigee before spiraling back up to apogee again in a cyclical process. Refer to Table XXI on page 160 for phasing details.

where τ has been defined in Eq. (1.10) on page 13. The spin rate in the ECF frame can be expressed as

$$\omega_s^F = \omega_s^I - \omega_\oplus = -n\tau - \omega_\oplus \tag{2.8}$$

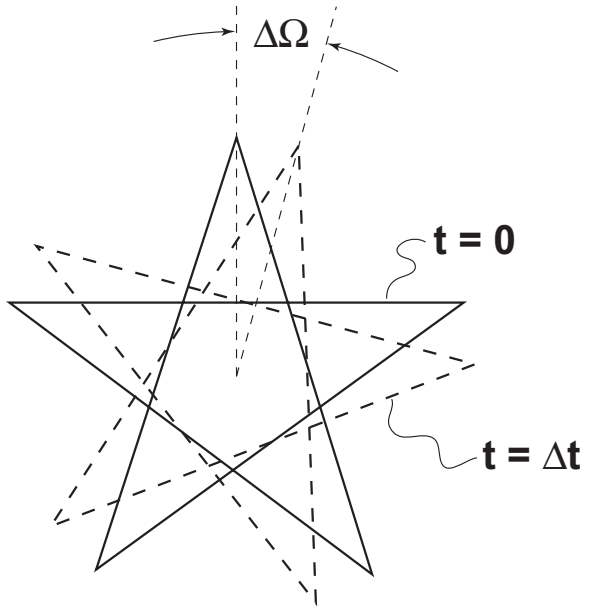

Fig. 27. The Lone Star Constellation is shown here at two different instants of time.

CHAPTER III

APPLYING THE FC THEORY: EXAMPLE PROBLEMS

In Chapter II, specific choices for the various design parameters were investigated. One can easily see the myriad of combinations among the parameters and the limitless possibilities afforded by the *Flower Constellation* theory. In order to try and gain a better grasp on how to use the *Flower Constellation* theory, this chapter will give some specific procedures and examples on how to use the theory as a design tool. In particular, this chapter will recreate some current constellation techniques utilizing *Flower Constellation* theory in addition to showing new and never-before-seen constellations.

A. Basic Design Procedure

A general design procedure is outlined in Figure 28. From a mission design perspective, usually one will have a good idea of the desired orbit period for the satellites. Knowing this, the values of N_p and N_d are specified via Equation (1.9). As discussed in previous chapters, the values for N_p and N_d can be adjusted as needed while still maintaining a particular value for τ (See Section II.2).

Having specified the orbit period, the next step is to choose the height of perigee and the orbit inclinations. The choice of inclination is coupled with the choice of height of perigee. If circular orbits result, then the value of inclination can be chosen as needed to affect the overall shape of the constellation. However, eccentric orbits will more than likely require one of the critical inclinations to maintain the initial constellation geometry without exerting undesirable levels of control effort.

The remaining orientation angle that needs to be established at this point is the argument of the perigee, ω. As discussed in the previous chapter, setting this value to 90° or 270° will ensure that the line of apsides is pointing towards the northern or southern

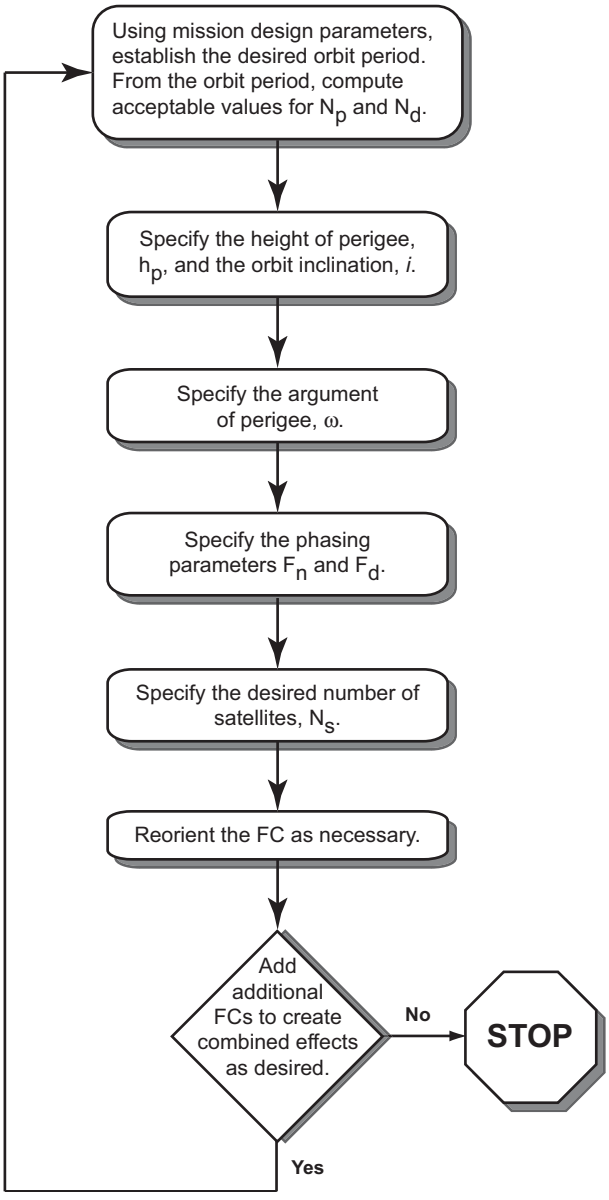

Fig. 28. This flowchart illustrates a basic FC design procedure.

hemispheres, respectively. Varying the argument of the perigee will cause the shape of the *petals* to alter.

Lastly, in order to obtain the final locations of each satellite in the *Flower Constellation*, one must specify the phasing parameters F_n and F_d. Note that a given choice of F_n and F_d may belong to more than one particular *Flower Constellation*. In other words, a particular constellation design may have requirements that are satisfied simultaneously by two or more particular design solutions. The following section describes some common choices for the value of F_n and F_d.

B. Common Phasing Choices

As discussed previously, there are only a certain number of permissible locations for a satellite to be placed in an orbit. Based upon this, it becomes apparent that each satellite in the constellation will be assigned a unique (Ω_k, M_k) pair. Otherwise, two satellites will be impossibly placed in the same physical location. The choice of F_n and F_d directly impact how these satellites are placed into the constellation.

Special interest is given when the choice of F_n and F_d fall into one of the following three cases:

(1) When $F_n = 1$ and $F_d = N_s$, then the N_s satellites are uniformly distributed and the so-called *sequential juggling effect* is apparent. See below for a description of this effect.

(2) When F_n and F_d are relatively prime and $F_d \leq N_s$, then the N_s satellites are uniformly distributed in F_d equally spaced orbits.

(3) When $F_n = N_d$ and $F_d = AN_p + BN_d$ where A and B are integers that can be freely chosen, then a secondary closed path forms on top of the relative path.

If the first phasing scheme is chosen with $F_n = 1$ and $F_d = N_s$, then the corresponding complete *Flower Constellation* will have N_s satellites evenly distributed about the Earth and evenly distributed along the relative path. In this case, the satellite with the largest true anomaly is continuously replaced in what we call a *sequential juggling* effect. The *sequential juggling* effect is essentially an artifact of the phasing rule of Equation (1.19). While a minimum of $N_p + N_d$ satellites are required to achieve the sequential juggling effect, any number of satellites may be selected for the desired application. Choosing a number of satellites below $N_p + N_d$ will result in having a number of *petals* remaining unoccupied for a period of time. It is obvious that the *stationarity* and *coverage* increase with the number of satellites. Consider that a ($N_p = 3,\ N_d = 1,\ N_s = 4$) *Flower Constellation* with $\omega = 270^\circ$ and $i_{cr} = 63.4^\circ$, requires only four satellites to achieve nearly complete coverage of the northern hemisphere![9]

For the second phasing scheme, the appropriate choice of F_n and F_d allows the flexibility to specify precisely the number of orbits that will be used to construct the *Flower Constellation*. Specifically, when $F_n \perp F_d$ (i.e. $\text{GCD}(F_n, F_d) = 1$), one can specify the number of orbits by setting F_d to that desired number. Furthermore, one can utilize the parameter $\eta_{s/o}$ to aid in the selection of F_d. However, as discussed previously, one distinct orbit cannot accept more than N_d satellites and there is a maximum of $F_d N_d$ satellites for a given *Flower Constellation*. If more than $F_d N_d$ satellites are required for a particular application, then either N_d or F_d or both must be increased.

In the third phasing scheme, a secondary closed path in the shape of a regular figure such as an ellipse, circle, or helix is formed. This secondary path is most distinguishable when there are enough intersections between the flower petals (i.e. when the number of flower petals is sufficiently large). Examples of the various categories of *Flower Constellations* and the appropriate phasing choices are given in Chapter II. This can be a useful design tool to satisfy specific mission criteria.

C. Galileo Constellation Example

Consider that you would like to construct a constellation with a given number of satellites, N_s, placed into a given number of orbit planes, η_o. The Galileo Constellation proposed by the European Space Agency has 30 satellites (27 are active and 3 are spares arrayed along with the other satellites) placed into 3 orbit planes.[21] The orbits are circular with an altitude of $23,616\,km$ above the Earth inclined at 56°.

Using the definition of the parameter η_o (See Section II.A.4.c), it is clear that if $N_s = 30$ and $\eta_o = 3$, then $N_d = 10$. Furthermore, examining the definition of $\eta_{s/o}$ (See Section II.A.4.b), one can see immediately that $F_d = 3$.

Now that N_d and F_d have been specified, one needs to find the value of N_p that will achieve the required orbit altitude. To that end, solve Equation (1.9) with $a = 29,994.1363\,km$, $n = 1.2153863 \times 10^{-4}\,rad/sec$, $T = 14.36\,hr$, $N_d = 10$, $e = 0$, $i = 56^\circ$, and $J_2 = 1.08 \times 10^{-3}$. The result is a rational value for N_p. Therefore, one must choose the integer value of N_p closest to that result.

In this case, the optimum integer value is $N_p = 17$. This results in a semi-major axis of $29,292\,km$, or an altitude of $22,913\,km$. A more precise solution can be obtained by using a rational value for τ instead of selecting integer values for N_p. Figure 29 shows the 3 inertial orbit planes in addition to the relative path that is generated.

D. JOCOS Example

In Pennoni and Bella,[11] 7 satellites are placed into circular orbits inclined at 75° at an altitude of $13,900\,km$. The following orbit parameters are given: The given orbit altitude can be used to compute the orbit period of approximately 8 *hrs* or $\tau = 1/3$. This leads to a basic choice for the number of petals and the number of days to repeat as $N_p = 3$ and $N_d = 1$. Examining Table V, one can see that the node values are spaced at 30° increments.

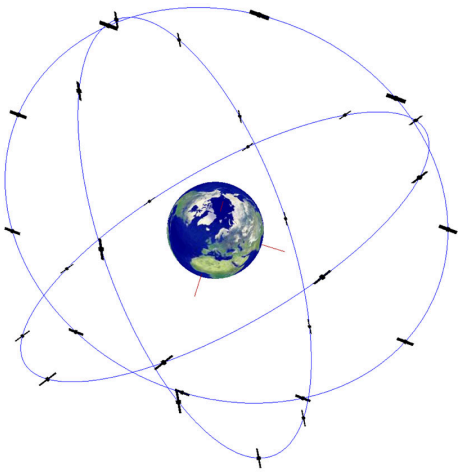

(a) 30 Satellites in Three ECI Orbit Planes

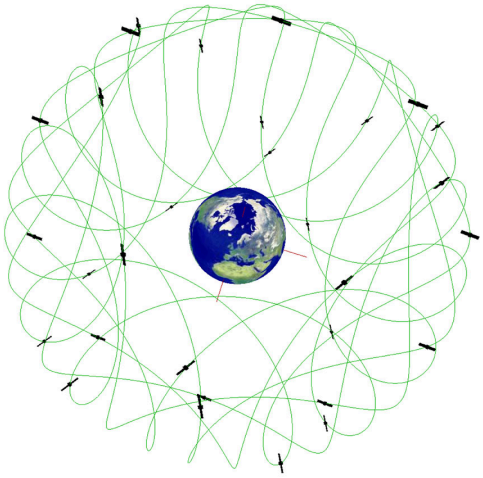

(b) Relative Path

Fig. 29. The FC version of ESA's Galileo Constellation - a 17-10-30-1-3 *Flower Constellation* with $i = 56^\circ$, and $h_p = 22,913\,km$.

Table V. Orbital parameters given for the 6+1 JOCOS system.[11]

Satellite	Ω	M_0
1	120°	90°
2	90°	180°
3	60°	-90°
4	30°	0°
5	0°	90°
6	-30°	180°
7	-60°	-90°

Based upon this, one finds that $360^\circ/30^\circ = 12$. Thus, $F_d = 12$. In this case, $F_n = 1$ as the simplest choice and the number of satellites, N_s, is 7. The initial values for the RAAN and mean anomaly angles are set to $\Omega_0 = 120^\circ$ and $M_0 = 90^\circ$, respectively.

One can easily verify using Equation (1.26) and Equation (1.27) that the values given in Table V are duplicated precisely. Using these values for the FC design parameters, the resultant *Flower Constellation* is shown in Figure 30.

E. LOOPUS Examples

In Peter Dondl's 1984 paper entitled *LOOPUS Opens a New Dimension in Satellite Communications*,[12] several examples of the LOOPUS concept are presented. In this section, the *Flower Constellation* theory will be employed to duplicate two of the examples presented as closely as possible based upon the information provided in the paper. Note that, in general, to generate a LOOPUS type constellation, the *Flower Constellation* parameters have the following relationship:

$$N_d = N_p + 1 \tag{3.1}$$

where the number of LOOPUS positions (as described in Dondl's work) equals the value of $2N_p$ (i.e. N_p loops in both the northern and southern hemispheres).

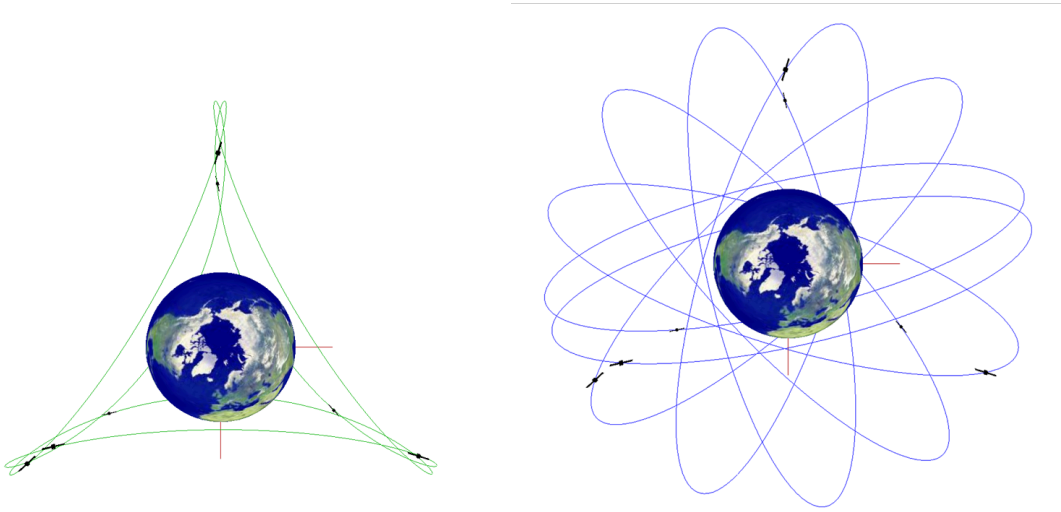

(a) Polar view showing the relative path

(b) Polar view showing the ECI orbits

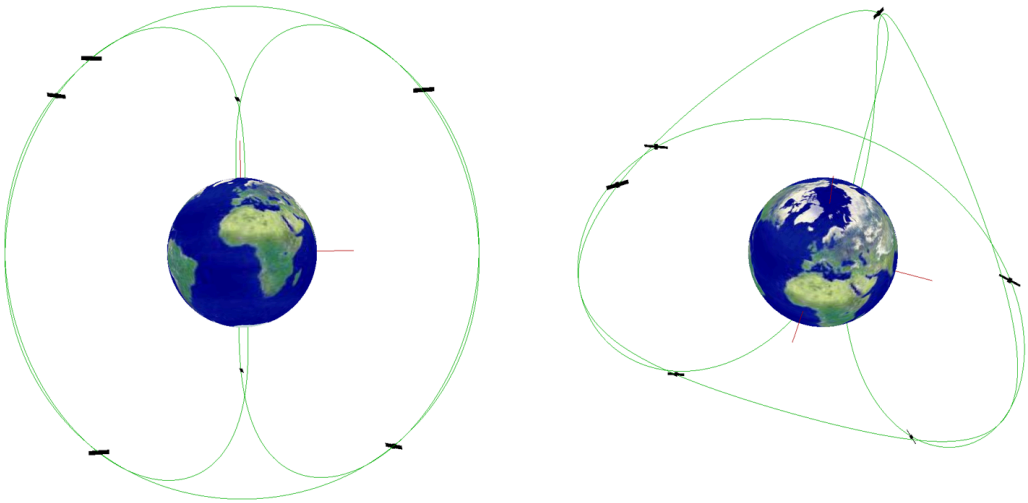

(c) Equatorial View

(d) Isometric View

Fig. 30. A 3-1-7-1-12 *Flower Constellation* is employed to re-create the 6+1 JOCOS constellation.[11] The *Flower Constellation* has $i = 75^\circ$, $h_p = 13,900\,km$ and $\omega = 270^\circ$. The initial RAAN was set to $\Omega_0 = 120^\circ$ while the initial mean anomaly was set to $M_0 = 90^\circ$

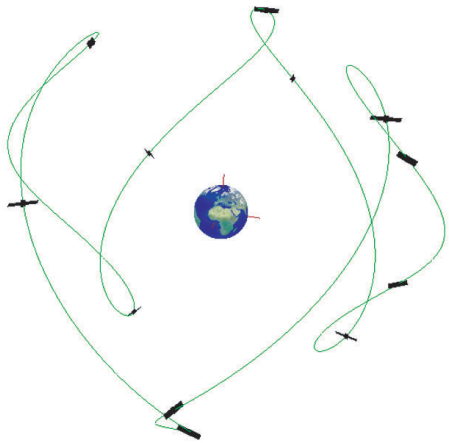

Fig. 31. A 3-4-12-11-12 *Flower Constellation* is employed to duplicate the example problem presented in Dondl's Section 5.2.[12] $i = 54.7^\circ$, $h_p = 44,165\ km$, $\omega = 270^\circ$.

1. Example from Dondl Section 5.2

In this example problem, Dondl specifies that there should be 6 LOOPUS positions in total with 12 satellites in the constellation. The orbit inclination should be 54.7°, the orbit period is 32 *hrs*, the period of repetivity is 96 *hrs*, and the height of perigee is to be greater than $44,000\ km$.

The *Flower Constellation* parameters N_p and N_d follow easily from the the orbit period information. In order to satisfy the above criteria, $N_p = 3$ and $N_d = 4$. Note that $N_p = 3$ will generate 6 LOOPUS positions as required. Because the orbit inclination is set to something other than the critical inclination, circular orbits are required, which results in a radius of $44,165\ km$ that satisfies the orbit period requirements.

The phasing of the parameters of *Flower Constellation* was chosen to be $F_n = 11$ and $F_d = 12$. This phasing arrangement spread the 12 satellites evenly about the relative ground track. Note that this choice gives a total of 48 available slots for satellites to occupy in the

Flower Constellation. Figure 31 shows the resulting *Flower Constellation* that duplicates Dondl's LOOPUS example problem.

2. Example from Dondl Section 6

This second LOOPUS example requires a 24 *hr* period of repetition with a 12 *hr* orbit period. The orbit inclination is set to the critical inclination and the semi-major axis is $26,562\,km$. In this case, the values of the *Flower Constellation* parameters are easy to solve, $N_p = 2$ and $N_d = 1$. Note that these parameters do not follow the general guideline given in Equation (3.1) because this example chosen by Dondl is essentially a set of Molinya orbits that traditionally create a *loop* in their ground track because of their extremely long dwell time near apogee. The phasing parameters were set to $F_n = 1$ and $F_d = 3$ to duplicate Dondl's system. However, the phasing parameters can be chosen at will to provide more available slots to place satellites into. Figure 32 shows the resulting *Flower Constellation*.

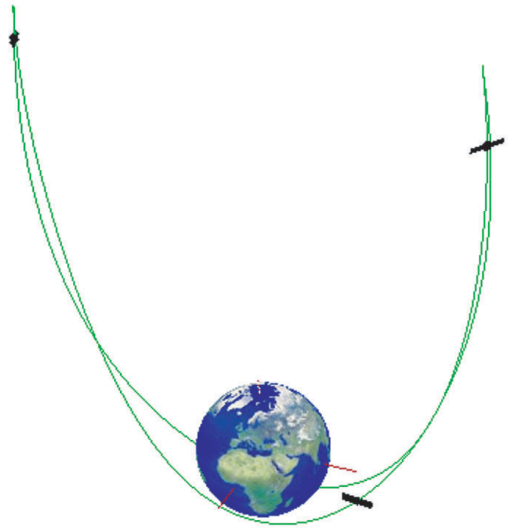

Fig. 32. A 2-1-3-1-3 *Flower Constellation* is employed to duplicate the example problem presented in Dondl's Section 6.[12] $i = 63.4^\circ$, $h_p = 600\,km$, $\omega = 270^\circ$.

F. COBRA Example

In this section, the *Basic 6-Satellite Teardrop Array* described in Table III of Draim et al.[15] will be duplicated using the *Flower Constellation* theory. The common orbit parameters given for each of the two repeat ground track orbits are a semi-major axis of $20,261$ *km*, eccentricity equal to 0.6458, and an inclination of 63.41°. The argument of perigee is set to either 232° or 308°. The initial RAAN values are 138.5° and 100.2°.

To construct the equivalent *Flower Constellation* one will need to combine two *Flower Constellations*. Each of the repeat ground track orbits of the COBRA Teardrop Array has three satellites placed into it. Thus, $N_s = 3$ for both *Flower Constellations*. Also, since three orbit planes are desired with one satellite per orbit, then it is clear that the phasing parameters must be $F_n = 1$ and $F_d = 3$. From the semi-major axis and eccentricity given, one can determine that the height of perigee for each of the COBRA orbits is $h_p = a(1-e) - R_\oplus \approx 800$ *km*. The anomalistic orbit period is found to be $T \approx 8$ *hrs*. For an 8 *hr* orbit, $\tau = 1/3$, which leads to $N_p = 3$ and $N_d = 1$ as a basic choice for the number of petals and the number of days to repeat.

The values above are approximate calculations due to the lack of precision of the data provided in Draim et al. and the fact that the final values depend upon the values used for the equatorial radius of the Earth, $R_\oplus$, and the Earth's gravitational parameter, $\mu_\oplus$. That being said, elsewhere in Draim et al. it is stated that the standard COBRA orbit period is eight hours. Figure 33 shows the resultant *Flower Constellation* that re-creates the basic 6-satellite COBRA Teardrop Array.

G. Constructing Secondary Closed Paths

As discussed in Section I.C, there are specific requirements on the choice of parameters in order to ensure that a secondary close path is formed. Figure 34 provides a sample of four

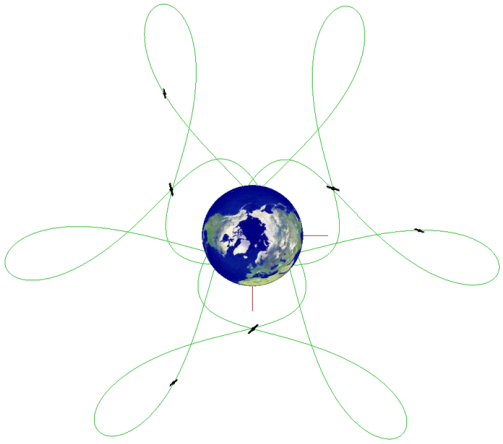

(a) Polar view showing the relative path

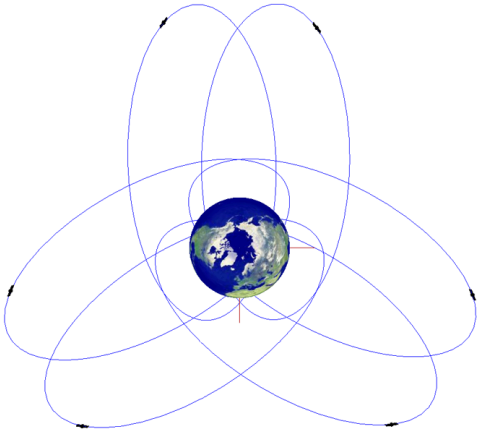

(b) Polar view showing the ECI orbits

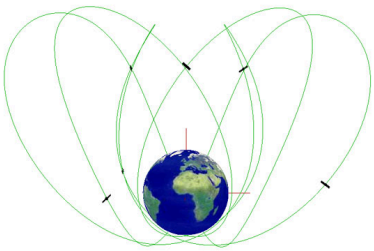

(c) Equatorial View

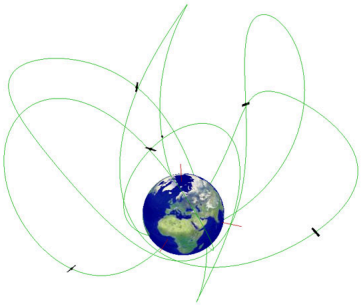

(d) Isometric View

Fig. 33. Two 3-1-3-1-3 *Flower Constellations* are employed to re-create the basic 6-satellite COBRA Teardrop Array.[15] Each *Flower Constellation* has $i = 63.41^\circ$ and $h_p = 800\ km$. The argument of perigee is either $\omega = 232^\circ$ or $\omega = 232^\circ$. The initial RAAN was set to either $\Omega_0 = 138.5^\circ$ or $\Omega_0 = 100.2^\circ$.

(a) 8-1-90-1-90 FC, $i = 165^\circ$, $\omega = 270^\circ$, $h_p = 3000\,km$

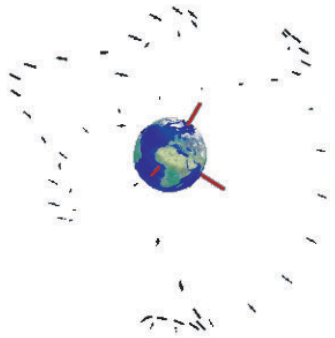

(b) 31-18-57-6-19 FC, $i = 63.4^\circ$, $\omega = 270^\circ$, $h_p = 22,967.988\,km$

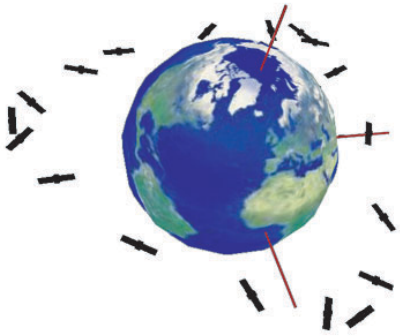

(c) 15-2-18-1-18 FC, $i = 180^\circ$, $\omega = 270^\circ$, $h_p = 3000\,km$

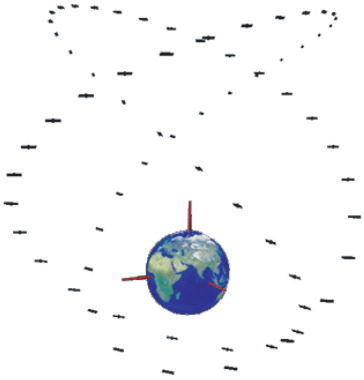

(d) 8-1-90-1-90 FC, $i = 165^\circ$, $\omega = 270^\circ$, $h_p = 3000\,km$

Fig. 34. Secondary closed paths can form on top of the relative orbit. Generally, these secondary closed paths spin about the axis of symmetry. Only the relative path is fixed.

constellations that have been generated using the concept of secondary closed paths.

In particular, recall that $F_n = N_d$ or $N_d = 1$ is required for a secondary closed path to form. Also, to completely visualize the secondary path, $N_s = F_d$. This section will examine how to create an example secondary closed path that is called the *The Lone Star Constellation*. Looking at Figure 35(a) on page 76, one can see that this constellation forms the shape of a five pointed star. This constellation closely resembles the star on flag of the State of Texas, hence the name. When viewing this constellation in motion, one would see the whole star spin about the axis of symmetry, which in this case is the spin axis of the Earth. Figure 35(b) and Figure 35(c) show the relative orbit and the Earth Centered Inertial (ECI) orbits, respectively, for this constellation.

Based upon the developments previously described, the construction of the Lone Star Constellation is relatively simple. In this case, five secondary petals are desired to form on top of the relative path already in place. To effect this design, the value of F_d must be chosen appropriately based upon the value of τ. In particular,

$$F_d = 5N_d - N_p \tag{3.2}$$

The values of N_d and N_p can be freely chosen to achieve a desired value of τ. In order to make the points of the star fairly sharp, $N_d = 23$ and $N_p = 38$ were found to be acceptable, which leads to $F_d = 5(23) - 38 = 77$. This particular constellation is rather large, smaller stars can be found by adjusting the values of N_d and N_p.

H. Potential Applications

1. Global Navigation Systems

One potential application of *Flower Constellations* is in the arena of Global Navigation Systems. The current GPS system and the Galileo constellation proposed by the European

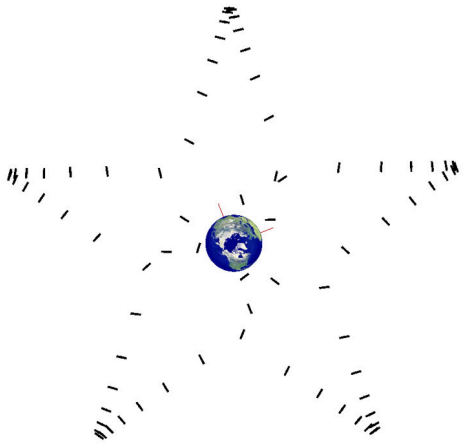

(a) North Pole view of the satellites only

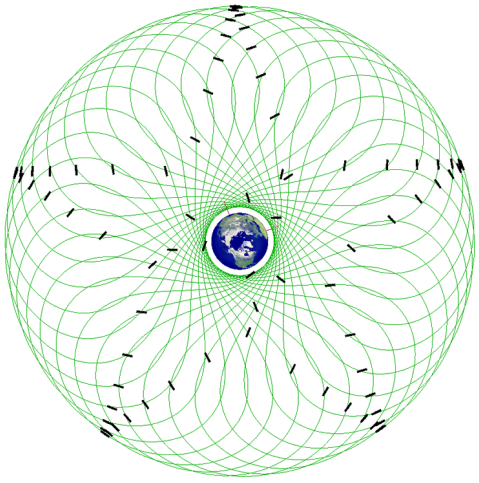

(b) North Pole view of the relative orbit

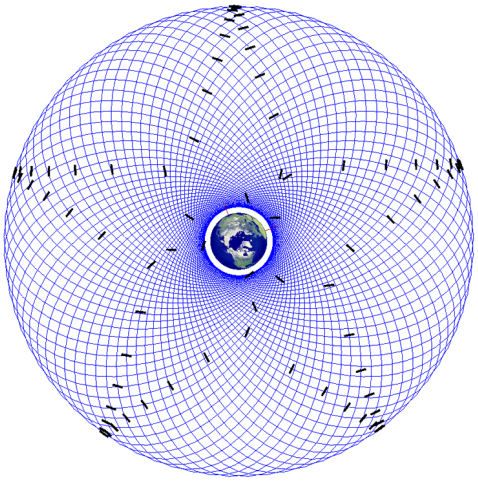

(c) North Pole view of the ECI orbits

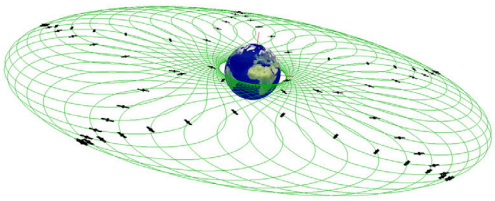

(d) Isometric view of the relative orbit

Fig. 35. The Lone Star Constellation - a 38-23-77-23-77 *Flower Constellation* with $i = 0^\circ$, $\omega = 270^\circ$, and $h_p = 1300\ km$.

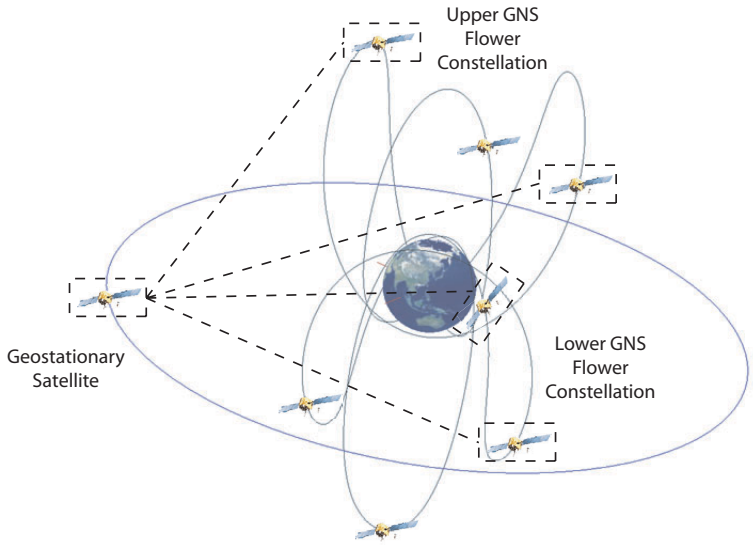

Fig. 36. ECF View of a double 3-1-5 *Flower Constellation* with $i_{cr} = 63.4^\circ$ and either $\omega = 90^\circ$ or 270°. The rectangles indicate satellites available to the geostationary satellite based upon a 55° cone angle. The orbits were generated by the Flower Constellation Visualization and Analysis Tool (FCVAT) and the accessibility was computed in AGI's STK. The access information was added for clarity. The FCVAT will eventually be able to import data from STK.

Union and the European Space Agency consists of large numbers of satellites in a Walker constellation (circular orbits). This creates a sphere of satellites surrounding the Earth, which is ideal for broadcasting navigation signals down to the Earth's surface and LEO. However, this system is ill suited to sending signals to MEO, HEO and GEO orbits. It may be possible to develop future global navigation systems using the *Flower Constellation* concepts that have the capability to broadcast signals not only to the planet surface but also to other orbiting satellites. This also may require antennae that broadcast in a wider cone than normally used for standard global positioning satellites.

Figure 36 shows a double 3-1-5 *Flower Constellation* with $i_{cr} = 63.4^\circ$ and $\omega = 90^\circ$ or 270° along with a test case geo-stationary satellite. Using STK software, the access

intervals between the geo-stationary satellites and the double *Flower Constellation* were computed. Each of the satellites were given a sensor with a 55° cone angle. While this sensor angle is arbitrary at the moment, future work will incorporate realistic sensor models. With this configuration, a minimum of 4 and up to 6 accesses were found to be available to the geo-stationary satellite at all times. Thus, obtaining a position fix is assured because of the quasi-stationary property of the *Flower Constellations*. More work is needed to determine sensor requirements and optimal number of petals and satellites. However, it has been shown that a global navigation system devised using a *Flower Constellation* that is uniformly distrubted in mean anomaly has superior GDOP and ADOP properties to that of every current system based upon preliminary analysis.[22]

2. Formation Flying Schemes

Some *Flower Constellations* can provide interesting opportunities in the field of formation flying. In particular, some new concepts in formation flying schemes can be introduced. The inclined ring formation is one example where future study into the relative motion of satellites belonging to a secondary closed path could prove useful (See Figure 11(d) on page 37). Some other examples of what could be considered formation flying is given in the following sections.

a. Follow the Leader

An interesting scenario arises when one selects a retrograde *Flower Constellation*. In Figure 37, a 4-1-51-5 *Flower Constellation* with $\omega = 270^\circ$ and $i_{cr} = 116.6^\circ$ is depicted. In this case, a *follow the leader* type of situation is generated.

Looking at the formation from a polar perspective, the satellites rotate clockwise about the Earth. In this manner, the formation appears to maintain almost a straight line as it rotates about the constellation axis of symmetry (i.e. the satellites appear to trace the outline

of square path). However, when viewed from an equatorial viewpoint, one will see that the *tail* satellite will descend towards perigee only to reappear on the opposite side of the Earth in the *lead* position. Likewise, the next to last satellite will then descend and reappear in the lead. *Flower Constellations* that form regular polygon shapes when viewed from one of the cardinal directions can be useful in Earth observation missions where gridding of information is a concern and will be subject of further study.

b. Asymmetric *Flower Constellations*

Another intriguing possibility is the use of restricted *Flower Constellations* for formation flying. By placing a number of satellites within a given range of RAAN values, we can bunch the satellites together in such a way as to act as a formation. Figure 38 shows an example of this. In this figure, both the relative orbit and the 5 inertial orbits of each satellite are shown. Additionally, one could consider having multiple *Flower Constellations* with multiple chains of satellites all placed within close proximity of each other.

c. Extreme *Flower Constellations*

Recently investigations have been conducted into the various choices for the number of petals and the number of days to repeat. Provided that N_p and N_d are increased on a relative scale to one another, *Flower Constellations*with reasonable periods and apogee heights can still be generated. However, as the number of petals becomes large, the relative path is no longer particularly relevant. Figure 39 shows one such “Extreme” *Flower Constellation*.

In this particular case, an apparent secondary path is formed on the relative path that resembles a 4 petal *Flower Constellation*. Interestingly, this apparent 4 petal constellation has groups of two satellites flying in formation. This can only be achieved because the number of petals is so large. Because of the large number of petals in this FC, the relative orbit is so dense that is has been omitted for clarity. Furthermore, by adding multiples

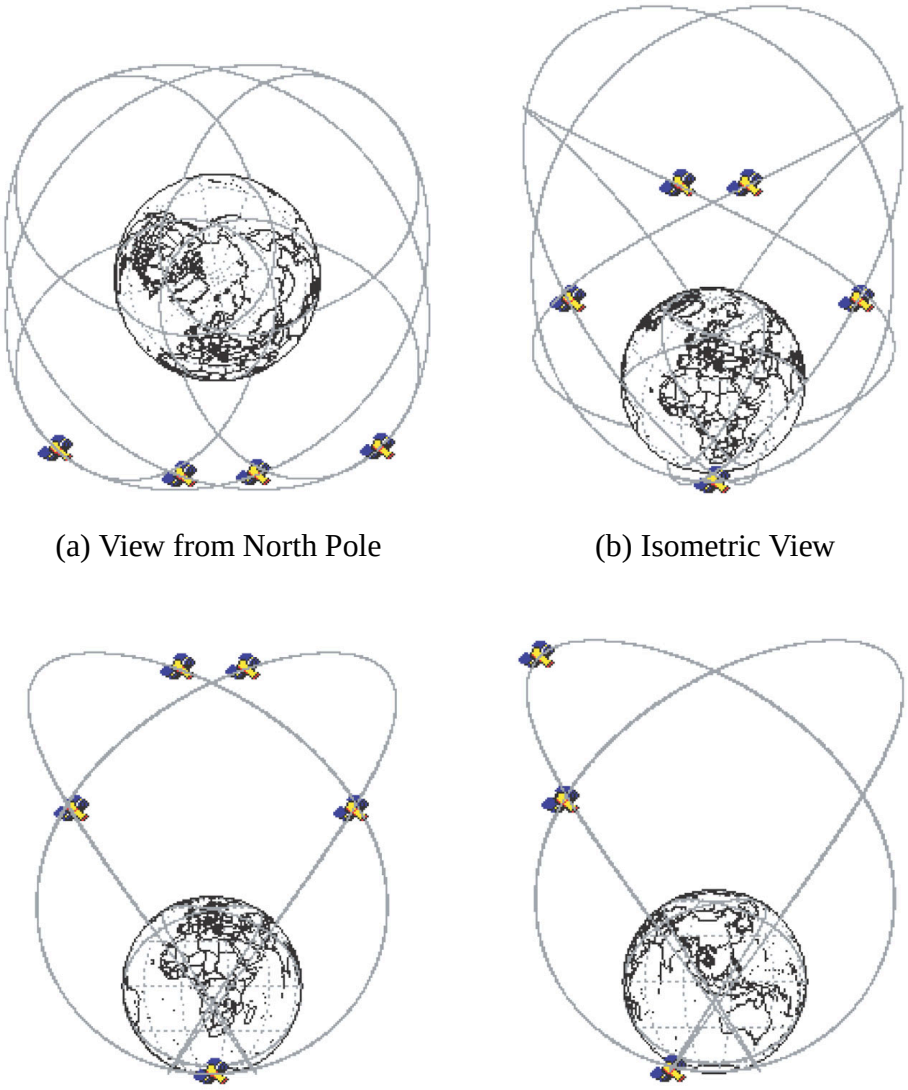

(a) View from North Pole

(b) Isometric View

(c) Equatorial View

(d) Equatorial View

Fig. 37. 3 ECF cardinal views (a,c,d) and an isometric view (b) of a 4-1-5 *Flower Constellation* with $\omega = 270^\circ$ and $i_{cr} = 116.6^\circ$. These graphics were generated with AGI's STK software.

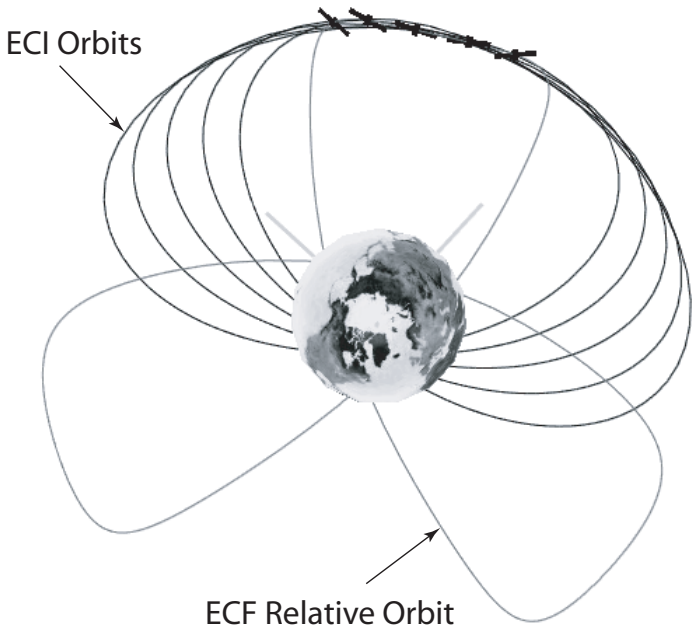

Fig. 38. A restricted *Flower Constellation* based upon a 3-1 *Flower Constellation*. Five satellites were placed with nodes evenly arrayed in a 45° range. The mean anomalies were then computed using the standard phasing rules.

of 51 satellites to this constellation, another satellite will be added to each group. Thus, to have groups of 3 satellites, all one must do is change the number of satellites to 153. Remember, though, that this is merely a method for generating the orbit parameters. In an actual mission design scenario, one would more than likely choose a single set of satellites flying in formation. The maximum number of satellites possible in this particular FC is $N_{s,max} = F_d N_d = 26,707$.

(a) View from North Pole

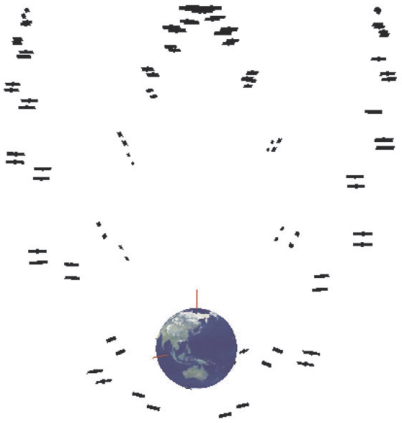

(b) Equatorial View

(c) Isometric view showing only the satellites

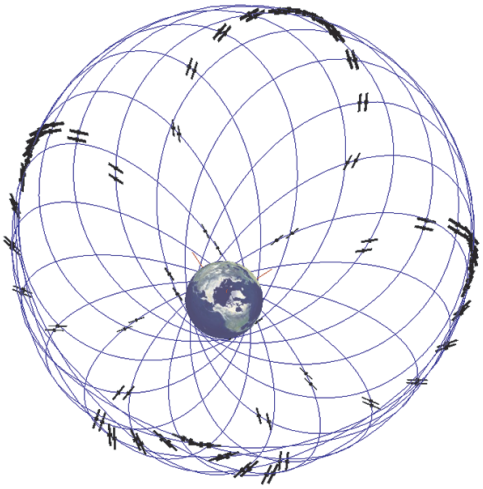

(d) Isometric view also showing the ECI orbits

Fig. 39. An “extreme” 2099-1571 *Flower Constellation* with 102 satellites. Curiously, this constellation appears to be a 4 petal flower. However, the relative path is completely different from that of a standard 4-1 FC. In this case, there are sets of two satellites flying in close formation with each other as they travel along the relative path.

CHAPTER IV

CONSTELLATION DESIGN VIA PROJECTION OF AN ARBITRARY SHAPE ONTO A FLOWER CONSTELLATION SURFACE

The inverse design of a *Flower Constellation* is a non-trivial process. One can reduce the complexity of the problem by specifying a number of the parameters *a priori*. Because the *Flower Constellations* are defined by eight parameters, if one were to leave all the parameters free in addition to adding other mission design constraints that might be unrelated to the *Flower Constellation* parameters themselves, then the process of finding a *Flower Constellation* that is optimal in some sense becomes exceedingly difficult. In that regard, the inverse design process on a single *Flower Constellation* is the subject of future work. In particular, genetic algorithms might be investigated as a potential way of specifying a cost function and obtaining an optimal solution of the *Flower Constellation* parameter set.

The inverse design process described in this chapter entails projecting an arbitrary shape onto a *Flower Constellation* surface and then computing the intersection. The choice of *Flower Constellation* specifies $a, e, i,$ and ω. Then, based upon a set of discrete intersection points, one can then compute the required right ascension of the ascending node (RAAN) and mean anomaly (MA) angles for each satellite to fix their location in space. The *Flower Constellation* surface is defined by selecting a base *Flower Constellation* and then revolving the relative orbit about the constellation axis of symmetry, which, in the case shown here, is the inertial $\hat{\mathbf{K}}$ axis. Figure 40 shows an example of a 5-2 *Flower Constellation* that has been revolved to form a surface.

Essentially, if one were to select a point on this surface, it would belong to a 5-2 *Flower Constellation* with a specific RAAN value. Thus, this surface can be thought of as an infinite set of identical *Flower Constellations* except for having differentially small variations in the RAAN. The objective, then, is to select a set of points on this surface that

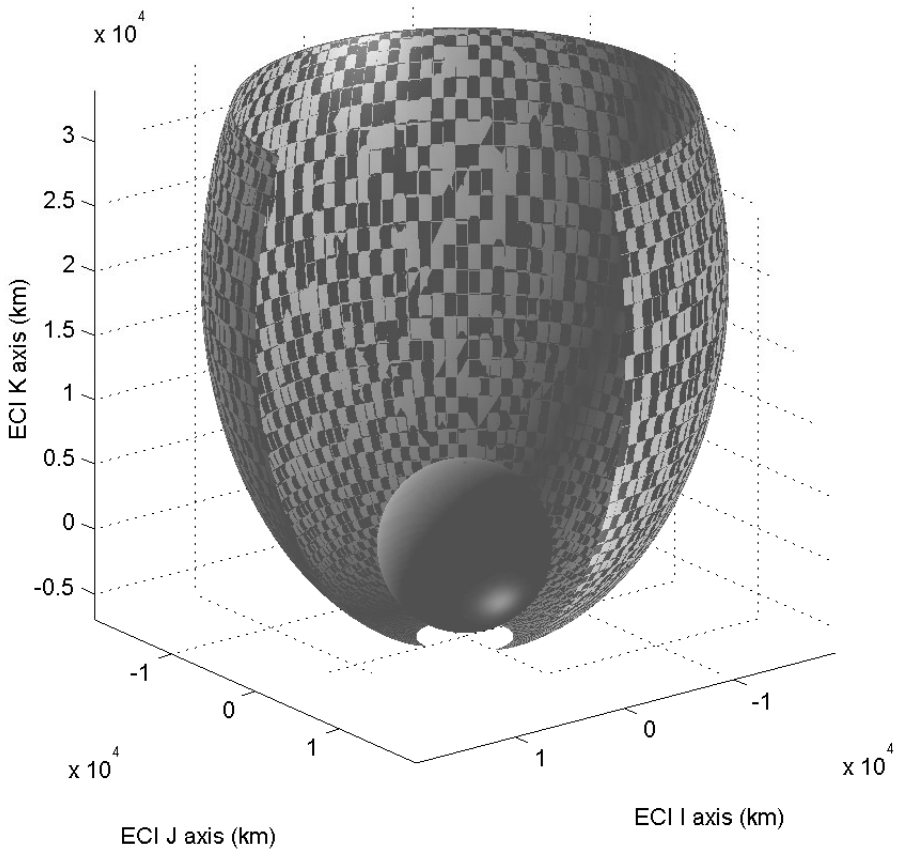

Fig. 40. A 5-2 *Flower Constellation* with $i = 63.4^\circ$, $\omega = 270^\circ$, and $h_p = 1500\ km$ that has been revolved about the ECI $\hat{\mathbf{K}}$ axis to form a surface. A section has been removed for clarity.

form a desired shape.

To that end, one needs to precisely locate the satellite on the specific *Flower Constellation*. Thus, for each RAAN selected, there will need to be a corresponding mean anomaly (MA) value chosen. In previous chpaters, there was a specific relationship between the RAAN and MA that was determined through physical constraints imposed by orbital dynamics. However, in this chapter, there is no physical relationship between the RAAN and MA but rather an algebraic one. This is due to the fact that each point selected

will, in general, belong to independent *Flower Constellations*. Thus, in this chapter, we will develop sets of equations where the RAAN and the MA are unknown variables that must be solved for simultaneously.

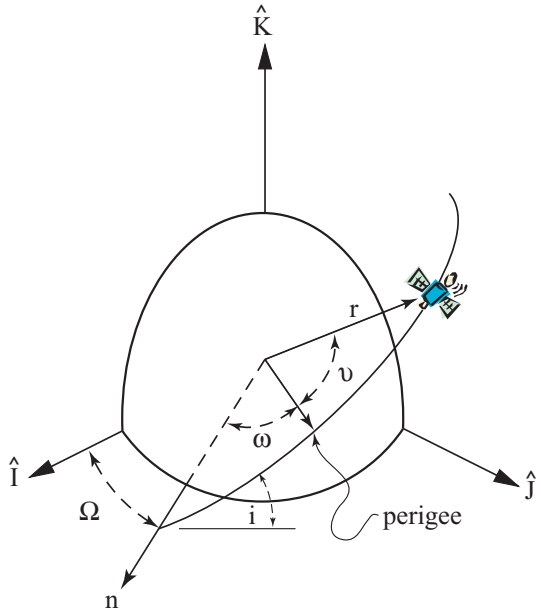

Fig. 41. The Earth Centered Inertial Frame and orbit parameters.

A. Projection from an Arbitrary View Plane

1. Some Definitions

First, begin with the inertial reference frame where the orbit parameters of the satellite are defined. Figure 41 depicts the right ascension of the ascending node (RAAN), Ω, the orbit inclination, *i*, the argument of perigee, ω, and the true anomaly, ν.

Denote the Earth Centered Inertial Frame by a superscript *I* with components of vectors expressed as:

$$I : \{ \hat{\mathbf{I}} \quad \hat{\mathbf{J}} \quad \hat{\mathbf{K}} \} \tag{4.1}$$

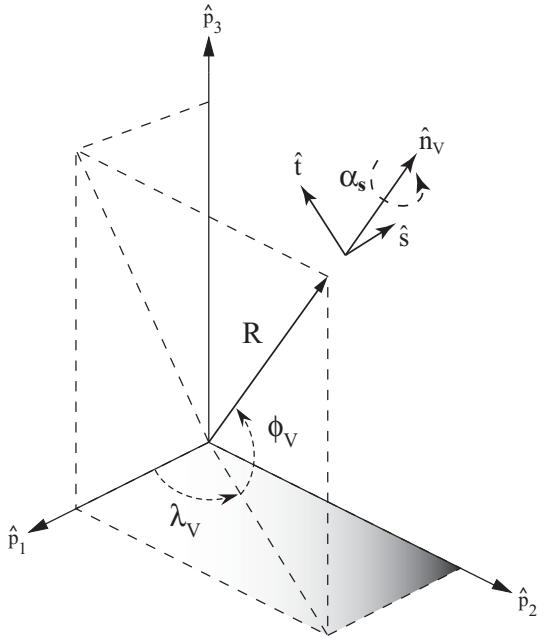

Fig. 42. The Camera Placement Frame and the View Frame.

For the purposes of this chapter, assume that the following orbit parameters have been properly selected to achieve the desired *Flower Constellation* shape: a, e, i, and ω. Chapter I describes how to solve for or select these orbit parameters based upon the *Flower Constellation* design parameters. A reference frame called the "Camera Placement" Frame in which we will orient the "View" Frame (See Figure 42) is defined. The Camera Placement Frame (CPF) is displaced from the Inertial frame by some predefined vector quantity. The CPF is constructed to be aligned with the inertial frame and will be described in more detail later. The View Frame is constructed by selecting two "viewing angles", λ_V and ϕ_V, which define the view normal, $\hat{\mathbf{n}}_V$.

$$\hat{\mathbf{n}}_V = \begin{bmatrix} \cos\phi_V \cos\lambda_V \\ \cos\phi_V \sin\lambda_V \\ \sin\phi_V \end{bmatrix} \tag{4.2}$$

Based upon this view normal, place a viewing plane perpendicular to the view normal at a distance of $|R|$ from the origin of the inertial reference frame. Thus, we can define

$$\mathbf{R} = |R|\hat{\mathbf{n}}_V \tag{4.3}$$

where $|R|$ is some predetermined value.

Vectors in the camera placement frame are denoted with a superscript P and vector components can be expressed in the camera placement frame as:

$$P : \{ \ \hat{\mathbf{p}}_1 \quad \hat{\mathbf{p}}_2 \quad \hat{\mathbf{p}}_3 \ \} \tag{4.4}$$

Vectors in the View Frame are denoted with a superscript V and vector components can be expressed in the View Frame as:

$$V : \{ \ \hat{\mathbf{n}}_V \quad \hat{\mathbf{s}} \quad \hat{\mathbf{t}} \ \} \tag{4.5}$$

Mapping from the View Frame to the camera placement frame is accomplished using the following transformation:

$$R_{PV} = R_3^T(\lambda_V)R_2^T(\phi_V)R_1^T(\alpha_s) \tag{4.6}$$

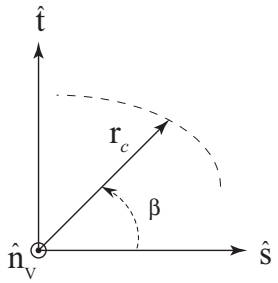

Fig. 43. The vector $\mathbf{r}_c$ is defined in the $\hat{\mathbf{s}}$-$\hat{\mathbf{t}}$ plane such that it is a function of the angle β.

where α_s is an angle that can be used to spin the view plane about the view normal if desired.

Having established the View Frame and the viewing plane, one can draw an arbitrary shape to project onto the *Flower Constellation* surface. One method is to define a vector $\mathbf{r}_c$ in the $\hat{\mathbf{s}}$-$\hat{\mathbf{t}}$ plane such that it is a function of the angle β (See Figure 43). The number of discrete values of β corresponds to the desired number of satellites in the final constellation or formation.

$$\mathbf{r}_c^V = |\mathbf{r}_c| \begin{bmatrix} 0 \\ \cos\beta \\ \sin\beta \end{bmatrix} \tag{4.7}$$

where $|\mathbf{r}_c| \equiv f(\beta)$.

2. Solving for the Unknowns

Having established the requisite reference frames, the problem can can be constructed. Figure 44 shows an example of projecting a circle from the $\hat{\mathbf{s}}$-$\hat{\mathbf{t}}$ viewing plane onto a *Flower Constellation* surface.

For each discrete value of β, a vector $\mathbf{r}_c$ is drawn from the origin of the View Frame. Then, the vector $\mathbf{r}_{proj}$ is constructed as the projection from $\mathbf{r}_c$ to the point of intersection with the *Flower Constellation* surface. This projection is perpendicular to the viewing plane; therefore, write the projection vector, $\mathbf{r}_{proj}$, in the V frame as

$$\mathbf{r}_{proj}^V = |\mathbf{r}_{proj}| \begin{bmatrix} -1 \\ 0 \\ 0 \end{bmatrix} \tag{4.8}$$

where $|\mathbf{r}_{proj}|$ is an unknown quantity.

Now, construct an equation in the View Frame which is nothing more than a vector

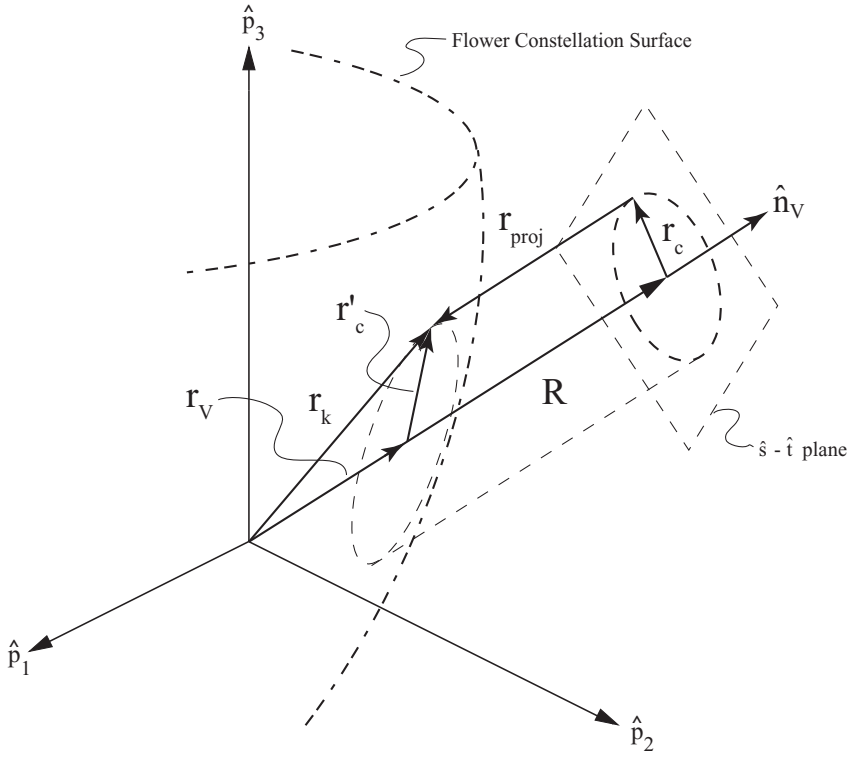

Fig. 44. Here we see that each satellite is located by projecting the shape from the **ŝ**-**t̂** plane to the surface of the *Flower Constellation*.

sum:

$$\mathbf{R}^V + \mathbf{r}_c^V + \mathbf{r}_{proj}^V - \mathbf{r}_k^V = 0 \tag{4.9}$$

where $\mathbf{r}_k^V$ is the unknown vector from the origin of the Camera Placement Frame to the point of intersection on the *Flower Constellation* surface expressed in the View Frame.

We can express $\mathbf{R}^V$ in this frame by

$$\mathbf{R}^V = |R| \begin{bmatrix} 1 \\ 0 \\ 0 \end{bmatrix} \tag{4.10}$$

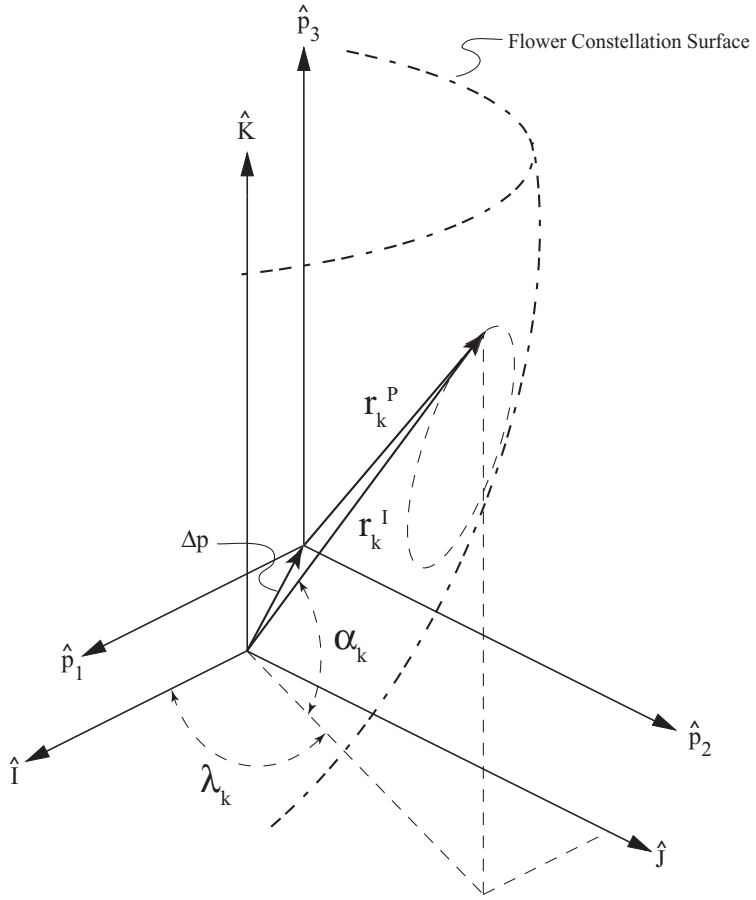

Fig. 45. This figure shows the relationship between the Camera Placement Frame and the Inertial Frame.

Substituting into the above equation, obtain:

$$|R|\begin{bmatrix}1\\0\\0\end{bmatrix}+|\mathbf{r}_c|\begin{bmatrix}0\\\cos\beta_k\\\sin\beta_k\end{bmatrix}+|\mathbf{r}_{proj}|_k\begin{bmatrix}-1\\0\\0\end{bmatrix}-\mathbf{r}_k^V=0 \tag{4.11}$$

which can be reduced down to

$$\mathbf{r}_k^V = \begin{bmatrix} |R| - |\mathbf{r}_{proj}|_k \\ |\mathbf{r}_c| \cos\beta_k \\ |\mathbf{r}_c| \sin\beta_k \end{bmatrix} \tag{4.12}$$

To express this vector in the Inertial Frame, use the transformation

$$\mathbf{r}_k^I = R_{IP}\mathbf{r}_k^P + \Delta\mathbf{p}^I = R_{IP}R_{PV}\mathbf{r}_k^V + \Delta\mathbf{p}^I \tag{4.13}$$

Recall that the Inertial and Camera Placement Frames are not rotated with respect to each other. Because the view plane can be arbitrarily oriented, rotating the CPF becomes unnecessary. Thus, these two frames are only separated by a linear displacement, $R_{IP} = I$. One can also express the vector $\mathbf{r}_k^I$ in the Inertial Frame as (See Figure 45):

$$\mathbf{r}_k^I = |\mathbf{r}_k^I| \begin{bmatrix} \cos\alpha_k \cos\lambda_k \\ \cos\alpha_k \sin\lambda_k \\ \sin\alpha_k \end{bmatrix} \tag{4.14}$$

where

$$|\mathbf{r}_k^I| = \frac{a(1-e^2)}{1+e\cos\nu_k}, \tag{4.15}$$

$$\alpha_k = tan^{-1}\left(\frac{-\sin i \sin\theta_k}{\sqrt{\cos\theta_k^2 + \sin\theta_k^2 \cos i^2}}\right), \tag{4.16}$$

$$\theta_k = \nu_k + \omega, \tag{4.17}$$

$$\lambda_k = \tan^{-1}\left(\frac{\tilde{\mathbf{r}}(2)}{\tilde{\mathbf{r}}(1)}\right), \tag{4.18}$$

$$\tilde{\mathbf{r}} = R_{IV}[\mathbf{r}_c^V(\beta_i) + \mathbf{R}^V] + \Delta\mathbf{p}^I \tag{4.19}$$

This leads to

$$|\mathbf{r}_k^I| \begin{bmatrix} \cos\alpha_k \cos\lambda_k \\ \cos\alpha_k \sin\lambda_k \\ \sin\alpha_k \end{bmatrix} = R_{PV} \begin{bmatrix} |R| - |\mathbf{r}_{proj}|_k \\ |\mathbf{r}_c| \cos\beta_k \\ |\mathbf{r}_c| \sin\beta_k \end{bmatrix} + \Delta\mathbf{p}^I \tag{4.20}$$

Here there are three equations in terms of two unknowns, ν_k and $|\mathbf{r}_{proj}|_k$. The parameters $a, e, i,$ and ω are defined by the choice of the *Flower Constellation* surface. One must solve these equations simultaneously for each discrete value of β to find the intersection points. To do this, one can use the Matlab Release 13 routine *fsolve*,[23] which attempts to find the solution to a non-linear set of equations. Thus, one can solve Equation (4.20) for the (λ_k, ν_k) pairs for each intersection point. The value of $|\mathbf{r}_{proj}|_k$ is only needed for the solution of the equations and won't be considered from this point on.

3. Finding the RAAN and MA

Now that the (λ_k, ν_k) pairs for each intersection point are known, a method to convert those to (Ω_k, M_k) pairs is desired. To that end, examine a vector expressed in two different ways in the Inertial frame:

$$\mathbf{r}_k^I = R_{IO} \begin{bmatrix} |\mathbf{r}_k^I| \\ 0 \\ 0 \end{bmatrix} = |\mathbf{r}_k^I| \begin{bmatrix} \cos\alpha_k \cos\lambda_k \\ \cos\alpha_k \sin\lambda_k \\ \sin\alpha_k \end{bmatrix} \tag{4.21}$$

where

$$R_{IO} = R_3^T(\Omega_k) R_1^T(i) R_3^T(\theta_k) \tag{4.22}$$

By expanding out the components of R_{IO}, find the following relationships:

$$f_1(\Omega_k) = \cos\Omega_k \cos\theta_k - \sin\Omega_k \sin\theta_k \cos i - \cos\alpha_k \cos\lambda_k = 0 \tag{4.23}$$

$$f_2(\Omega_k) = \sin\Omega_k \cos\theta_k + \cos\Omega_k \sin\theta_k \cos i - \cos\alpha_k \sin\lambda_k = 0 \tag{4.24}$$

$$f_3(\Omega_k) = \sin\theta_k \sin i - \sin\alpha_k = 0 \tag{4.25}$$

The third equation contains no useful information. Thus, one can solve the first two equations simultaneously, again using Matlab's *fsolve* routine. Because there are two valid equations with only one unknown, solving only one of the equations might not optimally satisfy the other. Therefore, a composite function is constructed to solve based upon the sum square of both equations:

$$f(\Omega_k) = \sqrt{\frac{1}{2}[f_1(\Omega_k)^2 + f_2(\Omega_k)^2]} = 0 \tag{4.26}$$

This was done to insure that both equations would be satisfied. Alternatively, one could algebraically combine the two equations into a single equation. Note that there are two possible solutions for the right ascension angle that are diametrically opposed to one another (corresponding to the ascending and descending nodes). To determine which value is correct, we employ a sanity check. Clearly, from Figure 41 on page 85, the value of the RAAN angle must be less than the current value of λ_k. In this way, we can select the only valid value of the Ω_k.

Now, standard classical equations are used to solve for the mean anomaly.

$$tan(\frac{E_k}{2}) = \sqrt{\frac{1-e}{1+e}} tan(\frac{\nu_k}{2}) \tag{4.27}$$

$$M_k = E_k + e\sin E_k \tag{4.28}$$

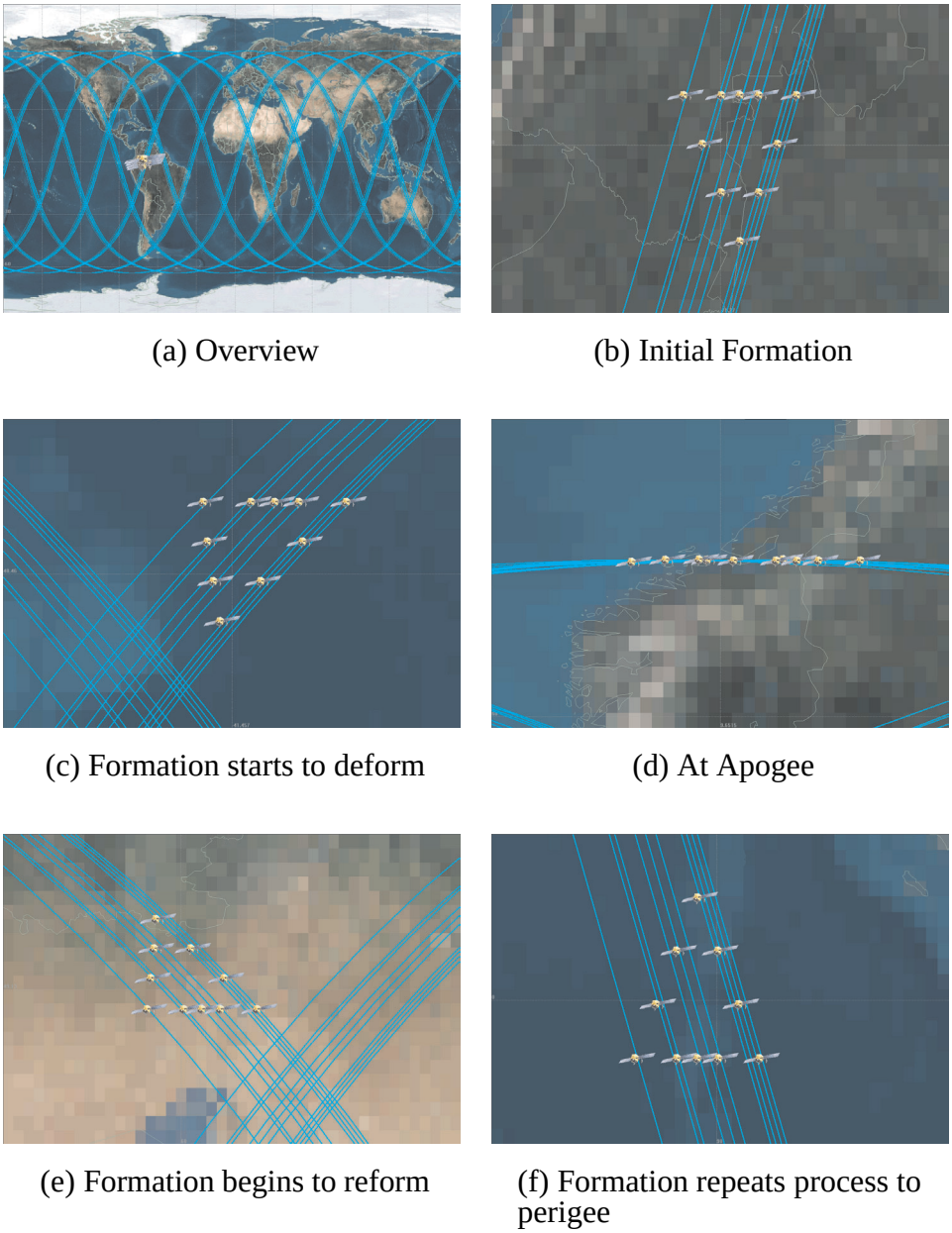

(a) Overview

(b) Initial Formation

(c) Formation starts to deform

(d) At Apogee

(e) Formation begins to reform

(f) Formation repeats process to perigee

Fig. 46. A 10-1 *Flower Constellation* surface with $i = 63.4^\circ$ and $\omega = 270^\circ$ was used to generate this triangle formation. As the formation approaches apogee and perigee, it collapses to a line before reforming. The original shape is formed twice on each petal. However, the shape inverts as it crosses from one side of the globe to the other. This figure was generated using AGI's Satellite Tool Kit software package and a two-body propagator.

4. A Triangle Formation Example

At this point, all of the orbit parameters required to precisely place each satellite in the formation have been determined. Each satellite has a common $a, e, i,$ and ω that were set based upon the desired *Flower Constellation* surface that the formation shape was being projected upon. Additionally, a technique for finding the requisite (Ω_k, M_k) pairs for each satellite to generate the desired formation shape was developed.

In this section, a triangle formation shape is created where the base of the triangle is desired to be 1000 *km* and the height is 500 *km*. The following design parameters were established:

$$|R| = 15,000\ km \qquad i = 63.4^\circ \qquad \omega = 270^\circ \qquad h_p = 1500\ km$$

$$N_p = 10 \qquad N_d = 1 \qquad N_s = 10 \qquad \lambda_V = 0^\circ \qquad \phi_V = 0^\circ$$

where i, ω, and h_p were used to establish the shape and orientation of the FC surface and N_p, N_d, and N_s are FC design parameters used to establish the number of "petals", the number of days to repeat, and the number of satellites in the constellation.

Based upon these parameters and using the *Flower Constellation* theory,[24] the semi-major axis and eccentricity of the FC surface are computed:

$$a = 9083.995\ km \qquad e = 0.23688$$

To construct the desired constellation/formation shape, a function is defined in Matlab v.6 to compute $\mathbf{r}_c$ as a function of β.

Matlab v. 6.0 Code

```
function [rc] = triangleshape(beta,a,b,c,h);
% These components are expressed in the view frame (n,s,t)
% a,b,c are vectors locating the vertices of the triangle
% h is the height of the triangle
alpha = atan2(b(2),b(1))+2*pi; %central angle from x axis to point b
gamma = atan2(a(2),a(1)); %central angle from x axis to point a
```

```
if (alpha < 0)
      alpha = alpha + 2*pi;
end
if (gamma < 0)
      gamma = gamma + 2*pi;
end
if ((beta >= 0 && beta <= pi/2) —— (beta >= alpha && beta <= 2*pi))
      slopebc = (b(2)-c(2))/b(1); % slope of line segment bc
      yintbc = c(2); % y-intercept of line segment bc
      x1 = c(2)/(tan(beta)-slopebc); % x coordinate of satellite
      y1 = slopebc*x1 + yintbc; % y coordinate of satellite
      rc = [ 0 x1 y1 ]';
elseif (beta > pi/2 && beta <= gamma)
      slopeac = (a(2)-c(2))/a(1); % slope of line segment ac
      yintac = c(2); % y-intercept of line segment ac
      x2 = c(2)/(tan(beta)-slopeac); % x coordinate of satellite
      y2 = slopeac*x2 + yintac; % y coordinate of satellite
      rc = [ 0 x2 y2 ]';
elseif (beta > gamma && beta <= 3*pi/2)
      rc = [ 0 -h/(3*tan(beta-pi)) -h/3 ]';
elseif (beta > 3*pi/2 && beta < alpha)
      rc = [ 0 h/(3*tan(beta-3*pi/2)) -h/3 ]';
else
      rc = [0 0 0]';
end
```

End Matlab v. 6.0 Code

Having established all the required parameters and set up a function to compute $\mathbf{r}_c$, one can now ready to solve for the RAAN and MA pairs for each satellite.

Table VI has the results for an 10 satellite triangle formation. When these orbit parameters are input into AGI's Satellite Toolkit software package,[25] one can visualize the formation. Figure 46 on page 94 shows a sequence of images demonstrating the deformation and reformation of the triangle formation as it moves from the equator to apogee and then back to the equator. A similar sequence is found when the satellites approach perigee. Note that, since this formation is non-symmetric, the shape inverts as it crosses from one side of the globe to the other.

Many design considerations go into the selection of the base *Flower Constellation* sur-

Table VI. Satellite phasing for a 10 satellite triangle formation based upon a 10-1 *Flower Constellation*.

Sat #	Ω (deg)	*M* (deg)	ν (deg)
1	1.27	74.84	90.00
2	1.20	73.67	88.80
3	1.13	72.50	87.59
4	359.92	73.67	88.80
5	358.72	74.84	90.00
6	357.53	76.00	91.20
7	358.81	76.00	91.19
8	359.45	76.00	91.19
9	0.08	76.00	91.19
10	1.35	76.00	91.20

face. However, the choice of a 10-1 *Flower Constellation* for this example was essentially arbitrary. By selecting a *Flower Constellation* that has multiple apogees arrayed around the Earth, the amount of time that the formation spends in the deformed state is reduced. Also, given that these formations are based upon repeating ground tracks, the multiple "petals" allows for better coverage of Earth. Choosing fewer petals means the formation would pass over a smaller region of the Earth. Therefore, the mission designer will need to experiment with all the options available for optimum results.

B. Projection From the Mercator Map

In this technique, the projection is made along radial lines from the center of the Earth through a set of geocentric latitude and longitude coordinates upward to the FC surface. Alternatively, the projection is made from the surface of the Earth such that each line of projection is parallel with each other. In this case, a centroid point is typically chosen to set the normal direction of the projection (e.g. a particular geodetic latitude and longitude coordinate where you would like to fix the surface normal direction). Again, once the intersection of the projected shape with the FC is found, the RAAN and MA pairs can be determined.

1. Geocentric Projection With a Circle Formation Example

For the geocentric projection case, one can express a vector from the origin of the ECF frame to the satellite in terms of either the geocentric latitude and longitude coordinates or in terms of the orbit elements. Note that the angle α in Eq. (4.16) on page 91 is equivalent to the geocentric latitude, ϕ_{gc}, expressed in terms of the satellite orbit elements. Thus, one

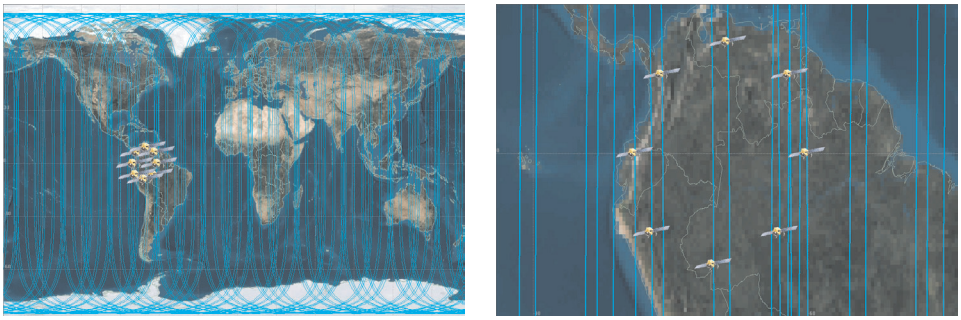

(a) Overview

(b) Initial Formation

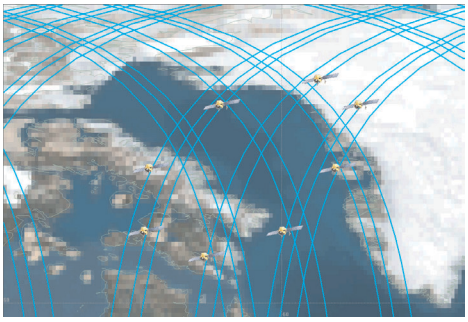

(c) Formation starts to deform

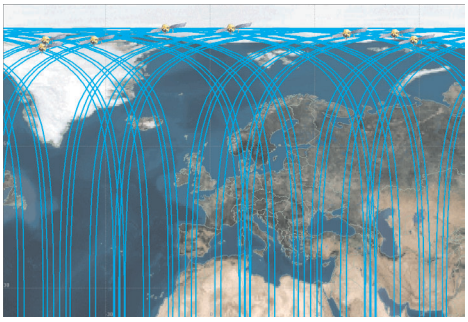

(d) At Apogee

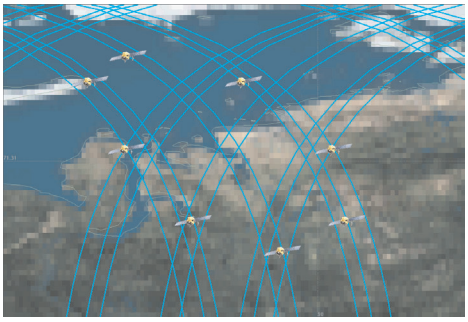

(e) Formation begins to reform

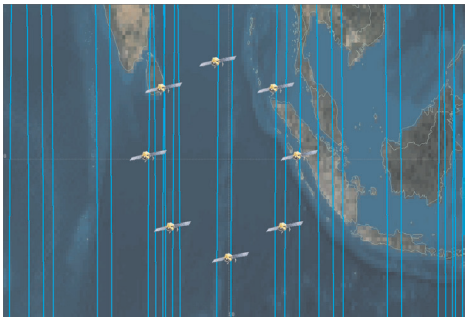

(f) Formation repeats process to perigee

Fig. 47. A 10-1 *Flower Constellation* surface with $i = 85.0^\circ$ and $\omega = 270^\circ$ was used to generate this circle formation. Note that the ground track has significantly longer straight sections as compared to those of Figure 46. Therefore, the formation maintains its geometry much longer on each pass. This figure was generated using AGI's Satellite Tool Kit software package and a two-body propagator.

can write

$$\tan\alpha = \tan\phi_{gc}$$
$$\frac{-\sin i \sin\theta}{\sqrt{\cos^2\theta + \sin^2\theta\cos^2 i}} = \tan\phi_{gc} \tag{4.29}$$

Rearrange Equation (4.29) to obtain:

$$f = \sin i \sin\theta_k + \tan\phi_{gc}\sqrt{\cos^2\theta_k + \sin^2\theta_k\cos^2 i} \tag{4.30}$$

Recall from Eq. (4.17) on page 91 that $\theta_k = \nu_k + \omega$. By specifying the desired geocentric latitude coordinate and knowing the base FC parameters, Equation (4.30) can be solved for ν_k with Matlab's *fsolve* routine. Once ν has been determined for each satellite, one can find the RAAN and MA values using the techniques described in Section A.3.

The geocentric latitude and longitude points can be specified directly or, for instance, one could use the Mercator Map equations:[26]

$$x = R_\oplus \lambda_{gc} \tag{4.31}$$
$$y = R_\oplus \ln\left[\tan\left(\frac{\phi_{gc}}{2} + \frac{\pi}{4}\right)\right] \tag{4.32}$$

where λ_{gc} and ϕ_{gc} are geocentric longitude and latitude coordinates.

A circle formation shape is created based upon a circle with a 1000 *km* radius. The following parameters were established:

$$i = 85.0^\circ \qquad \omega = 270^\circ \qquad h_p = 1500\ km$$
$$N_p = 10 \qquad N_d = 1 \qquad N_s = 8$$

As in the triangle formation example, using the *Flower Constellation* theory,[24] obtain

Table VII. Satellite phasing for a 8 satellite circle formation based upon a 10-1 *Flower Constellation*.

Sat #	Ω (deg)	M (deg)	ν (deg)
1	9.38	74.83	90.00
2	6.97	68.73	83.64
3	180.00	66.27	81.02
4	353.03	68.73	83.64
5	350.62	74.83	90.00
6	353.03	81.12	96.36
7	180.00	83.76	98.98
8	6.97	81.12	96.36

the semi-major axis and eccentricity. the following:

$$a = 9083.995\,km \qquad e = 0.132745$$

Figure 47 on page 99 shows the resulting formation based upon the computed RAAN and mean anomaly angles listed in Table VII. The sequence of images shows the deformation and reformation of the shape. Note that because the shape is symmetrical, it does not invert, per se, as in the case of the triangle formation.

2. Parallel Projection

For the parallel projection case, we modify our approach slightly compared the the geocentric projection technique. Here, a desired unit normal direction, $\hat{\mathbf{n}}$, is prescribed first as shown in Figure 48. Then a vector, $\mathbf{r}_1$ from the origin of the ECF frame is constructed to the discrete latitude and longitude coordinate points on the surface of the Earth. From that

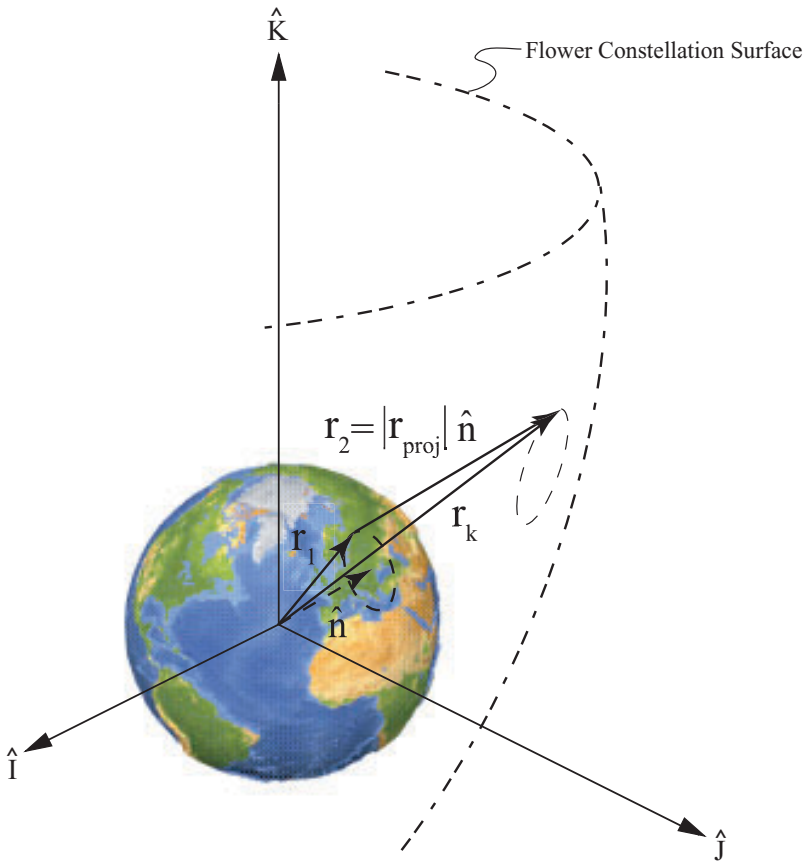

Fig. 48. For the parallel projection case, each of the satellites are positioned by projecting upwards from the surface of the Earth in a proscribed normal direction, $\hat{\mathbf{n}}$.

point, another vector, $\mathbf{r}_2$ is constructed from the Earth's surface to the intersection point with the FC surface. This second vector has the same unit normal as the desired nominal direction and has an unknown magnitude, $|\mathbf{r}_p|$, that must be determined. These two vectors can be written as follows:

$$\mathbf{r}_1 = R_\oplus \begin{bmatrix} \cos\lambda_{gc}\cos\phi_{gc} \\ \cos\lambda_{gc}\sin\phi_{gc} \\ \sin\lambda_{gc} \end{bmatrix} \tag{4.33}$$

$$\mathbf{r}_2 = |\mathbf{r}_p|\hat{\mathbf{n}} \tag{4.34}$$

Now recall Eq. (4.14) on page 91:

$$\mathbf{r}_k^I = |\mathbf{r}_k^I| \begin{bmatrix} \cos\alpha_k\cos\lambda_k \\ \cos\alpha_k\sin\lambda_k \\ \sin\alpha_k \end{bmatrix}$$

Using vector algebra, we can construct the following equation that must be solved for ν_k and $|\mathbf{r}_p|$:

$$\mathbf{r}_k^I = \mathbf{r}_1 + \mathbf{r}_2$$

$$|\mathbf{r}_k^I| \begin{bmatrix} \cos\alpha_k\cos\lambda_k \\ \cos\alpha_k\sin\lambda_k \\ \sin\alpha_k \end{bmatrix} = R_\oplus \begin{bmatrix} \cos\lambda_{gc}\cos\phi_{gc} \\ \cos\lambda_{gc}\sin\phi_{gc} \\ \sin\lambda_{gc} \end{bmatrix} + |\mathbf{r}_p|\hat{\mathbf{n}} \tag{4.35}$$

where Equations 4.15 through 4.19 are repeated here for convenience:

$$
\begin{aligned}
|\mathbf{r}_k^I| &= \frac{a(1-e^2)}{1+e\cos\nu_k}, \\
\alpha_k &= tan^{-1}\left(\frac{-\sin i \sin\theta_k}{\sqrt{\cos\theta_k^2+\sin\theta_k^2\cos i^2}}\right), \\
\theta_k &= \nu_k + \omega, \\
\lambda_k &= \tan^{-1}\left(\frac{\tilde{\mathbf{r}}(2)}{\tilde{\mathbf{r}}(1)}\right), \\
\tilde{\mathbf{r}} &= R_{IV}[\mathbf{r}_c^V(\beta_i)+\mathbf{R}^V]+\Delta\mathbf{p}^I
\end{aligned}
$$

Finally, we can compute the RAAN and MA for each satellite using the technique described in Section A.3. As this case is very similar to the geocentric projection, a graphical example has been omitted for brevity.

C. Other Examples

Any desired shape can be created using the techniques outlined in this chapter. Figure 49(a) shows a rectangular formation. One could even write text using satellites flying in formation. Figure 49(b) is an example of just that. The letters N, A, S, and A are spelled out using 44 satellites. While this formation is impractical for most purposes, it serves to demonstrate the flexibility and capabilities of this constellation/formation design technique.

D. Reorientation of the Constellation/Formation

In the previous examples given, the formation always collapsed to a line at apogee, which was always located in the northern hemisphere. However, this may not be desirable for some mission profiles. Thus, one can use a technique to reorient the base *Flower Constellation* surface as discussed in Chapter I. In this way, it is possible to rigidly reorient entire

(a) A rectangular formation on a 5-2 FC surface. This figure was generated using AGI's Satellite Tool Kit software package.

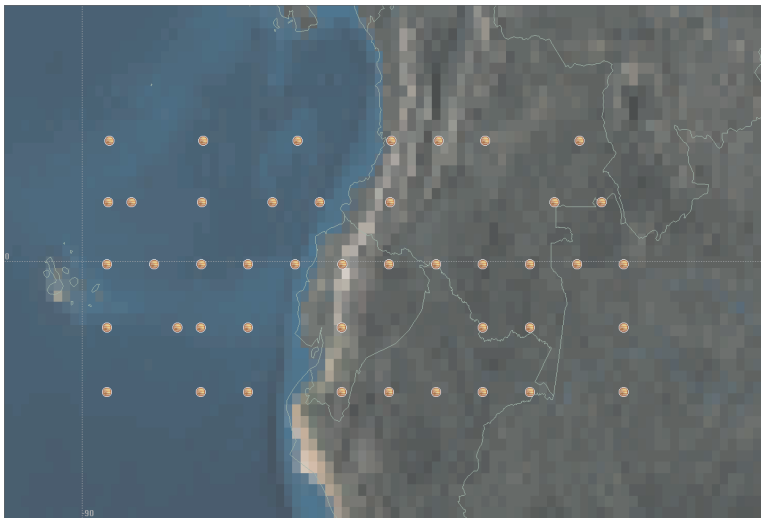

(b) Here, the text "NASA" is written on a 10-1 *Flower Constellation* surface using 44 satellites. This figure was generated using AGI's Satellite Tool Kit software package.

Fig. 49. Two examples of other kinds of constellations and formations that can be created with this technique.

constellations/formations. Note that this is a mathematical exercise and will generally be fuel prohibitive to maintain. Also note that this is not a reconfiguration, but rather a method for generating the required orbit elements at initial time.

Using this reorientation technique, the triangle formation from Figure 46 on page 94 was reoriented such that the original axis of symmetry was rotated 90° away. Table VIII shows the new orbital parameters for each satellite in the formation. Figure 50 on page 108 shows a sequence of images as the formation orbits the Earth.

Note that in this particular case, the inclination is for a retrograde orbit. This can be changed to a prograde orbit through a different selection of the reorientation angles. Also note that the inclination is no longer one of the critical inclinations. In general, reoriented FC's will require control to combat geopotential perturbations in order to maintain the integrity of the formation/constellation.

Table VIII. New orbital parameters for a 10 satellite triangle formation originally based upon a 10-1 *Flower Constellation* that has been reoriented 90° from the original axis of symmetry.

Sat #	*i* (deg)	ω (deg)	Ω (deg)	*M* (deg)	ν (deg)
1	100.54	155.54	23.65	63.12	90.01
2	100.60	155.56	23.67	61.97	88.75
3	100.65	155.58	23.70	60.83	87.48
4	101.64	155.88	24.15	61.97	88.75
5	102.62	156.18	24.60	63.12	90.01
6	103.60	156.47	25.05	64.27	91.25
7	102.55	156.15	24.57	64.25	91.24
8	102.03	156.00	24.32	64.25	91.24
9	101.51	155.84	24.09	64.25	91.24
10	100.48	155.52	23.62	64.27	91.25

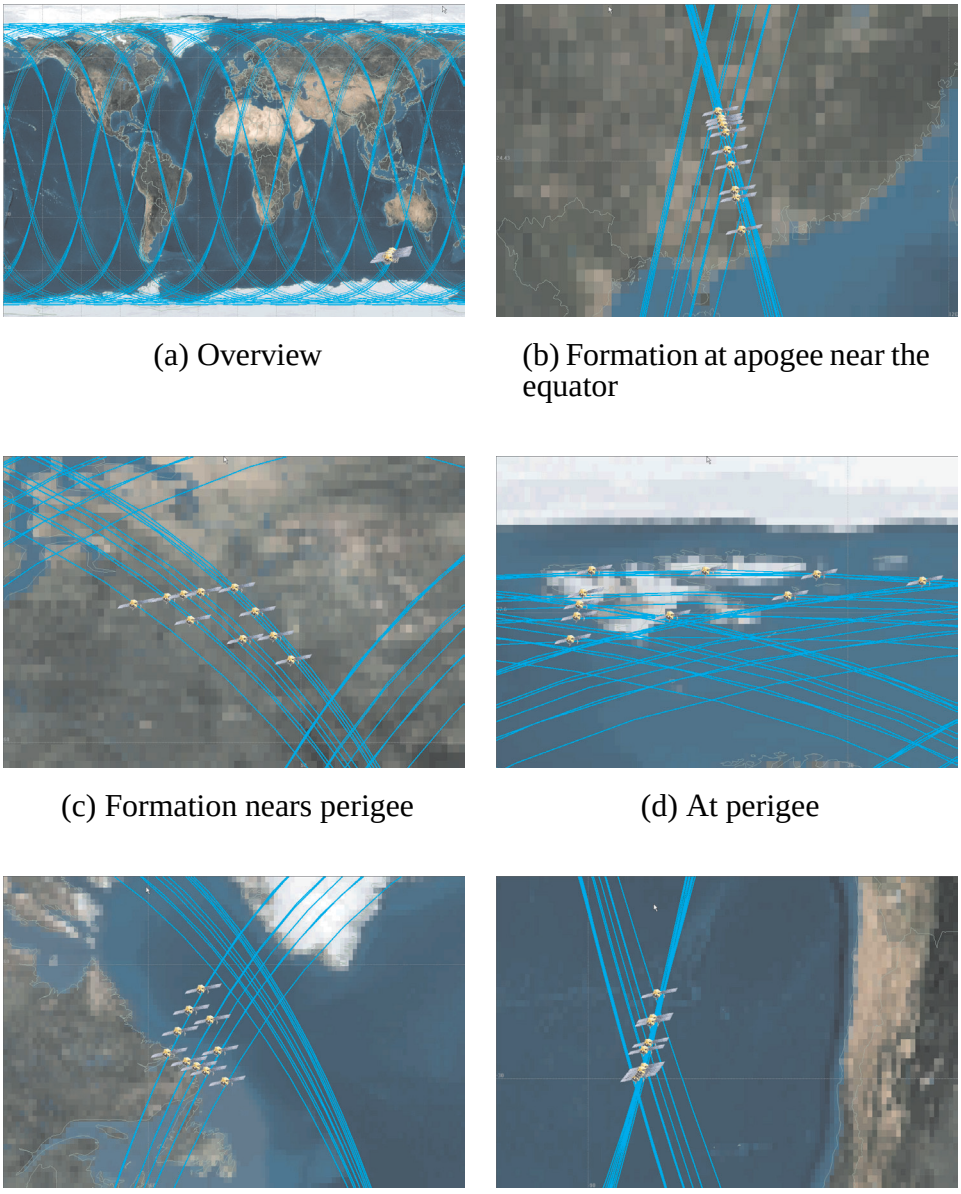

(a) Overview

(b) Formation at apogee near the equator

(c) Formation nears perigee

(d) At perigee

(e) Formation begins to deform as it approaches the equator again

(f) Formation repeats process from the equator

Fig. 50. The 10 satellite triangle formation from Figure 46 on page 94 has been reoriented 90° from the original axis of symmetry. Note that the location where the formation collapses to a line is no longer at the north pole, but rather at the equator. These figures were generated using AGI's Satellite Tool Kit software package.

CHAPTER V

PERTURBATION THEORY AND ITS EFFECT ON FC DESIGN

Because the Earth is an oblate spheroid, there are perturbations induced upon an orbit that cause it to shift position and alter shape over time. Among the primary perturbations affecting orbits in general are the J_2 effect (the first zonal component of the Earth's geopotential expansion), atmospheric drag, solar radiation pressure, and third-body interactions with other massive bodies in our solar system (e.g. luni-solar effects).

Atmospheric drag is of concern to many satellites that fall into the near Earth regime. There is some debate about the extent of this regime but it is generally held that above 1000 *km* in altitude, atmospheric drag is of little to no consequence. Earlier in Chapter I, it was pointed out that 600 *km* was a good threshold for a minimum altitude to ensure that atmospheric drag would not dominate the motion of the satellites in the constellation under consideration.

Other perturbations such as solar radiation pressure and third-body effects need to be evaluated on a case-by-case basis as they are strongly dependent upon the epoch time and the resultant orbit size. This chapter will look at summarizing the effects of solar radiation pressure and third-body interactions to give the constellation designer a guideline for choosing *Flower Constellation* parameters judiciously. For detailed analysis, refer to the cited literature.

The Joint Goddard Earth Model-2 (JGM-2) geopotential model, is one of the most accurate geopotential models today.[27] Currently there are on the order of 70×70 terms that have been evaluated through experiment. From this model, $J_2 = -1.08262692 \times 10^{-}3$ and is of the order of 10^{-3} while the remaining zonal terms are of the order 10^{-6} or less.[20] Therefore, in many instances, it is feasible to neglect zonal terms beyond the J_2 term and still obtain acceptable simulation accuracy.

However, this is not necessarily true for orbits that happen to have periods commensurate with the Earth's rotation rate. In this case, smaller tesseral harmonics can produced large amplitude oscillations in the orbit elements over time that might become unacceptable to the mission profile. The period of these motions varies depending upon the particular resonance that is excited. The next section in this chapter will examine in detail the problem of resonance as it pertains to the *Flower Constellations*.

A. Resonance Concerns

Flower Constellations have an additional concern regarding the Earth's geopotential field because many of these orbits are commensurate with the Earth's spin rate (i.e. the satellite mean motion is an integer multiple of the Earth's spin rate). In this situation and in cases of near commensurability, resonance effects created by the longitude dependent tesseral harmonics of the geopotential field must also be taken into account.

The disturbing potential introduced by Kaula in 1966 is given by:[28]

$$U = \frac{\mu}{r}\sum_{l=2}^{\infty}\sum_{m=0}^{l}\sum_{p=0}^{l}\sum_{q=-\infty}^{\infty}\frac{\mu}{a}\left(\frac{R_{\oplus}}{a}\right)^{l}F_{lmp}(i)G_{lpq}(e)S_{lmpq}(\omega,M,\Omega,\theta_{GMST}) \tag{5.1}$$

where the S functions contain the gravitational coefficients

$$S_{lmpq}(\omega,M,\Omega,\theta_{GMST}) = \begin{cases} C_{l,m}\cos\Theta_{lmpq} + S_{l,m}\sin\Theta_{lmpq} & \text{if } (l-m) \text{ is even} \\ -S_{l,m}\cos\Theta_{lmpq} + C_{l,m}\sin\Theta_{lmpq} & \text{if } (l-m) \text{ is odd} \end{cases} \tag{5.2}$$

where

$$\Theta_{lmpq} = (l-2p)\omega + (l-2p+q)M + m(\Omega - \theta_{GMST}) \tag{5.3}$$

The F and G functions are expressed as functions of the inclination and eccentricity:

$$F_{lmp}(i) = \sum_{t=0}^{\min(p,\,k)} \left[\frac{(2l-2t)!}{t!(l-t)!(l-m-2t)!2^{2l-2t}} \sin^{l-m-2t}(i) \right.$$
$$\left. \times \sum_{s=0}^{m} \binom{m}{s} \cos^{s}(i) \sum_{c} \binom{l-m-2t+s}{c} \binom{m-s}{p-t-c} (-1)^{c-k} \right] \tag{5.4}$$

where k is the integer part of $(l-m)/2$ and c is summed for all values for which the coefficients are not equal to zero.

$$G_{lpq}(e) = \frac{1}{(1-e^2)^{l-1/2}} \sum_{d=0}^{p'-1} \binom{l-1}{2d+l-2p'} \binom{2d+l-2p'}{d} \left(\frac{e}{2}\right)^{2d+l-2p'} \tag{5.5}$$

where $p' = p$ if $p \leq l/2$ and $p' = l-p$ if $p \geq l/2$.

$$\begin{aligned} \dot{\Theta}_{lmpq} &= (l-2p)\dot{\omega} + (l-2p+q)\dot{M} + m(\dot{\Omega} - \dot{\theta}_{GMST}) \\ &= (l-2p)\dot{\omega} + (l-2p+q)n + m(\dot{\Omega} - \omega_{\oplus}) \end{aligned} \tag{5.6}$$

Repeat ground track resonance occurs for terms where the condition $q = 0$ is satisfied or when $\dot{\Theta}_{lmpq} \approx 0$. This implies that

$$\dot{\Theta}_{lmpq} \approx 0 \Rightarrow (l-2p)(\dot{\omega} + \dot{M}) \approx m\left(\dot{\theta}_{GMST} - \dot{\Omega}\right) = m(\omega_{\oplus} - \dot{\Omega}) \tag{5.7}$$

which can be expressed as the ratio

$$\frac{P}{Q} \approx \frac{\dot{\omega} + \dot{M}}{\omega_{\oplus} - \dot{\Omega}} = \frac{m}{l-2p} \tag{5.8}$$

The values of $l, m,$ and p that satisfiy the resonance condition are $m = jP$ and $jQ = l-2p$ where $j = 1, 2, 3, \ldots$. These terms are considered critical because their rates vanish and lead to resonance oscillations with long periods. Based upon the above developments, the

resonance parameter, ε_Θ is defined

$$\varepsilon_\Theta = Q(\dot{\omega} + \dot{M}) - P(\omega_\oplus - \dot{\Omega}) \tag{5.9}$$

Note that when $\dot{\Theta}_{lmpq} = 0$, then exact resonance occurs (i.e. $\varepsilon_\Theta = 0$). When ε_Θ is small, then *deep* resonance occurs that leads to large amplitude oscillations with long periods. When ε_Θ is large, then *shallow* resonance occurs that have smaller motion amplitudes and shorter periods. The period of the resonance is

$$T_{res} = \frac{2\pi}{|\varepsilon_\Theta|} \tag{5.10}$$

Similarly, to determine whether or not tesseral harmonics will be a dominating factor, Garfinkel[29] introduced the resonance parameter, R.

$$R = \frac{T_c}{T} = 1 + \frac{s_o}{\Delta s} \tag{5.11}$$

where T_c is the circulation period (often called the beat period) defined by

$$T_c = \frac{2\pi/m}{(s_0/\Delta s)(\dot{\theta} - \dot{\Omega})}, \tag{5.12}$$

m is one of four summation indices in the standard potential function,[28] and T is the anomalistic orbit period. s_0 and Δs can be found from the following definition

$$s \equiv \frac{P}{Q} = s_0 + \Delta s \tag{5.13}$$

where s is the ratio of the nodal period of the satellite and the Earth's rotation rate and s_0 is the integer nearest s. Note that $\Delta s < 1$ and, when $\Delta s = 0$, the orbit is exactly commensurate with the Earth's rotation rate. When Δs is small, we say that the orbit is nearly commensurate. A *fundamental* resonance occurs when m (Equation (5.12)) equals s_0 and very weak higher *overtones* are apparent when m is an integer multiple of s_0. Thus, Equation (5.11) is derived for fundamental resonances.

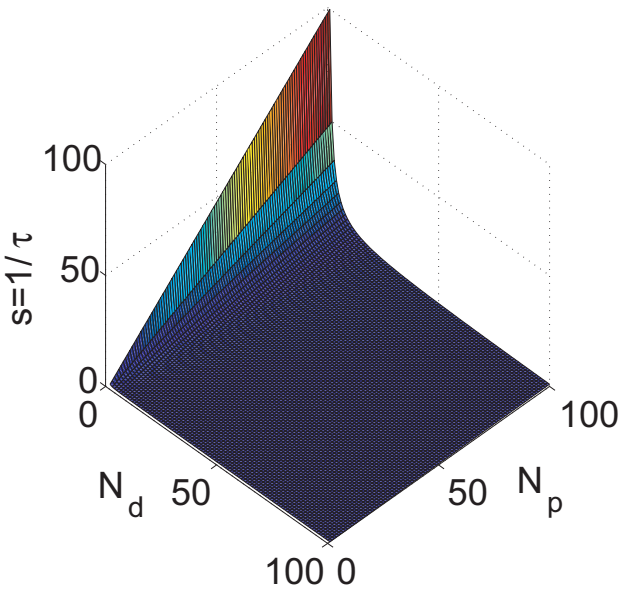

Fig. 51. A comparison of the resultant value of s for various values of N_p and N_d.

Recall from Equation (1.3) and Equation (1.2) that

$$T_{\Omega G} = 2\pi \left(\omega_{\oplus} - \dot{\Omega}\right)^{-1}$$

$$T_{\Omega} = 2\pi \left(\dot{M} + \dot{\omega}\right)^{-1}$$

Combining these two, one can write

$$\frac{T_{\Omega}}{T_{\Omega G}} = \frac{\left(\dot{M} + \dot{\omega}\right)}{\left(\omega_{\oplus} - \dot{\Omega}\right)} \tag{5.14}$$

where one can see from Equation (5.8) that

$$\frac{P}{Q} = \frac{T_{\Omega}}{T_{\Omega G}} \tag{5.15}$$

Clearly now from Equation (5.15) and Equation (1.1) one can write that

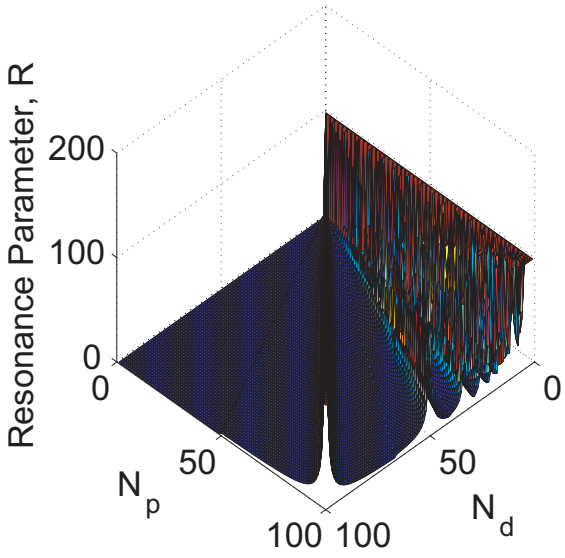

(a)

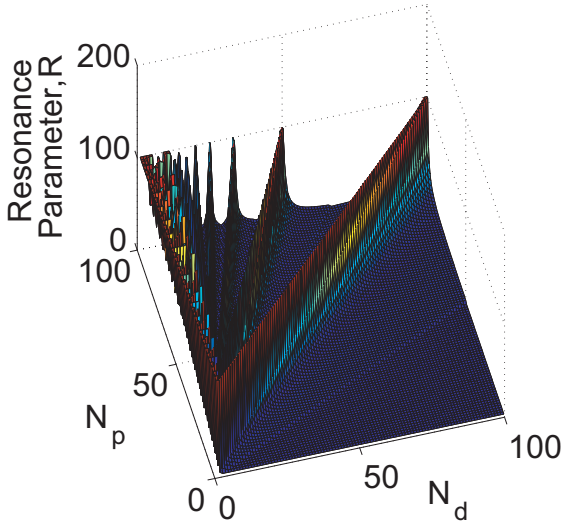

(b)

Fig. 52. Gedeon's resonance parameter can be used to determine whether or not resonance effects can be safely ignored. Values of R less than 10 have negligible resonance effects, R values in the low tens are in the *shallow* resonance regime, and R values in the high tens and hundreds are in the *deep* resonance regime. The spikes in this graph are located at an N_p, N_d pair where $\Delta s = 0$ and a fundamental resonance exists.

$$\frac{P}{Q} = \frac{N_p}{N_d} \tag{5.16}$$

Thus, for the purposes of the *Flower Constellations*,

$$s \equiv \frac{1}{\tau} = \frac{N_p}{N_d} \tag{5.17}$$

where τ is defined in Eq. (1.10) on page 13. Figure 51 graphically displays the variation in s for $1 \leq N_p \leq 100$ and $1 \leq N_d \leq 100$.

According to Gedeon, when the resonance parameter, R, is less than 10, then resonance effects are insignificant may be ignored. However, when R reaches values in the tens or higher, perturbations stemming from one or more critical tesseral harmonics becomes appreciable. This is called the *shallow* resonance regime. As $\Delta s \to 0$, R can reach into the hundreds and the orbit is said to be in *deep* resonance. Figure 52 depicts the resonance parameter for $1 \leq N_p \leq 100$ and $1 \leq N_d \leq 100$. For the *Flower Constellations*, a fundamental (deep) resonance occurs, for example, when $N_d = 1$ or when $N_d \mid N_p$ (i.e. $s \in \mathbb{N}$).

1. Station Keeping in the Presence of Resonance Effects for Nearly Circular Orbits

Resonance can affect all the orbit parameters in one way or another. However, the most pronounced effect caused by the resonance described in this chapter is found in what is termed the "stroboscopic mean node" [1],

$$\lambda_N = \frac{1}{s_0}(M + \omega) - (\theta_{GMST} - \Omega) \tag{5.18}$$

The classical method for controlling this effect is given by Gedeon[30] where he describes the stroboscopic mean node by introducing a "mean satellite" that "illuminates" the Earth with a stroboscopic flash light and crosses the equator at a longitude of $\lambda_N = \Omega - \theta_{GMST}$. After Q (or N_d) days, the mean satellite will be in the same position provided that $\dot{\lambda}_N = 0$ or will

[1] Gedeon[30] attributes this name to the suggestion of Dr. Boris Garfinkel

be $\int \dot{\lambda}_N dt$ away if $\dot{\lambda}_N \neq 0$. Therefore, λ_N only has physical meaning at integer multiples of Q (or N_d) days, which leads to the concept of a "stroboscopic mean node".

Bear in mind that the tesseral harmonic perturbations cause an acceleration in Ω, ω, and M and in order to determine λ_N, one must integrate the following second order differential equation that was derived by Gedeon:[30]

$$\ddot{\lambda}_N = \ddot{\Omega} + \frac{1}{s_0}(\ddot{M} + \ddot{\omega}) \tag{5.19}$$

$$= \frac{n^2}{s_0^2} \sum \left[1 + A \frac{m\dot{\lambda}_N - q\dot{\omega}}{n} \right] \frac{1}{m P_{lmpq}^2} - \sin m(\lambda_n - \overline{\lambda}_{lm}) + O(J_{lm}^2) \tag{5.20}$$

where

$$P_{lmpq} = \frac{1}{m} \left[\frac{(a/a_\oplus)^l}{3|F_{lmp}(i) G_{lpq}(e)| J_{lm}} \right]^{1/2} \tag{5.21}$$

$$\overline{\lambda}_{lm} = \lambda_{lm} + \frac{2\pi k}{m} - \left\{ \begin{array}{c} (1+\xi)\frac{\pi}{2m} \\ \xi \frac{\pi}{2m} \end{array} \right\}_{(l-m)\text{odd}}^{(l-m)\text{even}} + \frac{q}{m}\omega \tag{5.22}$$

$$\xi = \left\{ \begin{array}{c} +1 \\ -1 \end{array} \right\} \quad \text{if} \quad F_{lmp}(i) G_{lpq}(e) \left\{ \begin{array}{c} > \\ < \end{array} \right\} 0 \tag{5.23}$$

$$A = -\frac{s_o}{3m} \left[2(l+1) + \frac{e(1-e^2)^{1/2}}{1+(1-e^2)^{1/2}} \frac{G'}{G} + \frac{s_0 - \cos i}{(1-e^2)^{1/2} \sin i} \frac{F'}{F} \right] \tag{5.24}$$

and summation is performed over all critical indices. Note that $\overline{\lambda}_{lm}$ is the longitude of the stable node, which rotates at an angular velocity of $(q\dot{\omega}/m)$ in the equatorial plane.

The motion of the longitude of the mean node can be controlled by establishing a deadband region of $\pm\Delta\lambda$ that is centered away from a stable node by the amount β_{lm}. For small deadbands, Gedeon found that the amount of ΔV required on an annual basis can be computed as:

$$\frac{\delta V/V}{T} = \frac{n/s_0}{3} \left(\frac{V_c}{V} \right)^2 \sum \frac{1}{m P_{lmpq}^2} \sin m\beta_{lm} \tag{5.25}$$

where n is the mean motion expressed in radians per year, V_c is the circular orbit velocity, V is the velocity at the point of application of the orbit correction, and the summation is performed over all critical terms contributing to the resonance phenomena.

The stable node locations move depending upon the number and kind of critical terms included in the analysis. In order to determine β_{lm}, one must first locate the stable node by solving for those values of λ_0 that satisfy the following relationship:

$$\frac{\mu}{a}\sum\left(\frac{a_{\oplus}}{a}\right)^{l} J_{lm}F_{lmp}(i)G_{lpq}(e)\left\{\begin{array}{c}-\sin\\ \cos\end{array}\right\}_{(l-m)odd}^{(l-m)even}[m(\lambda_N-\lambda_m)-q\omega]=0 \qquad (5.26)$$

where, once again, the summation is performed over all critical indices.

2. Station Keeping in the Presence of Resonance Effects for Eccentric Resonant Orbits

The station keeping method presented by Gedeon was largely developed assuming very small orbit eccentricities. Ely and Howell[31] found that if one were to apply this method to highly eccentric orbits, then the method has the potential to become unstable. Ely and Howell addressed this issue by constructing a new method for east-west station-keeping for eccentric orbits called the EOSK algorithm. The EOSK algorithm is suitable for orbits that are nearly commensurate and also includes luni-solar effects. For complete details regarding the EOSK method, please refer to their paper.

3. Resonance and the Critical Inclination

It should also be mentioned that Delhaise and Henrard[32] showed that for 12 *hr* and 24 *hr* orbits that are inclined at the critical inclination chaotic motion can result. Their work was performed as part of a preliminary mission analysis for ESA's Archimedes project (See Section I.A). They looked at the Hamiltonian averaged over the mean motion and included

terms due to the Earth's geopotential, which is shown here up to the 2nd order zonal term:

$$\begin{aligned} H =& -\frac{\mu^2}{2L^2} - \omega_\oplus H - \frac{\mu^4}{L^6}\frac{R_\oplus^2 J_2}{4}\left(3\frac{H^2}{G^2}-1\right)\left(\frac{L}{G}\right)^3 \\ & - \frac{\mu^6}{L^{10}}\frac{R_\oplus^4 J_2^2}{4}[A(L,G,H)\cos 2g + C(L,G,H)] \\ & - \sum_{l,m,p,q} B_{lmpq} \left\{ \begin{array}{c} \cos\theta_{l,m,p,q} \\ \sin\theta_{l,m,p,q} \end{array} \right\} \begin{array}{l} \text{for } l-m \text{ even} \\ \text{for } l-m \text{ odd} \end{array} \end{aligned} \tag{5.27}$$

where

$$\theta_{l,m,p,q} = m(x_3 - \lambda_{lm}) + (l-2p)g \tag{5.28}$$

$$A(L,G,H) = -\frac{3}{16}\left(\frac{L^5}{G^5} - \frac{L^7}{G^7}\right)\left(1 - 16\frac{H^2}{G^2} + 15\frac{H^4}{G^4}\right) \tag{5.29}$$

$$\begin{aligned} C(L,G,H) =& \frac{15}{32}\frac{L^5}{G^5}\left(1 - \frac{18}{5}\frac{H^2}{G^2} + \frac{H^4}{G^4}\right) \\ & + \frac{3}{8}\frac{L^6}{G^6}\left(1 - 6\frac{H^2}{G^2} + 9\frac{H^4}{G^4}\right) \\ & - \frac{15}{32}\frac{L^7}{G^7}\left(1 - \frac{18}{5}\frac{H^2}{G^2} + \frac{H^4}{G^4}\right) \end{aligned} \tag{5.30}$$

$$B_{lmpq} = \frac{\mu}{a}\left(\frac{R_\oplus}{a}\right)^l F_{lmp}(i) G_{lpq}(e) J_{lm} \tag{5.31}$$

Note that λ_{lm} is the longitude of the major axis of symmetry of the (l,m) spherical harmonic, (l,g,h,L,G,H) are the Delaunay variables with respect to an Earth Centered Earth Fixed (ECEF) frame, the inclination and eccentricity functions $F_{lmp}(i)$ and $G_{lpq}(e)$ have already been given in Section V.A, and J_{lm} are the tesseral ($l \neq m$) and sectorial ($l = m$) geopotential spherical harmonic coefficients. The canonical variables used in Delhaise and Henrard's analysis can be written in terms of the *Flower Constellation* parameters as:

$$x_1 = l \qquad x_2 = g \qquad x_3 = \frac{N_d}{N_p}l + \Omega - \omega_\oplus t \tag{5.32}$$

$$y_1 = L - \frac{N_d}{N_p}H \qquad y_2 = G \qquad y_3 = H \tag{5.33}$$

The equilibrium points of the Hamiltonian can be found by solving

$$\frac{\mathrm{d}x_i}{\mathrm{d}t} = \frac{\partial H}{\partial y_i} = 0 \tag{5.34}$$

$$\frac{\mathrm{d}y_i}{\mathrm{d}t} = -\frac{\partial H}{\partial x_i} = 0 \quad \text{for} \quad i = 2,3 \tag{5.35}$$

where the terms $A, B_{l,m,p,q}$, and C are assumed to be constant, the values of the semi-major axis and eccentricity are determined as described in the *Flower Constellation* theory, and the inclination is a critical inclination. By expanding the total Hamiltonian about the equilibrium points up to quadratic terms and separating into a perturbed and non-perturbed form, one can obtain

$$H = H_o(x_3, y_3, x_2) + \varepsilon H_1(x_3, y_3, x_2, y_2) \tag{5.36}$$

with

$$H_0 = \frac{1}{2}(y_3 - y_3^*)^2 \left.\frac{\partial H}{\partial y_3^2}^2\right|_{y_i^*} - \sum_{l,m,p,q} B_{lmpq} \left\{ \begin{array}{l} \cos\theta_{l,m,p,q} \\ \sin\theta_{l,m,p,q} \end{array} \right\} \begin{array}{l} \text{for } l-m \text{ even} \\ \text{for } l-m \text{ odd} \end{array} \tag{5.37}$$

$$H_1 = \frac{1}{2}(y_2 - y_2^*)^2 \left.\frac{\partial H}{\partial y_2^2}^2\right|_{y_i^*} + (y_2 - y_2^*)(y_3 - y_3^*) \left.\frac{\partial H}{\partial y_2 \partial y_3}^2\right|_{y_i^*} - \frac{\mu^6}{L*^{10}} \frac{R_\oplus^4 J_2^2}{4} A(y_i^*) \cos 2x_2 \tag{5.38}$$

By modifying the new separable form of the total Hamiltonian using the classical action angle variables (ψ, J), one can create a quasi-integral $\overline{J}$. This quasi-integral can now be used to look at the level curves for canonical coordinate pairs (x_2, y_2) and (x_3, y_3). "Choatic motion is expected in the regions where level curves cross the separatrix associated with the resonance in mean motion."[32]

The tesseral terms employed in their analysis for the Molinya and Tundra type orbits are given in Table IX.

Table IX. Tesseral terms used by Delhaise and Henrard[32] to study the problem of resonance in mean motion for critically inclined orbits.

12 hr Orbit		24 hr Orbit	
l m p q	l m p q	l m p q	l m p q
2 2 0 -1	2 2 1 1	2 2 0 0	2 2 1 2
3 2 1 0	3 2 2 2	3 2 0 -1	3 2 1 1
5 2 2 0	4 4 1 0	3 2 2 3	4 2 1 0
4 4 2 2	5 4 2 1	3 3 0 0	3 3 1 2
5 4 3 3	6 4 3 2	3 3 2 4	4 3 0 -1
6 6 2 1	6 6 3 3	4 3 1 1	4 3 2 3
7 6 3 2	7 6 4 4	4 4 1 2	5 5 1 2
8 6 4 3	9 8 4 3		

B. Variation of the Orbit Elements

The orbit elements for each individual satellite in a *Flower Constellation* will vary based on the perturbations induced upon them. These variations can be classified as secular, short-period, and long-period effects. The classic orbit elements can be written as

$$\begin{aligned} a &= \bar{a} + \Delta a_{SP} + \Delta a_{LP} \\ e &= \bar{e} + \Delta e_{SP} + \Delta e_{LP} \\ i &= \bar{i} + \Delta i_{SP} + \Delta i_{LP} \\ \omega &= \bar{\omega} + \dot{\omega}_{sec}\Delta t + \Delta\omega_{SP} + \Delta\omega_{LP} \\ \Omega &= \bar{\Omega} + \dot{\Omega}_{sec}\Delta t + \Delta\Omega_{SP} + \Delta\Omega_{LP} \\ M &= M_0 + \dot{M}_{0,sec}\Delta t + \Delta M_{SP} + \Delta M_{LP} \end{aligned} \tag{5.39}$$

Secular effects (SEC) are the most pronounced in that the elements will grow as a linear function of time. Note that the elements $a, e,$ and $i,$ have no secular effects. Short-period (SP) and long-period (LP) perturbations give rise to bounded sinusoidal motions. A common practice is to average out the short period and long period effects so that only secular effects remain. This allows one to see the big picture of how perturbations are impacting orbit elements over time.

Analytic and semi-analytic theories studying secular, short-period, and long-period perturbations have been around since the 1960's. Brouwer,[33] Kozai,[34,35] Lyddane,[36] Merson,[37] and Deprit,[38] have all written classic works on treating orbit element propagation under the influence of geopotential perturbations in an analytic fashion. Some of these analytic theories include effects up to J_6; however, higher order terms beyond J_6 become extremely computationally expensive and are best reserved for modern automated symbolic manipulation.

From Vallado,[20] the secular rates of $\Omega, \omega,$ and M_0 originally derived by Merson,[37] including the first six zonal harmonics, can be expressed as:

$$\begin{aligned}\dot{\Omega}_{sec} = \frac{d\Omega}{dt} = &-\frac{3J_2R_\oplus^2 n\cos i}{2p^2} + \frac{3J_2^2R_\oplus^4 n\cos i}{32p^4}\left[12-4e^2-(80+15e^2)\sin^2 i\right] \\ &+\frac{15J_4R_\oplus^4 n\cos i}{32p^4}\left[8+12e^2-(14+21e^2)\sin^2 i\right] \\ &-\frac{105J_6R_\oplus^6 n\cos i}{1024p^6}\left[64+160e^2+120e^4-(288+720e^2+540e^4)\sin^2 i\right. \\ &\left.+(264+660e^2+495e^4)\sin^4 i\right]\end{aligned} \tag{5.40}$$

$$\begin{aligned}\dot{\omega}_{sec} = \frac{d\omega}{dt} =& \frac{3nJ_2R_\oplus^2}{4p^2}\left[4-5\sin^2 i\right] \\ &+ \frac{9nJ_2^2R_\oplus^4}{384p^4}\left[56e^2+(760-36e^2)\sin^2 i-(890+45e^2)\sin^4 i\right] \\ &- \frac{15J_4R_\oplus^4 n}{128p^4}\left[64+72e^2-(248+252e^2)\sin^2 i+(196+189e^2)\sin^4 i\right] \\ &+ \frac{105J_6R_\oplus^6 n}{2048p^6}\left[256+960e^2+320e^4-(2048+6880e^2+2160e^4)\sin^2 i\right. \\ &\left.+(4128+13080e^2+3960e^4)\sin^4 i-(2376+14520e^2+2145e^4)\sin^6 i\right]\end{aligned} \tag{5.41}$$

$$\begin{aligned}\dot{M}_{0,sec}\frac{dM_0}{dt} =& \frac{3nR_\oplus^2J_2\sqrt{1-e^2}}{4p^2}\left[2-3\sin^2 i\right] \\ &+ \frac{3nR_\oplus^4J_2^2}{512p^4\sqrt{1-e^2}}\left[320e^2-280e^4+(1600-1568e^2+328e^4)\sin^2 i\right. \\ &\left.+(-2096+1072e^2+79e^4)\sin^4 i\right] \\ &- \frac{45J_4R_\oplus^4e^2n\sqrt{1-e^2}}{128p^4}\left[-8+40\sin i-35\sin^2 i\right] \\ &+ \frac{35J_6R_\oplus^6n\sqrt{1-e^2}}{2048p^6}\left[-128+320e^2+240e^4+(1344-3360e^2-2520e^4)\sin i\right. \\ &\left.+(-1512+3780e^2+2835e^4)\sin^2 i-(-1848+4620e^2+3465e^4)\sin^4 i\right]\end{aligned} \tag{5.42}$$

where $p = a(1-e^2)$, $n^2a^3 = \mu$, and $J_2 = 1.0826269\times10^{-3}$, $J_4 = -1.62042999\times10^{-6}$, and $J_6 = 5.408436161399631\times10^{-7}$ are the zonal harmonic expansion coefficients given by the JGM-2 geopotential model.[20] Equation (5.40) was extended up to $O(J_{14})$ by King-Hele, Cook, and Rees.[39] Note that only even zonal terms cause a secular drift. Also, Kozai included J_2^3 terms and the coupled terms for J_2J_4.[35] Furthermore, using Brouwer's averaging method, the secular variation of the RAAN and argument of perigee due to the

J_2^2 term can be expressed as

$$\dot{\Omega}_{J_2^2} = \frac{3J_2^2 R_\oplus^4 n\cos i}{8p^4}\left[-9-e^2-6\sqrt{1-e^2}+\left(10-\frac{5}{4}e^2+9\sqrt{1-e^2}\right)\sin^2 i\right] \tag{5.43}$$

$$\dot{\omega}_{J_2^2} = \frac{9nJ_2^2 R_\oplus^4}{384p^4}\left[1062+168e^2+576\sqrt{1-e^2}+\left(-2382-108e^2-1584\sqrt{1-e^2}\right)\sin^2 i + \left(1290-135e^2+1080\sqrt{1-e^2}\sin^4 i\right)\right] \tag{5.44}$$

Kozai used a different method of averaging and generated secular variations due to the J_2^2 term as

$$\dot{\Omega}_{J_2^2} = \frac{3J_2^2 R_\oplus^4 n\cos i}{32p^4}\left[-216-24e^2+288\sqrt{1-e^2}+\left(240-30e^2-432\sqrt{1-e^2}\right)\sin^2 i\right] \tag{5.45}$$

$$\dot{\omega}_{J_2^2} = \frac{9nJ_2^2 R_\oplus^4}{384p^4}\left[192+56e^2-192\sqrt{1-e^2}+\left(-172+288\sqrt{1-e^2}\right)\sin^2 i+e^2\sin^4 i\right] \tag{5.46}$$

1. Numerical Simulations

The secular drift rates for the right ascension of the ascending node, the argument of perigee, and the mean anomaly are critical to the overall integrity of a *Flower Constellation*. These drift rates are a function of the geopotential harmonic coefficients, eccentricity, inclination, and the semi-major axis. Here the secular drift rates will be plotted as a function of τ instead of semi-major axis.

Figures 53 through 55 show the secular drifts at the critical inclination of 63.4°. What is important to note here is the choice of τ and eccentricity as it pertains to the three orbit elements. For the change in RAAN depicted in Figure 53 on page 126, as $\tau \to \infty$ coupled with circular and nearly circular orbits a large shift over one year is created. Highly eccentric orbits appear to have the smallest shift in RAAN.

The shift in the argument of perigee, as expected, is very small. Only a close approximation of the true critical inclination was used (i.e. only one decimal of precision). As one can see once again in Figure 54 on page 127, large values of τ lead to large changes in the argument of perigee. Also note that in this truncated perturbation expansion where only J_2 zonal terms are considered(See Equation (5.41)), as the eccentricity goes to one, the perturbation goes to zero.

For the mean anomaly at the critical angle, the smallest secular change occurs in highly eccentric orbits and for small τ. This is shown in Figure 55 on page 128. Figures 56 through 58 shows the same scenario as before except that even zonal terms up to J_6 have been included. Note that qualitatively, incorporating higher harmonics has very little change in the overall secular drift rate.

Now consider the secular drift rates when the orbit inclination is some other desired inclination besides the critical inclination. Figures 59 through 61 depicts the secular drift rate for orbits at an inclination of 27.5° and includes up to J_6 zonal harmonics along with Kozai's J_2^3 and $J_2 J_4$ terms. Here one will notice that there is a significant change in the argument of perigee drift and the mean anomaly drift. The right ascension of the ascending node is unaffected by inclination for all intents and purposes. The inclusion of the higher order harmonics changes the qualitative results only slightly. The major shift occurs due to the orbit inclination being something other than a critical inclination.

In general, the perturbation of the argument of the perigee and the mean anomaly is the most critical to the *Flower Constellations*. A secular drift in the RAAN is not critical for most *Flower Constellations* because it has no effect on the overall shape or character of the *Flower Constellation*. The *Flower Constellation* merely spins about the axis of symmetry (reoriented *Flower Constellations* require additional analysis). The shift in the argument of perigee, however, will cause the line of apsides to rotate. The effect on the relative path is somewhat akin to a flower"wilting" in the sun. Perturbations of the mean

anomaly will cause the carefully orchestrated and synchronized patterns to deviate creating a potential for collision. Therefore, the mission designer must decide upon an orbit period knowing that certain values of τ will cause significant changes in the phasing and that inclination choices other than the critical inclination will most likely require a consistent level of control throughout the constellation lifetime.

2. Incorporating Higher Order Zonal Harmonics

In Section I.2, the anomalistic orbit period was determined as a function of the semi-major axis, the height of perigee, the orbit inclination, and J_2. However, if one is wanting to perform a more detailed analysis using higher order perturbations, then these must be included into the computation of the nodal period as well.

Eq. (1.9) on page 13 can be written in the more general form

$$T_\Omega = \frac{N_d}{N_p}\left(\frac{2\pi}{\omega_\oplus - \dot{\Omega}}\right)\left(1 + \frac{\dot{M}_0 + \dot{\omega}}{n}\right) \tag{5.47}$$

One can now substitute in the 6th order perturbative terms given in Eqs. (5.40) through (5.46) and solve for the semi-major axis just as was done in Section I.B.3. Given that this system of equations is highly nonlinear, a good initial guess for the semi-major axis would be the solution containing only the J_2 term.

C. Effects of Third-Body Interactions

Satellites that are in medium to high Earth orbits will more than likely require the inclusion of perturbative effects stemming from the gravitational pull of the moon and Sun. These so-called luni-solar effects in particular and third-body effects in general can cause long term changes to the orbit elements of a satellite. Third-body effects only evidence secular perturbations in the RAAN and argument of perigee while long-period perturbations can be

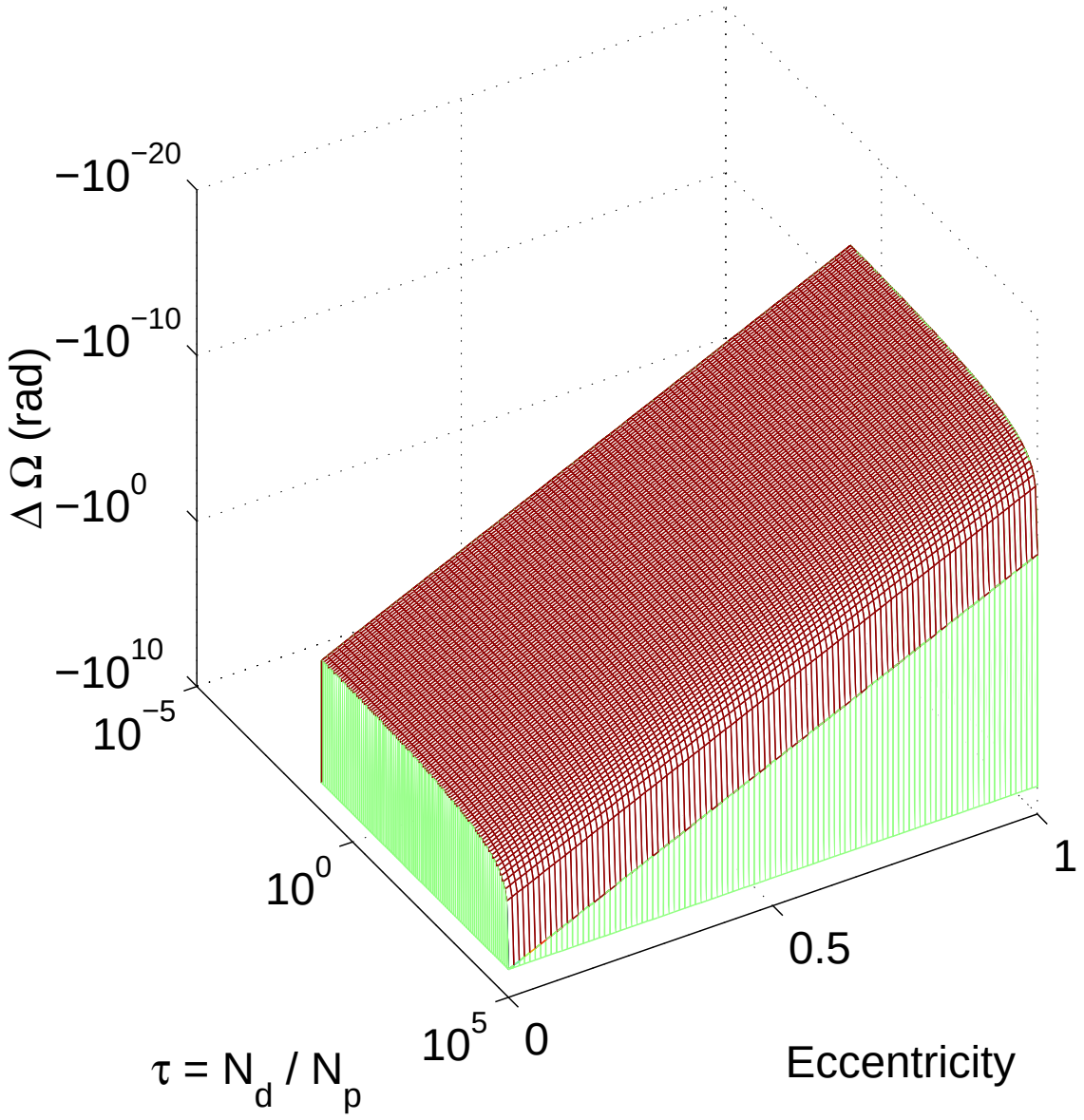

Fig. 53. The change in the RAAN over one year is plotted for various values of τ and eccentricity at the critical orbit inclination of 63.4°. Only the J_2 zonal term has been included.

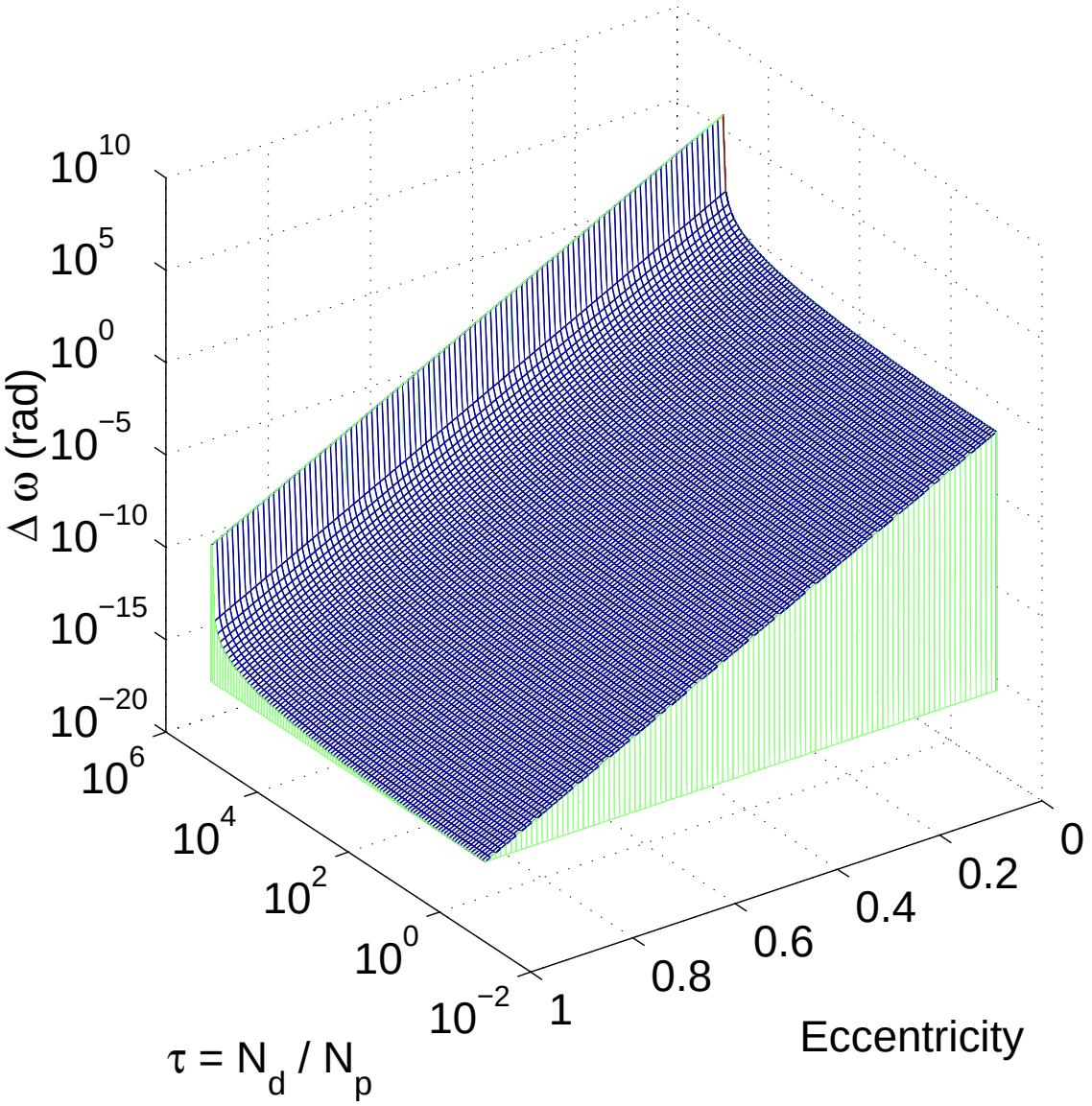

Fig. 54. The change in the argument of the perigee over one year is plotted for various values of τ and eccentricity at the critical orbit inclination of 63.4°. Only the J_2 zonal term has been included.

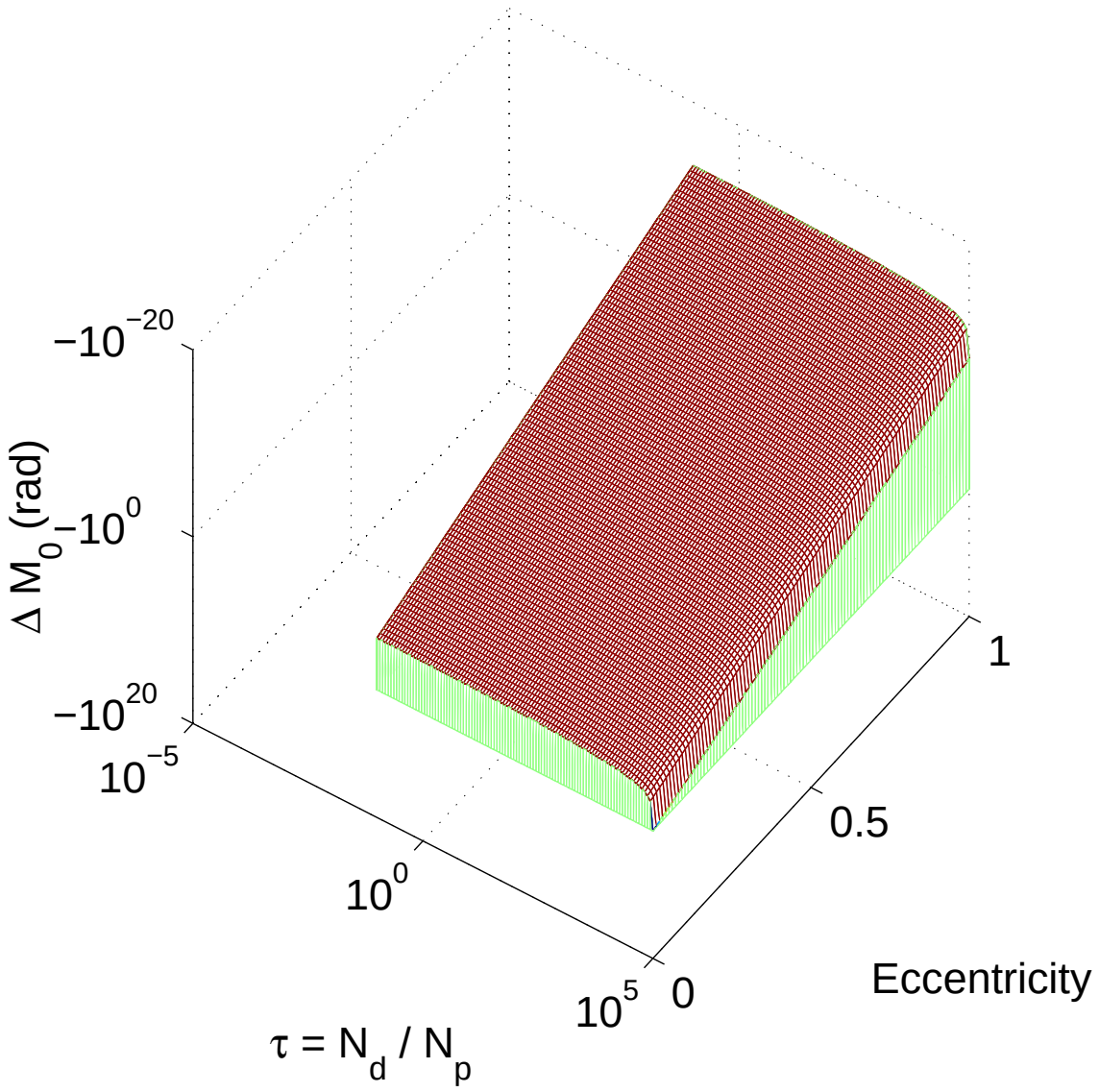

Fig. 55. The change in the mean anomaly over one year is plotted for various values of τ and eccentricity at the critical orbit inclination of 63.4°. Only the J_2 zonal term has been included.

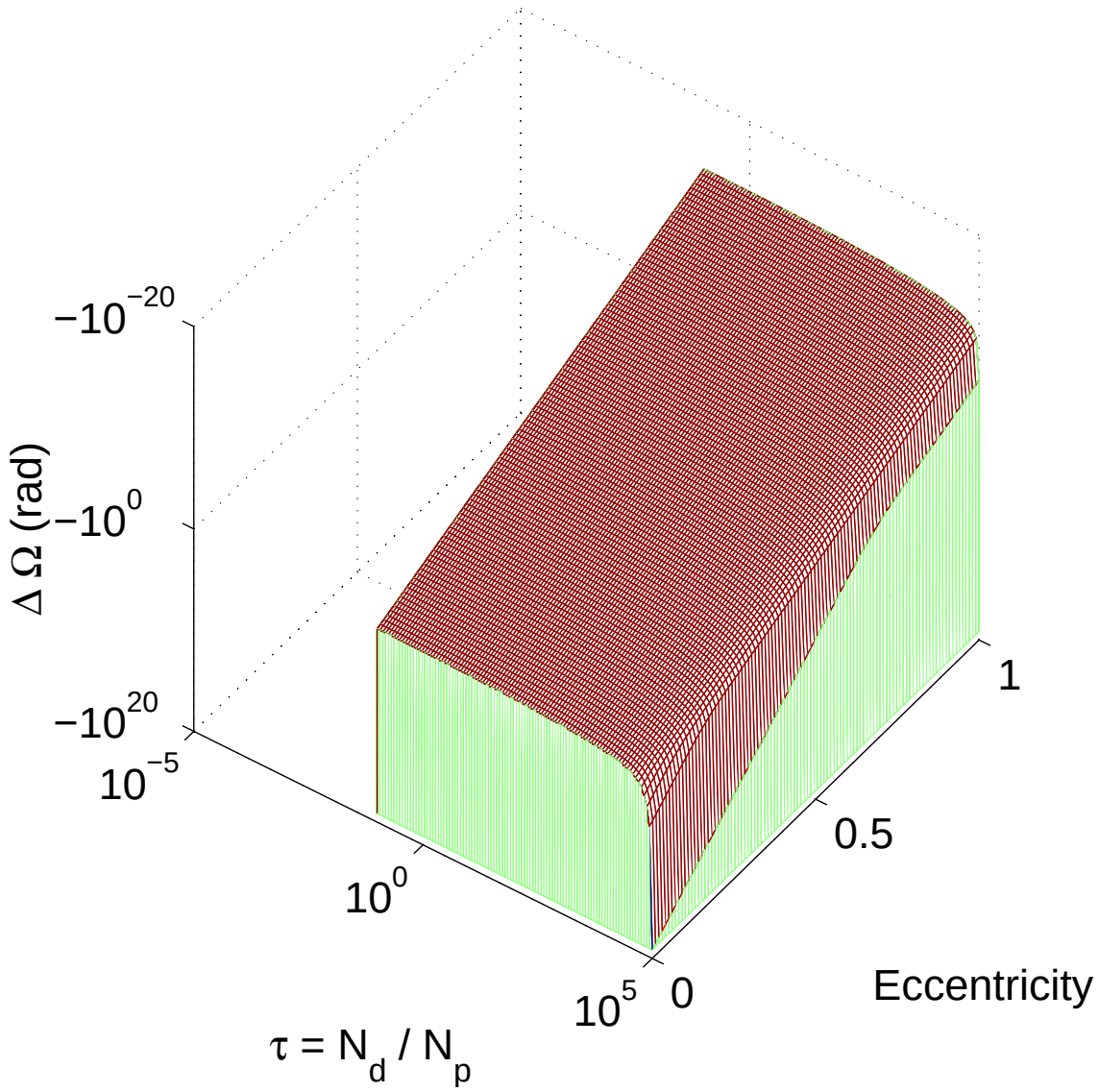

Fig. 56. The change in the RAAN over one year is plotted for various values of τ and eccentricity at the critical orbit inclination of 63.4°. Zonal terms up to J_6 have been included.

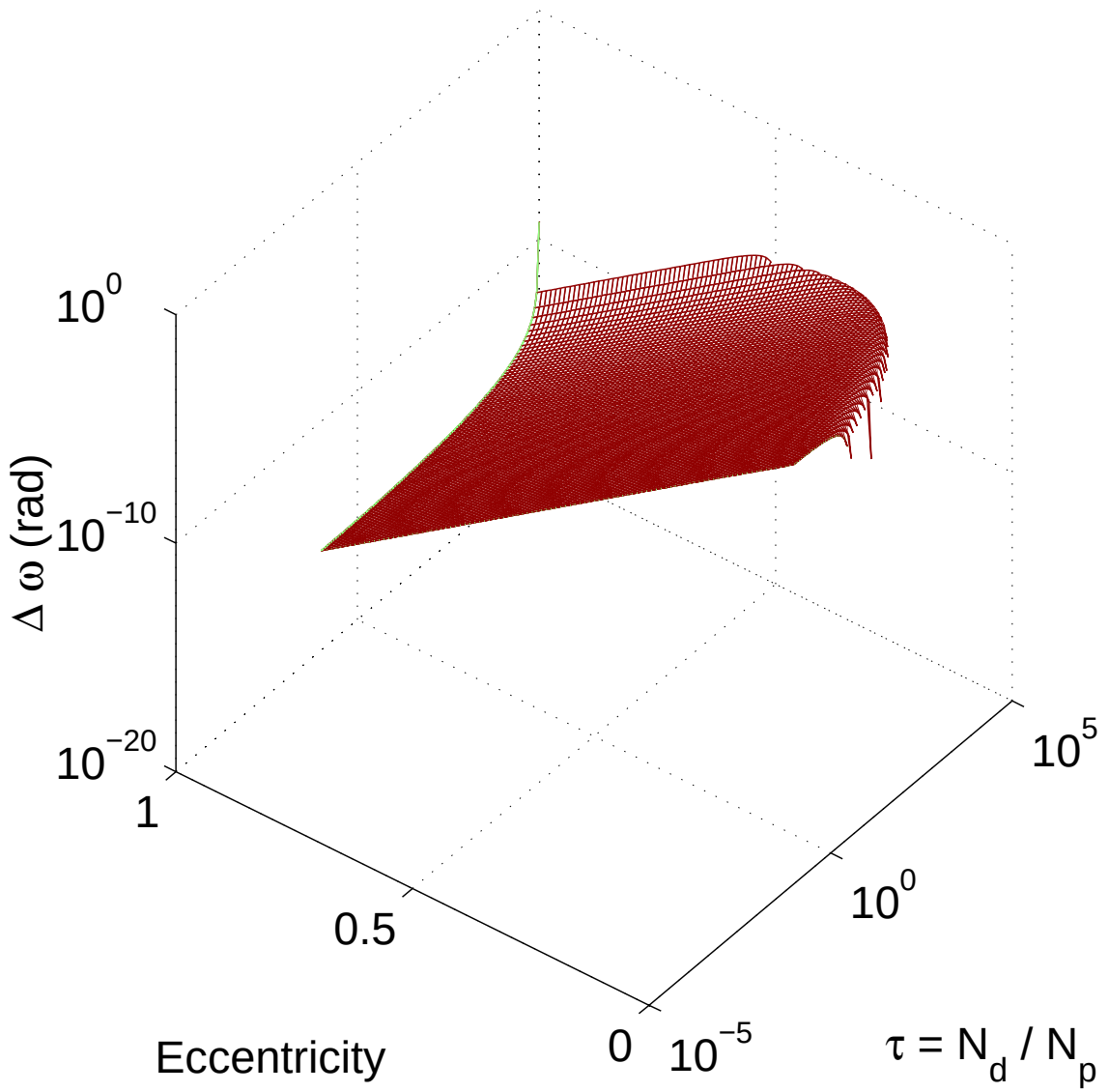

Fig. 57. The change in the argument of the perigee over one year is plotted for various values of τ and eccentricity at the critical orbit inclination of 63.4°. Zonal terms up to J_6 have been included.

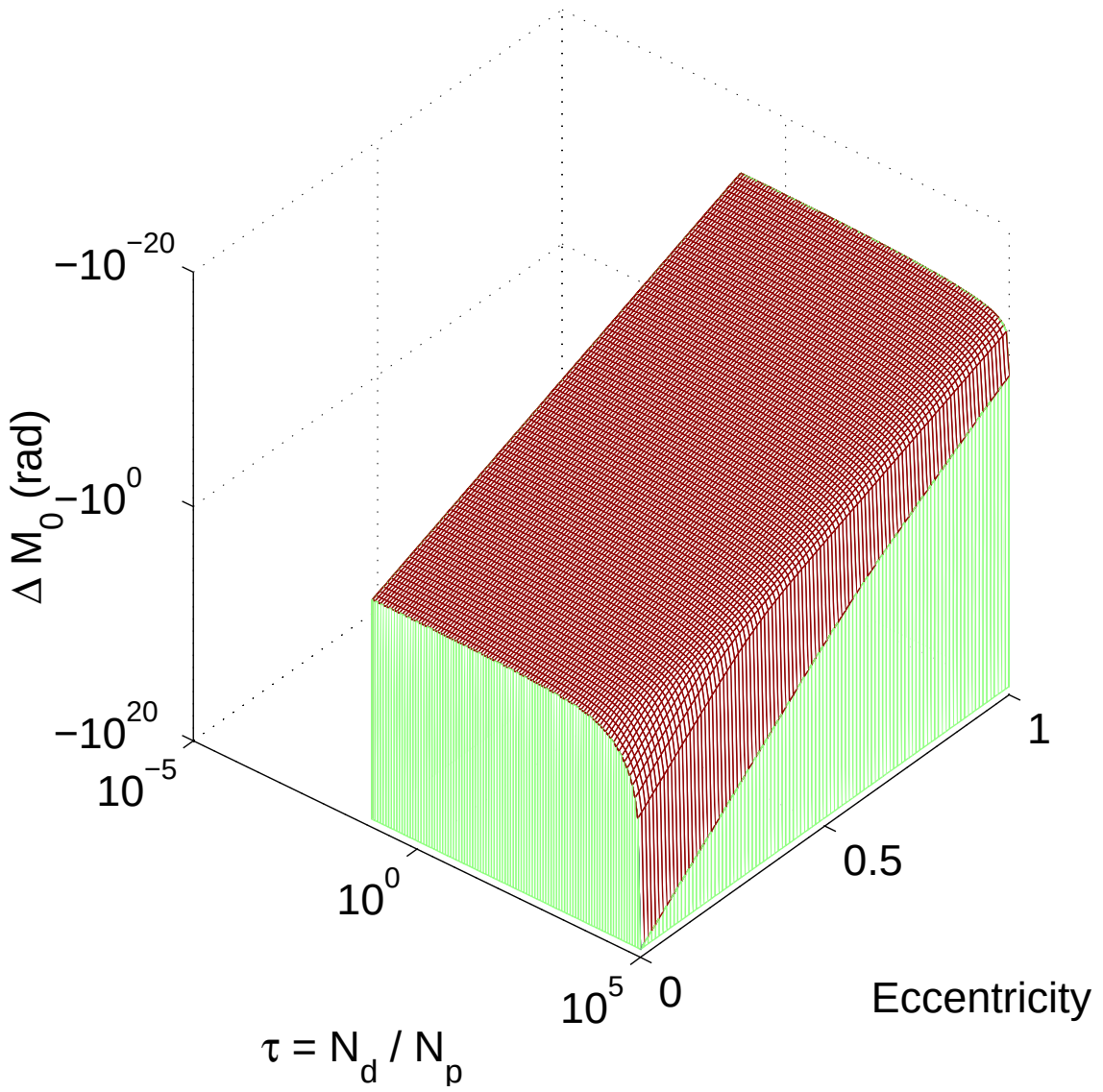

Fig. 58. The change in the mean anomaly over one year is plotted for various values of τ and eccentricity at the critical orbit inclination of 63.4°. Zonal terms up to J_6 have been included.

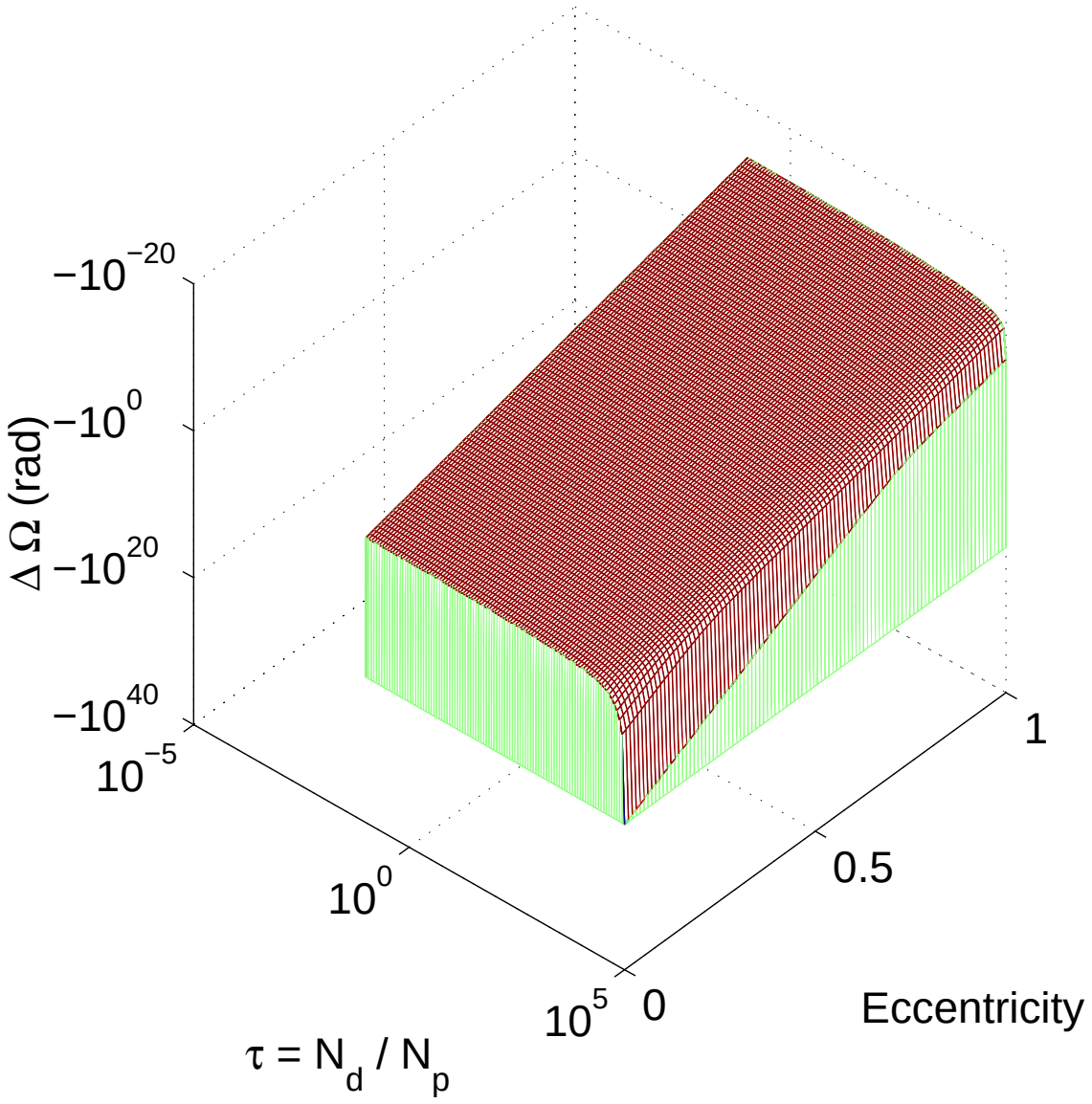

Fig. 59. The change in the RAAN over one year is plotted for various values of τ and eccentricity at an orbit inclination of 27.5°. Zonal terms up to J_6 have been included along with Kozai's J_2^3 and $J_2 J_4$ terms.

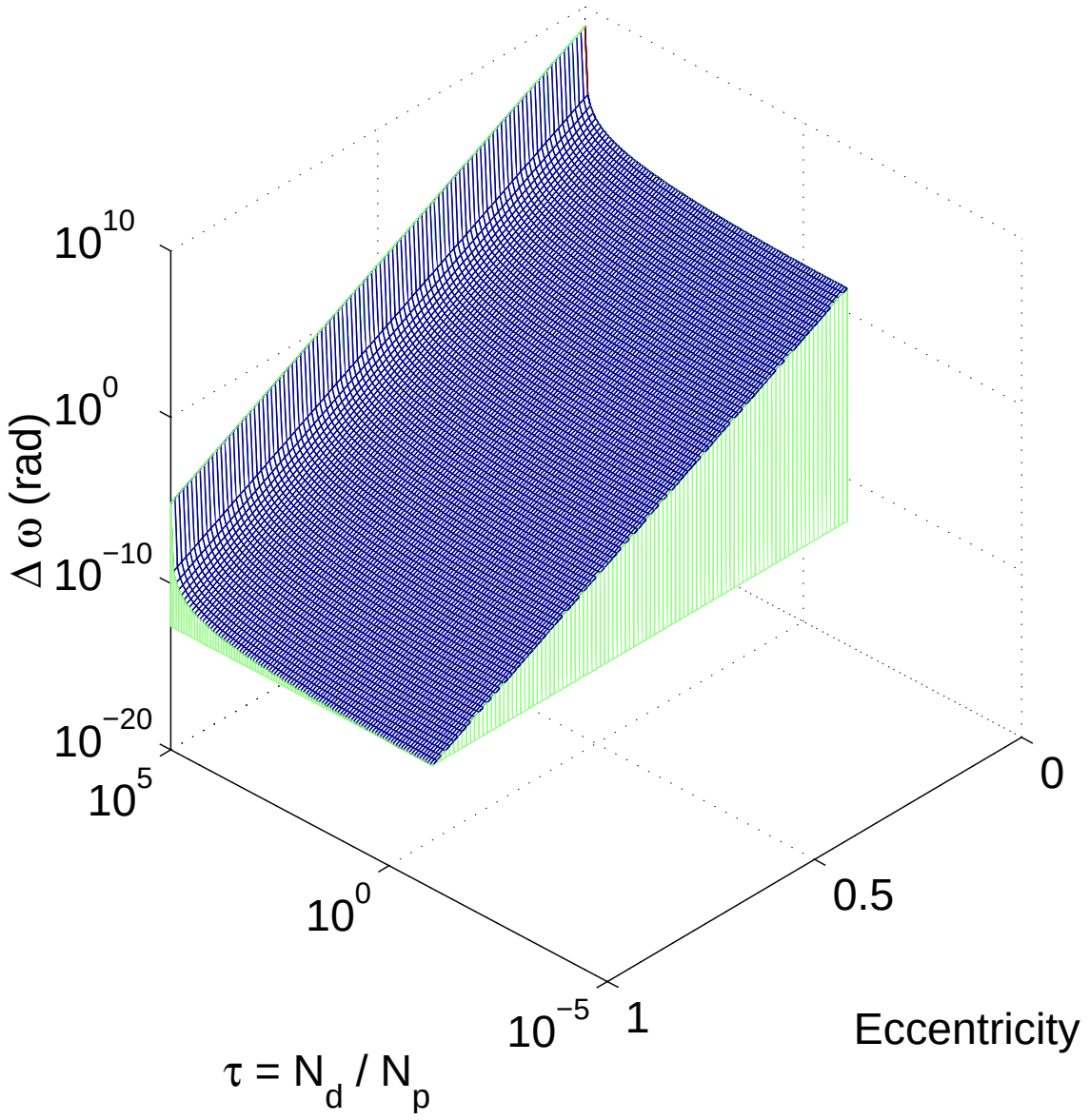

Fig. 60. The change in the argument of the perigee over one year is plotted for various values of τ and eccentricity at an orbit inclination of 27.5°. Zonal terms up to J_6 have been included along with Kozai's J_2^3 and $J_2 J_4$ terms.

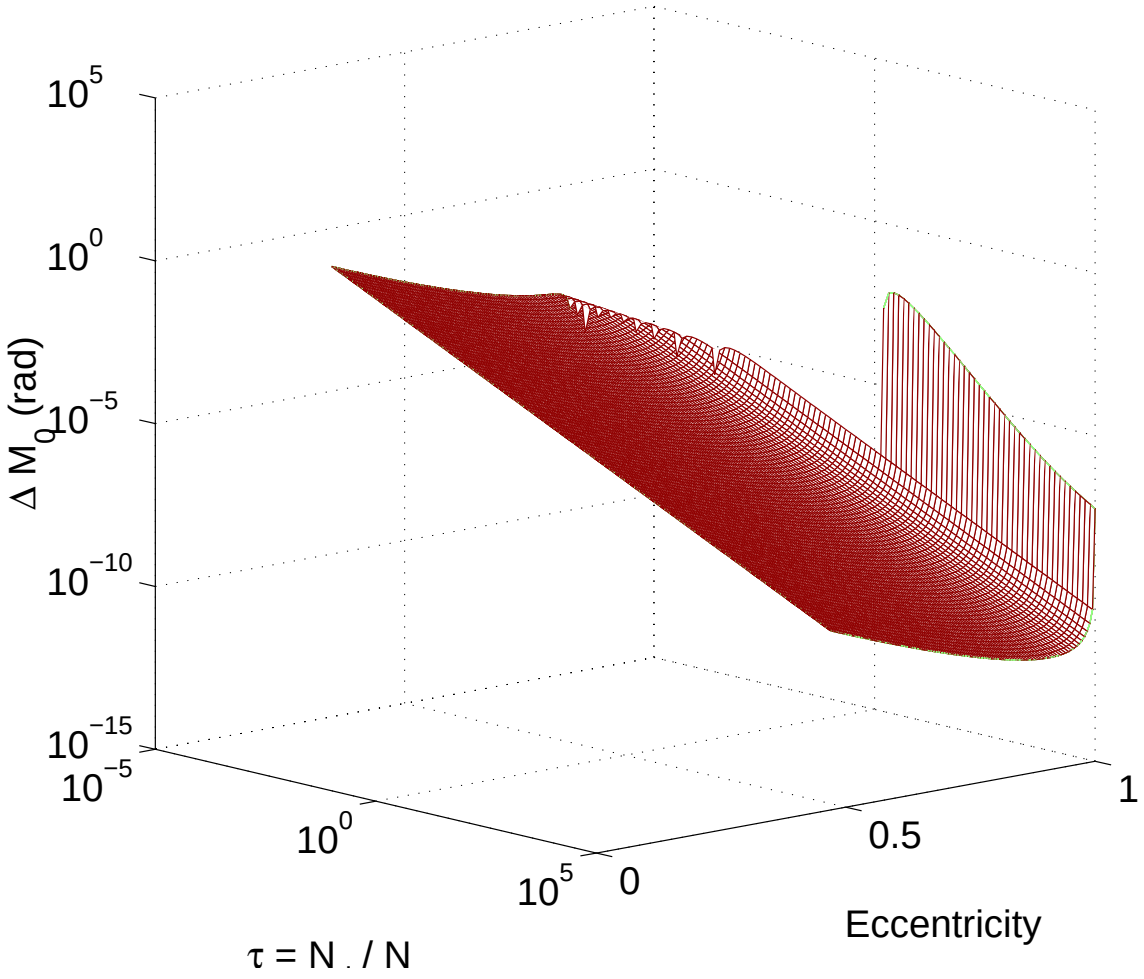

Fig. 61. The change in the mean anomaly over one year is plotted for various values of τ and eccentricity at an orbit inclination of 27.5°. Zonal terms up to J_6 have been included along with Kozai's J_2^3 and $J_2 J_4$ terms.

seen in the eccentricity, orbit inclination, RAAN, and argument of the perigee. Resonance can also occur when the time rate of change of the arguments of periodic terms approaches zero.[40]

Assuming that the third body is in a general eccentric orbit, Smith[41] determined that the secular rate of change of for the RAAN and argument of the perigee can be expressed as

$$\dot{\Omega}_{sec} = \frac{3\mu_3(1-e^2)^3(1+5e^2)[2-3\sin^2 i^3]^{3/2}}{8r_3^3 n(1-e_3^2} \cos i \tag{5.48}$$

$$\dot{\omega}_{sec} = \frac{3\mu_3(1-e^2)^3[2-3\sin^2 i_3]}{16r_3^3 n(1-e_3^2)^{3/2}} \left[4-5\sin^2 i+5e^2\left(3-\frac{7}{2}\sin^2 i\right)\right] \tag{5.49}$$

where variables with the subscript 3 refer to the third body and variables without subscripts refer to the satellite.

Kamel, Ekman, and Tibbitts[42] presented a method for analyzing east-west station-keeping requirements for nearly synchronous satellites under the influence of luni-solar perturbations. A two maneuver approach was presented that keeps important tesseral harmonic terms. The authors found that the initial semi-major axis of the satellite deviates in a fashion dependent upon the initial relative position of the satellite to the Moon and Sun.

D. Effect of Solar Radiation Pressure

Solar radiation pressure (SRP) can become a significant factor in a perturbation analysis for a satellite at an altitude above 800 *km*. Above this altitude, solar radiation pressure forces can exceed those of atmospheric drag. The periodic variations of the orbit parameters as induced by solar radiation pressure can have periods of up to one year due to the Earth's yearly rotation about the Sun. SRP is generally very small for most satellites except for those with large surface areas and a low overall mass (e.g. Solar Sails). Satellites that pass into and out of shadow as they orbit the Earth can have complex periodic effects.

The rate of change of the orbit elements due to SRP effects for a satellite in sunlight for its entire orbit can be expressed as[20]

$$\dot{a} = 0 \tag{5.50}$$

$$\dot{e} = \frac{3\sqrt{1-e^2}}{2na} S_P \tag{5.51}$$

$$\dot{r}_p = -a\dot{(}e) \tag{5.52}$$

$$\dot{i} = \frac{3We\cos\omega}{2na\sqrt{1-e^2}} \tag{5.53}$$

$$\dot{\Omega} = -\frac{3We\sin\omega}{2na\sqrt{1-e^2}\sin i} \tag{5.54}$$

$$\dot{\omega} = -\left(\frac{3\sqrt{1-e^2}}{2nae} R_p + \dot{\Omega}\cos i\right) \tag{5.55}$$

where

$$R_P = F_{SR}\left\{\left[\cos^2\left(\frac{\varepsilon}{2}\right)\cos(\omega+\Omega-\lambda_\odot)+\sin^2\left(\frac{\varepsilon}{2}\right)\cos(\omega+\Omega+\lambda_\odot)\right]\cos^2\left(\frac{i}{2}\right)\right.$$
$$\left[\cos^2\left(\frac{\varepsilon}{2}\right)\cos(\omega-\Omega+\lambda_\odot)+\sin^2\left(\frac{\varepsilon}{2}\right)\cos(\omega-\Omega-\lambda_\odot)\right]\sin^2\left(\frac{i}{2}\right)$$
$$\left.+\frac{1}{2}[\cos(\omega-\lambda_\odot)-\cos(\omega+\lambda_\odot)]\sin i\sin\varepsilon\right\} \quad (5.56)$$

$$S_P = F_{SR}\left\{\left[\cos^2\left(\frac{\varepsilon}{2}\right)\sin(\omega+\Omega-\lambda_\odot)+\sin^2\left(\frac{\varepsilon}{2}\right)\cos(\omega+\Omega+\lambda_\odot)\right]\cos^2\left(\frac{i}{2}\right)\right.$$
$$\left[\cos^2\left(\frac{\varepsilon}{2}\right)\sin(\omega-\Omega+\lambda_\odot)+\sin^2\left(\frac{\varepsilon}{2}\right)\cos(\omega-\Omega-\lambda_\odot)\right]\sin^2\left(\frac{i}{2}\right)$$
$$\left.-\frac{1}{2}[\sin(\omega-\lambda_\odot)-\sin(\omega+\lambda_\odot)]\sin i\sin\varepsilon\right\} \quad (5.57)$$

$$W\sin\omega = -\frac{F_{SR}}{2}\left\{[\cos(\omega+\Omega-\lambda_\odot)-\cos(\omega-\Omega-\lambda_\odot)]\sin\left(\frac{i}{2}\right)\cos^2\left(\frac{\varepsilon}{2}\right)\right.$$
$$[\cos(\omega+\Omega+\lambda_\odot)-\cos(\omega-\Omega-\lambda_\odot)]\sin\left(\frac{i}{2}\right)\sin^2\left(\frac{\varepsilon}{2}\right)$$
$$\left.+[\cos(\omega+\lambda_\odot)-\cos(\omega-\lambda_\odot)]\cos i\sin\varepsilon\right\} \quad (5.58)$$

$$W\cos\omega = \frac{F_{SR}}{2}\left\{[\sin(\omega+\Omega-\lambda_\odot)-\sin(\omega-\Omega-\lambda_\odot)]\sin\left(\frac{i}{2}\right)\cos^2\left(\frac{\varepsilon}{2}\right)\right.$$
$$[\sin(\omega+\Omega+\lambda_\odot)-\sin(\omega-\Omega-\lambda_\odot)]\sin\left(\frac{i}{2}\right)\sin^2\left(\frac{\varepsilon}{2}\right)$$
$$\left.+[\sin(\omega+\lambda_\odot)-\sin(\omega-\lambda_\odot)]\cos i\sin\varepsilon\right\} \quad (5.59)$$

and F_{SR} is the SRP disturbing acceleration, $\lambda_\odot$ is the ecliptic longitude of the Sun, and $\varepsilon \approx 23.5^\circ$. Note that a resonance occurs when $\dot{\omega} \pm \dot{\Omega} \pm \dot{\lambda}_\odot = 0$ or when $\dot{\omega} \pm \dot{\Omega} = 0$. For a complete discussion of the effects of solar radiation pressure including detailed equations for when a satellite moves into and out of sunlight, please refer to Vallado,[20] Burns et al.,[43] and Cook.[40]

E. Frozen Orbits

In general, all of the perturbations discussed in this chapter prevent the orbit ground track from repeating precisely in addition to destroying carefully planned constellation geometry. While the symmetry of the *Flower Constellation* will be maintained (each orbit essentially experiences identical perturbations), the original design of the *Flower Constellation* will be lost. By judicious choice of the orbit parameters, one can attempt to eliminate and/or minimize the effect of some of the geopotential perturbations. In that regard, when we choose a parameter such that it will eliminate a known perturbation, the orbit is said to be *frozen*.

The J_2 effect can be characterized by linearizing the aspherical gravitational potential equation. From this, we find that J_2 perturbation affects only Ω, ω, and the mean anomaly M. The secular equations resulting from this linearization are given in the previous section in Eq. (1.5). More extensive analysis can be done to include not only the zonal harmonics, but also tesseral and sectorial harmonics. However, the resulting equations will be much more complex and are beyond the scope of this section.

The change in the argument of the perigee will cause the line of apsides to move. While the symmetry of the *Flower Constellation* will be maintained (each orbit experiences identical perturbations), the original design of the *Flower Constellation* will be lost. The argument of perigee can be frozen by selecting one of the critical inclinations, specifically $i = 63.4^\circ$ or $i = 116.6^\circ$. Note that the choice of critical inclination will have a major impact upon both the shape and behavior of the *Flower Constellation*. However, any inclination can be selected provided that the control effort required to maintain the *Flower Constellation* falls within acceptable limits for the mission.

For the specific case that the orbit inclination is a critical inclination, i_{cr}, Equation

(1.9) can be simplified because $\dot{\omega}$ is now zero, which results in

$$T = \frac{2\pi}{\omega_{\oplus}} \frac{N_d}{N_p} \left(1 + 2\xi \frac{n}{\omega_{\oplus}} \cos i_{cr} \right)^{-1} \left\{ 1 + \xi \left[(2 - 3\sin^2 i_{cr}) \sqrt{1 - e^2} \right] \right\} \tag{5.60}$$

Equation (5.60) governs the anomalistic period for a *Flower Constellation* under the influence of the J_2 perturbation when the inclination is a critical inclination.

CHAPTER VI

CONCLUSIONS AND FUTURE WORK

The fundamental theory of *Flower Constellations* has been presented. The concepts of the Broglio Clover, LOOPUS, and JOCOS systems among others have been extended to a general method for generating constellations of satellites with orbits that are compatible with a rotating reference frame. Based upon the phasing scheme adopted in this work, it was shown that unique *Flower Constellations* can be generated using what is termed "secondary closed paths." The existence and uniqueness of secondary closed paths were proved and the specific choices of *Flower Constellation* parameters that create secondary paths were derived.

A new, and more general, phasing scheme is being considered for future work. Eq. (1.27) on page 19 will be expressed in the following way

$$\Delta M_0 = 2\pi \frac{F_n}{F_d} \frac{N_p}{N_d} + \frac{2\pi F_h}{N_d} \tag{6.1}$$

where F_h is a new phasing parameter that allows the placement of satellites be shifted. This is an effort to alleviate the requirement that satellites be placed sequentially. Incorporating this new phasing parameter will require a new study of secondary closed paths.

Guidelines for designing a constellation of satellites using the *Flower Constellation* technique have also been presented. A variety of categories of *Flower Constellations* that could be achieved above and beyond the simple flower petals that were originally conceived when this work first began were also presented. Examples of how to generate currently known constellation types were demonstrated using the *Flower Constellation* theory.

Future work will focus on the inverse process whereby a designer would specify the desired shape and then the required *Flower Constellation* parameters to generate that constellation would be determined. While not explicitly presented herein, creating an arbitrar-

ily defined shaped onto a single relative trajectory proved to be enormously difficult. Thus, future work will be necessary to formalize an optimal method of *Flower Constellation* parameters. One such technique under consideration is genetic algorithms.

One inverse design technique based upon the Flower Constellation concept is presented. Using a number of methods, an arbitrarily prescribed shape is projected onto a *Flower Constellation* surface which is constructed from an infinite set of relative trajectories that are differentially separated in RAAN. The intersection of the projected shape and the *Flower Constellation* surface is computed, and then the satellites are placed at these intersection points to create a constellation/formation. These formations collapse to a line at apogee, but reform twice on each "petal". Non-symmetric formations will invert as they cross from one side of the globe to the other.

Further work needs to be performed in the application of *Flower Constellations* to telecommunications, coverage, global navigation, and formation flying. While telecommunications and coverage have been explored over the last decade or so to a certain extent, there are other unique applications of *Flower Constellations* that have not yet been fully exploited. Additionally, the lifetime of *Flower Constellations* and the cost to launch these kinds of constellations versus more traditional ones needs to be investigated.

Perturbations due to the Earth's oblateness, solar radiation pressure, third-body effects, and resonance were explored. Much work has already been done in the literature regarding the perturbation and control of resonant orbits. Because there are an infinity of *Flower Constellations* that all have varying choices for the orbit parameters, performing a perturbation study is very difficult if one desires to try and convey some sense of generality for all *Flower Constellations*. Therefore, encapsulated results for the various perturbations were presented with appropriate citations so that the mission designer can perform a perturbation analysis on a particular *Flower Constellation* of interest.

REFERENCES

[1]Broglio, L., "Una Politica Spaziale per il Nostro Paese, Prospettive del Progetto San Marco: Il Sistema Quadrifoglio," Centro di Ricerca Progetto San Marco, Internal Report, 1981.

[2]Castronuovo, M. M., Bardone, A., and Ruscio, M. D., "Continuous Global Earth Coverage By Means of Multistationary Orbits," *Advances in the Astronautical Sciences*, Vol. 99, 1998, pp. 1021–1039.

[3]Turner, A. E., "Non-Geosynchronous Orbits for Communications to Off-Load Daily Peaks in Geostationary Traffic," American Astronautical Society, AAS Paper 87-547, 1987.

[4]Nugroho, J., Draim, J., and Hudyarto, "A Satellite System Concept for Personal Communications for Indonesia," Paper Presented at the United Nations Indonesia Regional Conference on Space Science and Technology, Bandung, Indonesia, 1993.

[5]Walker, J., "Some Circular Orbit Patterns Providing Continuous Whole Earth Coverage," *British Interplanetary Journal*, Vol. Soc. 24, 1971, pp. 369–384.

[6]Walker, J., "Satellite Constellations," *British Interplanetary Journal*, Vol. Soc. 37, 1984, pp. 559–572.

[7]Beste, D., "Design of Satellite Constellations for Optimal Continuous Coverage," *IEEE Transactions on Aerospace and Electronic Systems*, Vol. 14(3), 1978, pp. 466–473.

[8]Proulx, R., Smith, J., Draim, J., and Cefola, P., "Ellipso Gear Array - Coordinated Elliptical/Circular Constellations," American Astronautical Society, AAS Paper 98-4383, 1998.

[9]Draim, J., "Elliptical Orbit MEO Constellations: A Cost-Effective Approach for Multi-Satellite Systems," *Space Technology*, Vol. 16, No. 1, 1996.

[10]Solari, G. and Viola, R., "M-HEO: The Optimal Satellite System for the Most Highly Populated Regions of the Northern Hemisphere," Integrated Space/Terrestrial Mobile Networks Action Final Summary, ESA COST 227 TD(92)37, 1992.

[11]Pennoni, G. and Bella, L., "JOCOS: A Triply Geosynchonous Orbit for Global Communications An Application Example," *Tenth International Conference on Digital Satellite Communications*, Vol. 2, 1995, pp. 646–652.

[12]Dondl, P., "LOOPUS Opens a Dimension in Satellite Communications," *International Journal of Satellite Communications*, Vol. 2, 1984, pp. 241–250, First published 1982 in German.

[13]Rouffet, D., “The SYCOMORES System [Mobile Satellite Communications],” IEE Colloquium on ‘Highly Elliptical Orbit Satellite Systems’ (Digest No.86), pp. 6/1-6/20, 1989.

[14]Norbury, J., “The Mobile Payload of the UK T-Sat Project,” IEE Colloquium on ‘Highly Elliptical Orbit Satellite Systems’ (Digest No.86), pp. 7/1-7/7, 1989.

[15]Draim, J. E., Inciardi, R., Cefola, P., Proulx, R., and Carter, D., “Demonstration of the COBRA Teardrop Concept Using Two Smallsats in 8-hr Elliptic Orbits,” 15th Annual/USU Conferece on Small Satellites, SSC01-II-3, 2001.

[16]Berretta, G., “The Place of Highly Elliptical Orbit Satellites in Future Systems,” IEE Colloquium on ‘Highly Elliptical Orbit Satellite Systems’ (Digest No.86), pp. 1/1-1/4, 1989.

[17]Girolamo, S. D., Luongo, M., and Soddu, C., “Use of Highly Elliptic Orbits for New Communication Services,” *RBCM - J. of the Braz. Soc. Mechanical Sciences*, Vol. XVI, 1994, pp. 143–149, AAS 98-172.

[18]Stuart, J. and Smith, D. J., “Review of the ESA Archimedes Study 1,” IEE Colloquium on ‘Highly Elliptical Orbit Satellite Systems’ (Digest No.86), pp. 2/1-2/4, 1989.

[19]Carter, D., “When is the Groundtrack Drift Rate Zero?” CSDL Memorandum ESD-91-020, 1991, Cambridge, MA: Charles Stark Draper Laboratory.

[20]Vallado, D. A., *Fundamentals of Astrodynamics and Applications*, McGraw-Hill, New York, 2nd ed., 2001.

[21]European Space Agency (ESA), “What is Galileo?” http://www.esa.int/esaNA/GGGMX650NDC_index_0.html, Accessed October 15, 2004.

[22]Park, A., Wilkins, M. P., and Mortari, D., “Uniformly Distributed Flower Constellation Design Study for Global Navigation System,” American Astronautical Society, AAS Paper 04-297, Maui, HI, February 8-12, 2004.

[23]“Matlab Release 13,” The Mathworks, Natick, MA, http://www.mathworks.com, Accessed October 15, 2004.

[24]Mortari, D., Wilkins, M. P., and Bruccoleri, C., “The Flower Constellations,” John L. Junkins Astrodynamics Symposium, AAS Paper 03-274, College Station, TX, May 24, 2003.

[25]“Satellite Tool Kit 5.0,” Analytical Graphics, Inc., Exton, PA, http://www.agi.com, Accessed October 15, 2004.

[26]Snyder, J. P., “Map Projections Used by the U.S. Geological Survey,” U.S. Geological Survey Bulletin 1532, 1982, 2nd ed.

[27]Vetter, J. R., "The Evolution of Earth Gravity Models Used in Astrodynamics," *APL Technical Digest*, Vol. 15, No. 4, pp. 319–335, Johns Hopkins University, Laurel, MD.

[28]Kaula, W. M., *Theory of Satellite Geodesy*, Blaisdell Publishing Company, Waltham, MA, 1966.

[29]Garfinkel, B., "Tesseral Harmonic Perturbations of an Artificial Satellite," *The Astronomical Journal*, Vol. 70, 1965, pp. 784–786.

[30]Gedeon, G., "Tesseral Resonance Effects on Satellite Orbits," *Celestial Mechanics*, Vol. 1, 1969, pp. 167–189.

[31]Ely, T. A. and Howell, K. C., "East-West Stationkeeping of Satellite Orbits With Resonant Tesseral Harmonics," *Acta Astronautica*, Vol. 46, No. 1, 2000, pp. 1–15.

[32]Delhaise, F. and Morbidelli, A., "The Problem of Critical Inclination Combined with a Resonance in Mean Motion in Artificial Satellite Theory," *Celestial Mechanics and Dynamical Astronomy*, Vol. 55, 1993, pp. 261–280.

[33]Brouwer, D., "Solutions of the Problem of Articifical Satellite Theory Without Drag," *Astronomical Journal*, Vol. 64, No. 1274, 1959, pp. 378–397.

[34]Kozai, Y., "The Motion of a Close Earth Satellite," *Astronomical Journal*, Vol. 64, No. 1274, 1959, pp. 367–377.

[35]Kozai, Y., "Second-Order Solution of Articifical Satellite Theory Without Drag," *Astronomical Journal*, Vol. 67, 1962, pp. 446.

[36]Lyddane, R. H., "Small Eccentricities of Inclinations in the Brouwer Theory of the Artificial Satellite," *Celestial Mechanics*, Vol. 36, No. 2, 1963, pp. 191–205.

[37]Merson, R. H., "The Motion of a Satellite in an Axi-Symmetric Gravitation Field," *Geophysical Journal of the Royal Astronomical Society*, Vol. 4, No. 17, 1961.

[38]Deprit, A., "The Main Problem in the Theory of Artificial Satellites to Order Four," *Journal of Guidance and Control*, Vol. 4, No. 2, 1981, pp. 201–206.

[39]King-Hele, D., G. E. C. and Rees, J. M., "Determination of the Even Harmonics in the Earth's Gravitational Potential," *Geophysical Journal of the Royal Astronomical Society*, Vol. 8, No. 119, 1963.

[40]Cook, G. E., "Luni-Solar Perturbations of the Orbit of an Earth Satellite," *Geophysical Journal of the Royal Astronomical Society*, Vol. 6, No. 271, 1962.

[41]Smith, M. S. and Service, C. R., "Space Debris: A Growing Problem," CRS Report for Congress, The Library of Congress, 1991.

[42]Kamel, Ahmed, D. E. and Tibbits, R., "East-West Stationkeeping Requirements of Nearly Synchronous Satellites Due to Earth's Triaxiality and Luni-Solar Effects," *Celestial Mechanics*, Vol. 8, 1973, pp. 129–148.

[43]Burns, R., Gabor, M. J., McLaughlin, C. A., and Luu, K. K., "Solar Radiation Pressure Effects on Formation Flying of Satellites with Different Area to Mass Ratios," AIAA Paper 2000-4132, 2000.

[44]Weisstein, E. W., "Algebraic Numbers," From MathWorld–A Wolfram Web Resource. http://mathworld.wolfram.com/AlgebraicNumber.html, Accessed October 15, 2004.

[45]Weisstein, E. W., "Rational Numbers," From MathWorld–A Wolfram Web Resource. http://mathworld.wolfram.com/RationalNumber.html, Accessed October 15, 2004.

[46]Weisstein, E. W., "Counting Numbers," From MathWorld–A Wolfram Web Resource. http://mathworld.wolfram.com/CountingNumbers.html, Accessed October 15, 2004.

[47]Weisstein, E. W., "Constructible Numbers," From MathWorld–A Wolfram Web Resource. http://mathworld.wolfram.com/ConstructibleNumber.html, Accessed October 15, 2004.

[48]Weisstein, E. W., "Congruence," From MathWorld–A Wolfram Web Resource. http://mathworld.wolfram.com/Congruence.html, Accessed October 15, 2004.

[49]Weisstein, E. W., "Greatest Common Divisor," From MathWorld–A Wolfram Web Resource. http://mathworld.wolfram.com/GreatestCommonDivisor.html, Accessed October 15, 2004.

[50]Weisstein, E. W., "Extended Greatest Common Divisor," From MathWorld–A Wolfram Web Resource. http://mathworld.wolfram.com/ExtendedGreatestCommonDivisor.html, Accessed October 15, 2004.

[51]Weisstein, E. W., "Divides," From MathWorld–A Wolfram Web Resource. http://mathworld.wolfram.com/Divides.html, Accessed October 15, 2004.

[52]Weisstein, E. W., "Relatively Prime," From MathWorld–A Wolfram Web Resource. http://mathworld.wolfram.com/RelativelyPrime.html, Accessed October 15, 2004.

[53]Weisstein, E. W., "Division Lemma," From MathWorld–A Wolfram Web Resource. http://mathworld.wolfram.com/DivisionLemma.html, Accessed October 15, 2004.

[54]Weisstein, E. W., "Floor Function," From MathWorld–A Wolfram Web Resource. http://mathworld.wolfram.com/FloorFunction.html, Accessed October 15, 2004.

[55]Weisstein, E. W., “Ceiling Function,” From MathWorld–A Wolfram Web Resource. http://mathworld.wolfram.com/CeilingFunction.html, Accessed October 15, 2004.

[56]Weisstein, E. W., “Euclidean Algorithm,” From MathWorld–A Wolfram Web Resource. http://mathworld.wolfram.com/EuclideanAlgorithm.html, Accessed October 15, 2004.

APPENDIX A

SOME MATHEMATICAL CONCEPTS AND DEFINITIONS

Algebraic Numbers

Consider the equation

$$a_n x^n + a_{n-1} x^{n-1} + \cdots + a_1 x^1 + a_0 x^0 = 0 \tag{A.1}$$

where the a_i's are integers and where a root of Equation (A.1) is r such that r satisfies no similar equation of degree $< n$, then r is an *algebraic number* of degree n. r is an *algebraic integer* when r is an algebraic number and $a_n = 1$.

Furthermore, consider

$$b_n x^n + b_{n-1} x^{n-1} + \cdots + b_1 x^1 + b_0 x^0 = 0 \tag{A.2}$$

where the b_i's are now algebraic numbers themselves, then any root r of Equation (A.2) is also an algebraic number. Any number that is not algebraic is termed *transcendental* (e.g. the numbers e and π are both transcendental).[44]

Rational Numbers

A *rational number* is any number that can be expressed as the ratio of two integers p and q where p is the numerator, q is the denominator, and $q \neq 0$. Trivially, any rational number is also an algebraic number.[45]

Table X. Integer symbols.

Example Set	Name	Symbol
$\{\ldots,-2,-1,0,1,-2,\ldots\}$	Integers	$\mathbb{Z}$
$\{1,2,3,\ldots\}$	Positive Integers	$\mathbb{N}$ or $\mathbb{Z}^+$
$\{0,1,2,3,\ldots\}$	Non-negative Integers	$\mathbb{Z}^*$
$\{0,-1,-2,-3,\ldots\}$	Non-positive Integers	$\{0\}\cup\mathbb{Z}^-$
$\{-1,-2,-3,\ldots\}$	Negative Integers	$\mathbb{Z}^-$

Counting Numbers

A number of non-standard terms exist that all refer to the set of integers. Counting numbers, natural numbers, and whole numbers are being used interchangeably in the literature. Table X gives the notation that is used for this work when referring to integers.[46]

Constructible Numbers

A *constructible number* is any number that can be represented by a finite number of additions, subtractions, multiplications, divisions, and finite square root extractions of integers. These numbers fall on a line segment that can be constructed using only a straightedge and a compass. "All rational numbers are constructible, and all constructible numbers are algebraic numbers."[47]

Congruence

Given two arbitrary numbers *a* and *b*, if one can demonstrate that their difference *a-b* is an integral multiple of a divisor *c* (i.e. $c \mid (a-b)$), then *a* and *b* are said to be *congruent modulo c*.[48] *c* is called the modulus and the statement *a is congruent to b modulo c* can be

expressed as

$$a \equiv b(\bmod c) \tag{A.3}$$

Note that the symbol $\equiv$ represents congruency and should not be confused with the equivalence sign. If $c \nmid (a-b)$, then a is *not* congruent with b modulo c, which is expressed as

$$a \not\equiv b(\bmod c) \tag{A.4}$$

Greatest Common Divisor

For any two positive integers a and b, the greatest common divisor, expressed as GCD(a,b), is the largest divisor common to both a and b.[49] GCD(a,b) is can also be written simply as (a,b). For example, GCD$(10,5) = 5$, GCD$(2,3) = 1$, and GCD$(30,36) = 6$.

If $(a,b) = c$, then c is the largest possible integer that satisfies

$$a = cx \tag{A.5}$$

$$b = cy \tag{A.6}$$

where x and y are positive integers. One can therefore state that there exists an integer relationship between a and b of the form

$$ay - bx = 0 \tag{A.7}$$

Furthermore, one can employ the Euclidean algorithm to find the greatest common divisor of two integers.

The greatest common divisor can be computed using prime factorization (i.e. con-

structed using factors that are prime). The prime factorizations of a and b are

$$a = \prod_i p_i^{\alpha_i} \tag{A.8}$$

$$b = \prod_i p_i^{\beta_i} \tag{A.9}$$

where p_i are the prime factors. Therefore,

$$\mathrm{GCD}(a,b) = \prod_i p_i^{\min(\alpha_i,\beta_i)} \tag{A.10}$$

where *min* represents the minimum. For example, consider $\mathrm{GCD}(30,36) = 6$.

$$30 = 2^1 \cdot 3^1 \cdot 5^1$$

$$36 = 2^2 \cdot 3^2 \cdot 5^0$$

which leads to

$$\mathrm{GCD}(30,36) = 2^1 \cdot 3^1 \cdot 5^0 = 6$$

The GCD is commutative, associative, distributive, and idempotent:

$$\mathrm{GCD}(na,nb) = n\mathrm{GCD}(a,b) \tag{A.12}$$

$$\mathrm{GCD}(a,b,c) = \mathrm{GCD}(\mathrm{GCD}(a,b),c) = \mathrm{GCD}(a,\mathrm{GCD}(b,c)) \tag{A.13}$$

$$\begin{aligned}\mathrm{GCD}(ab,cd) =& \mathrm{GCD}(a,c)\mathrm{GCD}(b,d) \\ &\times \mathrm{GCD}\left(\frac{a}{\mathrm{GCD}(a,c)}, \frac{d}{\mathrm{GCD}(b,d)}\right)\mathrm{GCD}\left(\frac{c}{\mathrm{GCD}(a,c)}, \frac{b}{\mathrm{GCD}(b,d)}\right)\end{aligned} \tag{A.14}$$

$$\mathrm{GCD}(a,b) = \mathrm{GCD}(b,a) \tag{A.15}$$

$$\mathrm{GCD}(a,a) = a \tag{A.16}$$

Extended Greatest Common Divisor

The greatest common divisor of two integers a and b that also satisfies the constraint that $\text{GCD}(a,b) = ra + sb$ where r and s are given integers is called the *extended greatest common divisor*.[50]

Divides

If a and b are both integers and the ratio a/b is also an integer, then b is said to *divide* a. This can be written $b \mid a$ and read as b *divides* a. Furthermore, one can say that a is divisible by b and that b is a divisor of a.[51]

Relatively Prime

Two integers are considered relatively prime if they have no common positive divisors or factors between them.[52] The notation for *greatest common divisor* is given as (a,b) (See Section A.A). If two integers a and b are relatively prime, then $(a,b) = 1$. *Coprime* and *stranger* are two terms also used to describe relatively prime integers. Relatively prime integers can be written as $a \perp b$.

Division Lemma

When ac is divisible by a number b that is relatively prime to a (i.e. $b \mid ac$ where $b \perp a$), then c must be divisible by b.[53]

Floor and Ceiling Function

The greatest integer function $\lfloor x \rfloor$, or the *floor* function, provides the largest integer that is less than or equal to x.[54] Alternatively, the smallest integer function $\lceil x \rceil$, or the *ceiling*

function, provides the smallest integer that is greater than or equal to x.[55]

Euclidean Algorithm

An algorithm is find the greatest common divisor of two numbers a and b is called the *Euclidean Algorithm* or, sometimes, *Euclid's Algorithm*.[56] Let $a = bq + r$ then find a number u such that divides both $u \mid a$ and $u \mid b$ (i.e. $a = su$ and $b = tu$). Based upon this, $u \mid r$ since

$$r = a - bq = su - qtu = (s - qt)u \tag{A.17}$$

One can also find a number v such that $v \mid b$ and $v \mid r$ (i.e. $b = s'v$ and $r = t'v$) since

$$a = bq + r = s'vq + t'v = (s'q + t')v \tag{A.18}$$

Hence, all common divisors of a and b are also common divisors of b and r from which the Euclidean Algorithm can be written

$$q_1 = \left\lfloor \frac{a}{b} \right\rfloor \qquad a = bq_1 + r_1 \qquad r_1 = a - bq_1 \tag{A.19}$$

$$q_2 = \left\lfloor \frac{b}{r_1} \right\rfloor \qquad b = q_2 r_1 + r_2 \qquad r_2 = b - q_2 r_1 \tag{A.20}$$

$$q_3 = \left\lfloor \frac{r_1}{r_2} \right\rfloor \qquad r_1 = q_3 r_2 + r_3 \qquad r_3 = r_1 - q_3 r_2 \tag{A.21}$$

$$q_4 = \left\lfloor \frac{r_2}{r_3} \right\rfloor \qquad r_2 = q_4 r_3 + r_4 \qquad r_4 = r_2 - q_4 r_3 \tag{A.22}$$

$$q_n = \left\lfloor \frac{r_{n-2}}{r_{n-1}} \right\rfloor \qquad r_{n-2} = q_n r_{n-1} + r_n \qquad r_n = r_{n-2} - q_n r_{n-1} \tag{A.23}$$

$$q_{n+1} = \left\lfloor \frac{r_{n-1}}{r_n} \right\rfloor \qquad r_{n-1} = q_{n+1} r_n + 0 \qquad r_n = \frac{r_{n-1}}{q_{n+1}} \tag{A.24}$$

For integer solutions, the Euclidean Algorithm terminates when $q_{n+1} \mid r_{n-1}$ exactly making r_n the greatest common divisor of a and b (i.e. $\mathrm{GCD}(a, b) = r_n$).

APPENDIX B

THE *Flower Constellation* VISUALIZATION AND ANALYSIS TOOL

Flower Constellations have many potential applications. To aid in the analysis of this potential, it is important to be able to properly visualize the constellation. For many *Flower Constellations*, viewing these orbits on a Mercator projection does not adequately represent the complete shape. Major software applications such as AGI's Satellite Tool Kit (STK)[25] are available that allows one to view three dimensional graphics of satellite orbits. Until very recently when AGI released version 5.0, STK could only show ECF relative orbits in a static way (i.e. the camera can not be easily moved to view the relative orbits from any angle). Also, STK at the time did not allow one to view the relative and inertial orbits simultaneously.

Therefore, our group undertook the task of creating a JAVA application that would simplify the task of design and study of *Flower Constellations* that is now called The *Flower Constellation* Visualization and Analysis Tool (FCVAT). Thanks to the efforts of Christian Bruccoleri, a 3D animation and analysis tool that allows the user to input the basic parameters of a *Flower Constellation* along with specifying the phasing requirements is available for use. Because JAVA is relatively platform independent it is also possible to make this software available to other users as a web-based application. It is virtually impossible to fully understand the implications of complex constellations without a visualization tool of this nature. At the time of this writing, our group is in active discussions with companies such as AGI to integrate the FCVAT as either a third-party add on or as an integral part of existing commercial software.

APPENDIX C

EXAMPLE CONSTELLATION PHASING DATA

Table XI. Satellite Phasing for a 8-1-9-1-9 *Flower Constellation*.

$a = 10541.042\ km$	$e = 0.1577554$	$h_p = 2500.000\ km$	
Sat #	Node (deg)	Mean Anom (deg)	True Anom (deg)
1	0.00	0.00	0.00
2	40.00	40.00	53.54
3	80.00	80.00	98.12
4	120.00	120.00	134.10
5	160.00	160.00	165.20
6	200.00	200.00	194.80
7	240.00	240.00	225.90
8	280.00	280.00	261.88
9	320.00	320.00	306.46

Table XII. Satellite phasing for a 4-1-4-1-4 *Flower Constellation*.

$a = 16732.862\ km$	$e = 0.5829681$	$h_p = 600.000\ km$	
Sat #	Node (deg)	Mean Anom (deg)	True Anom (deg)
1	0.00	0.00	0.00
2	90.00	0.00	0.00
3	180.00	0.00	0.00
4	270.00	0.00	0.00

Table XIII. Satellite phasing for a 769-257-4-1-4 *Flower Constellation*.

$a = 20305.549\ km$	$e = 0.6661929$	$h_p = 400.000\ km$	
Sat #	Node (deg)	Mean Anom (deg)	True Anom (deg)
1	0.00	0.00	0.00
2	90.00	87.90	150.73
3	180.00	178.60	179.61
4	270.00	269.30	208.10

Table XIV. Satellite phasing for a 3-1-4-1-7 *Flower Constellation*.

$a = 20270.418\ km$	$e = 0.6557478$	$h_p = 600.000\ km$	
Sat #	Node (deg)	Mean Anom (deg)	True Anom (deg)
1	0.00	0.00	0.00
2	205.71	102.86	156.60
3	257.14	308.57	229.79
4	308.57	154.29	172.85

Table XV. Satellite phasing for a 4-1-5-1-5 *Flower Constellation*.

$a = 16732.862\ km$	$e = 0.0000434$	$h_p = 10354.000\ km$	
Sat #	Node (deg)	Mean Anom (deg)	True Anom (deg)
1	0.00	0.00	0.00
2	72.00	72.00	72.00
3	144.00	144.00	144.00
4	216.00	216.00	216.00
5	288.00	288.00	288.00

Table XVI. Satellite phasing for a 3-1-4 and 3-2-4 *Flower Constellation*.

	$a = 20270.418\ km$	$e = 0.6557478$	$h_p = 600.000\ km$	
Sat #	(a) Node (deg)	(a) Mean Anom (deg)	(b) Node (deg)	(b) Mean Anom (deg)
1	0.00	0.00	0.00	0.00
2	90.00	90.00	180.00	180.00
3	180.00	180.00		
4	270.00	270.00		
Sat #	(c) Node (deg)	(c) Mean Anom (deg)	(d) Node (deg)	(d) Mean Anom (deg)
1	0.00	0.00	0.00	0.00
2	0.00	180.00	90.00	45.00
3	180.00	90.00	180.00	270.00
4	180.00	270.00	270.00	135.00

Table XVII. Satellite phasing for a 12-1-13-1-13 *Flower Constellation*.

$a = 8044.321\ km$	$e = 0.0000$	$h_p = 1666.000\ km$	
Sat #	Node (deg)	Mean Anom (deg)	True Anom (deg)
1	0.00	0.00	0.00
2	27.69	27.69	27.69
3	55.38	55.38	55.39
4	83.08	83.08	83.08
5	110.77	110.77	110.77
6	138.46	138.46	138.46
7	166.15	166.15	166.15
8	193.85	193.85	193.85
9	221.54	221.54	221.54
10	249.23	249.23	249.23
11	276.92	276.92	276.92
12	304.62	304.62	304.61
13	332.31	332.31	332.31

Table XVIII. Satellite phasing for a 12-1-26-1-26 *Flower Constellation.*

$a = 8044.321\ km$	$e = 0.0000229$	$h_p = 1666.000\ km$	
Sat #	Node (deg)	Mean Anom (deg)	True Anom (deg)
1	0.00	0.00	0.00
2	13.85	193.85	193.85
3	27.69	27.69	27.69
4	41.54	221.54	221.54
5	55.38	55.38	55.39
6	69.23	249.23	249.23
7	83.08	83.08	83.08
8	96.92	276.92	276.92
9	110.77	110.77	110.77
10	124.62	304.62	304.61
11	138.46	138.46	138.46
12	152.31	332.31	332.31
13	166.15	166.15	166.15
14	180.00	360.00	360.00
15	193.85	193.85	193.85
16	207.69	27.69	27.69
17	221.54	221.54	221.54
18	235.38	55.38	55.39
19	249.23	249.23	249.23
20	263.08	83.08	83.08
21	276.92	276.92	276.92
22	290.77	110.77	110.77
23	304.62	304.62	304.61
24	318.46	138.46	138.46
25	332.31	332.31	332.31
26	346.15	166.15	166.15

Table XIX. Satellite phasing for a 31-11-30-7-10 *Flower Constellation*.

$a = 21133.149\ km$	$e = 0.2723216$	$h_p = 9000.000\ km$	
Sat #	Node (deg)	Mean Anom (deg)	True Anom (deg)
1	0.00	0.00	0.00
2	0.00	261.82	233.54
3	0.00	163.64	170.24
4	36.00	291.27	259.81
5	36.00	193.09	187.80
6	36.00	94.91	123.85
7	72.00	320.73	294.96
8	72.00	222.55	205.92
9	72.00	124.36	145.48
10	108.00	350.18	342.28
11	108.00	252.00	226.05
12	108.00	153.82	164.29
13	144.00	281.45	250.28
14	144.00	183.27	181.95
15	144.00	85.09	115.60
⋮	⋮	⋮	⋮
25	288.00	301.09	270.31
26	288.00	202.91	193.71
27	288.00	104.73	131.51
28	324.00	330.55	309.39
29	324.00	232.36	212.33
30	324.00	134.18	151.97

Table XX. Satellite phasing for a 37-18-57-6-19 *Flower Constellation*.

$a = 26080.990\ km$	$e = 0.0000327$	$h_p = 19702.000\ km$	
Sat #	Node (deg)	Mean Anom (deg)	True Anom (deg)
1	0.00	0.00	0.00
2	18.95	221.05	221.05
3	18.95	101.05	101.06
4	18.95	341.05	341.05
5	37.89	202.11	202.10
6	37.89	82.11	82.11
7	37.89	322.11	322.10
⋮	⋮	⋮	⋮
53	341.05	18.95	18.95
54	341.05	258.95	258.94
55	341.05	138.95	138.95
56	360.00	240.00	240.00
57	360.00	120.00	120.00

Table XXI. Satellite phasing for a 15-7-49-23-49 *Flower Constellation*.

$a = 25367.718\ km$	$e = 0.3937911$	$h_p = 9000.000\ km$	
Sat #	Node (deg)	Mean Anom (deg)	True Anom (deg)
1	0.00	0.00	0.00
2	7.35	35.69	75.28
3	14.69	71.37	116.71
4	22.04	4.20	10.47
5	29.39	39.88	81.57
6	36.73	75.57	120.28
7	44.08	8.40	20.74
8	51.43	44.08	87.39
9	58.78	79.77	123.66
10	66.12	12.59	30.66
11	73.47	48.28	92.79
12	80.82	83.97	126.89
13	88.16	16.79	40.09
14	95.51	52.48	97.81
15	102.86	88.16	129.97
⋮	⋮	⋮	⋮
30	213.06	6.30	15.64
31	220.41	41.98	84.54
32	227.76	77.67	121.99
33	235.10	10.50	25.75
34	242.45	46.18	90.14
35	249.80	81.87	125.29
36	257.14	14.69	35.44
37	264.49	50.38	95.34
38	271.84	86.06	128.45
39	279.18	18.89	44.59
40	286.53	54.58	100.19
41	293.88	90.26	131.46
42	301.22	23.09	53.15
43	308.57	58.78	104.71
44	315.92	94.46	134.36
45	323.27	27.29	61.11
46	330.61	62.97	108.96
47	337.96	98.66	137.15
48	345.31	31.49	68.48
49	352.65	67.17	112.95

VITA

Matthew Paul Wilkins was born in Waco, TX on July 1, 1974. He attended high school at Waco-Midway from 1988 until 1992. In the Fall of 1992 he enrolled in Texas A&M University and subsequently graduated *cum laude* with a B.S. degree in Aerospace Engineering in the Spring of 1997. During his undergraduate career, Matt worked as a Co-Op Design Engineer at Johnson Engineering Corporation. Among the many projects he worked on, the most extensive was the design of a complete mock-up of the external airlock for the Space Shuttle High-Fidelity Crew Compartment Trainer. Immediately after graduating, Matt interned at United Space Alliance where he developed a computer simulation of tracking orbital debris and then predicting their orbits. This initial study led up to his Master's Thesis work, also at Texas A&M University, under the direction of Dr. Kyle T. Alfriend. Matt graduated with an M.S. degree in Aerospace Engineering in May of 2000, whereupon he immediately continued on towards the completion of his Ph.D. That summer, Matt also worked for the Naval Research Laboratory under the direction of Dr. Shannon Coffey and investigated transitioning from a general perturbations to a special perturbations space object catalog. During the first year of his Doctoral work, Matt also served as the Graduate Student Council president at Texas A&M University. As GSC President, Matt had the opportunity to represent the entire graduate student body to the University community and work on their behalf. Matt spent most of his 7 years in graduate school serving in some capacity with the GSC as either a representative of the Aerospace Engineering Department, the GSC Treasurer, the GSC President, or the GSC Legislative Affairs Liaison. Additionally, Matt was heavily involved over the years with organizing the University's annual premier student research competition called the Student Research Week, which is heavily funded by the Graduate Student Council. The following address may be used to reach Matt: P.O. Box 1401, Pearsall, TX, 78061